Polymers at Membranes

Dissertation
zur Erlangung des akademischen Grades
Doktor der Naturwissenschaften (Dr. rer. nat.)
in der Wissenschaftsdisziplin Theoretische Physik

eingereicht an der
Mathematisch-Naturwissenschaftlichen Fakultät der Universität Potsdam

angefertigt am
Max-Planck-Institut für Kolloid- und Grenzflächenforschung in Golm

von

Markus Breidenich

geboren am 18. Mai 1972 in Düren

Potsdam, im August 2000

Zusammenfassung

Lipidmembranen sind die Grundbausteine der Zelloberfläche. Die in der Membran vorliegende Doppelschicht-Struktur entsteht durch Selbstaggregation der Lipidmoleküle in Wasser. Neben den Lipiden enthält die Zellmembran eine Vielzahl weiterer Bestandteile, zu deren zahlreichen Aufgaben der Ionentransport ebenso zählt wie die Schutzfunktion gegen mechanische und chemische Beschädigungen der Zelle.

Während der Ionentransport durch Proteine in der Zellmembran geregelt wird, sorgt ein von der Membran ausgehendes Netzwerk von Filamenten im Inneren der Zelle für zusätzliche Stabilität der Lipidschicht. Außen ist die Zellmembran mit einer Vielzahl von Zuckermolekülen bedeckt, die die Schutzfunktion wahrnehmen.

Die Beeinflussung der Membran durch derartige kettenähnliche Proteine soll im Rahmen dieser Arbeit anhand eines vereinfachten biomimetischen Systems studiert werden. Letzteres dient als Minimalmodell für die Zellmembran, in welchem der Einfluß verankerter Polymere auf die Lipidmembran untersucht wird.

Zu den grundlegenden Größen, die durch verankerte Polymere beeinflusst werden, zählen die Krümmung und Steifigkeit der Membran. Eine freie, nicht mit Polymeren bedeckte Membran hat eine im Mittel verschwindende Krümmung. Einseitig auf der Membran verankerte Polymere induzieren eine Krümmung, die die Membran von den Polymeren weg biegt. Grund hierfür ist der Druck, den eine Polymerkette durch Stöße mit der Membran auf diese ausübt. Die Berechnung des Druckes, der im Ankersegment stets ein Zug an der Membran ist, erlaubt es, explizit die Form der Membran unter dem Einfluss der Polymere zu bestimmen. In der Nähe des Ankers nimmt die Membran Kegelgestalt an, während sie sich in großem Abstand einem Katenoid annähert, einer Minimalfläche mit verschwindender Krümmung. Bei einer Bedeckung mit vielen Polymeren ergibt sich das Gesamtprofil der Membran, ebenso wie ihre Krümmung, als lineare Superposition der einzelnen Polymereffekte. Mittels einer Monte Carlo-Simulation können die perturbativ berechneten Resultate bestätigt werden.

Im Rahmen desselben Formalismus ist auch die Wechselwirkung der Polymere, die durch die Membran induziert wird, zugänglich. Diese ist attraktiv, jedoch vernachlässigbar bei Berücksichtigung der sterischen Repulsion der Ketten verschiedener Polymere. Beides, sowohl die Wechselwirkung zwischen Polymer und Membran, als auch die Wechselwirkung der Polymere untereinander, haben Einfluss auf die Krümmung der Membran und müssen somit bei der Auswertung von Experimenten herangezogen werden. Von Interesse sind ebenso Polymere, die an beiden Enden verankert sind und Polymere, welche die Membran durchdringen. Letztere Situation ist biologisch motiviert im Hinblick auf den Transport von DNA durch die Zellmembran.

In einem weiteren Teil der Arbeit geht es um den Einfluss eines Wechselwirkungspotentials zwischen Polymer und Membran, das zu der bisher betrachteten entropischen Repulsion hinzutritt. Es zeigt sich, dass ein attraktives Potential die ursprünglich induzierte Krümmung verkleinert. Im Limes starker Adsorption, in welchem das Polymer ganz auf der Membran lokalisiert ist, verschwindet der Polymerdruck und die durch diesen induzierte Krümmung der Membran. Monte Carlo-Simulationen hierzu dienen dem Vergleich mit der theoretischen Vorhersage.

Im letzten Teil der Arbeit werden Polymerlösungen und deren Einfluss auf die Krümmung der Membran betrachtet. Im Grenzfall einer rein sterischen, repulsiven Wechselwirkung zwischen Polymeren und Membran biegt sich diese, im Gegensatz zur verankerten Situation, zur Lösung hin. Bei Hinzunahme von Adsorption biegt sich die Membran im Limes starker Attraktion der Polymere von

der Lösung weg.

Contents

Chapter 1

Introduction

1.1 Biomembranes and biomimetic systems

Membranes which are decorated by polymers provide simple model systems of biological membranes such as the plasma membrane of the cell. Its structure is displayed in figure 1.1. A detailed introduction into the biology of the cell membrane is given in [1, 2, 3, 4]. The main purpose of the cell membrane is to separate and protect the inside, which contains the life carrying components, from the outside, the environment of the cell. On the other hand the membrane has to garantee transport between inside and outside. Ion channels, composed of proteins, which are embedded in the membrane, regulate transport of ions and small molecules between inner and outer part of the cell [2].

Other inclusions of the membrane have large tails, which extrude from the membrane both in the inner and in the outer direction. The intracellular side is called the cytoskeleton, consisting of a network of filaments which stabilizes the flexible membrane. The extracellular part consists of the glycocalix and the extracellular matrix. The membrane on this side is decorated by glycolipids and glycoproteins, which protect the cell against mechanical and chemical attack.

The backbone of the cell membrane is given by the lipid bilayer. Bilayers are one possible self-assembled structure [5, 6, 7, 8, 9] formed by molecules, such as lipids, which have two parts, namely a hydrophilic and a hydrophobic part. If those molecules are dissolved in water, they tend to form aggregates in order to avoid contacts between the hydrophobic parts and the water in such a way that the hydrophilic groups of the molecule are exposed to the water. In figure 1.2 we show a variety of different aggregates such as a cylindrical micelle, a bilayer and a vesicle.

In order to understand certain aspects of the behavior of biological membranes we will in the following study much simpler objects which we call **biomimetic membranes**[1]. These are model systems which allow to investigate the physical properties of biological membranes by focusing on the basic and characteristic aspects. Polymer-decorated membranes serve as a biomimetic system for the cell membrane. On the other hand the investigation of these supramolecular structures might lead to new materials and biotechnical applications. Both experimental [11, 12, 13, 14] and theoretical [15, 16] work has been done in this area of research.

We will now introduce the components of our model system, namely the lipid bilayer and the anchored polymers.

[1] mimesis (gr.) imitation

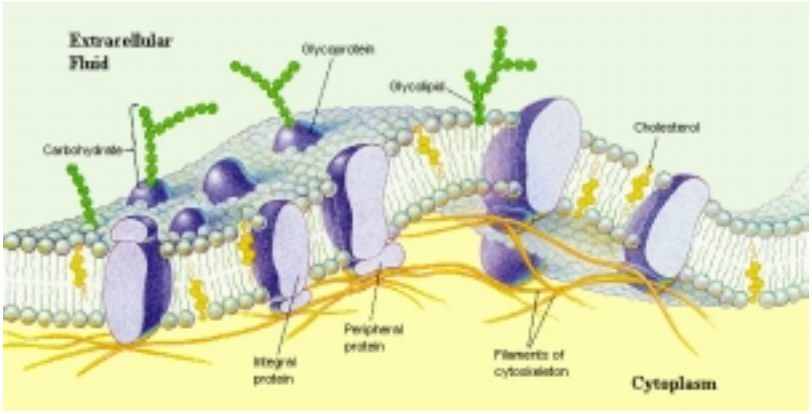

Figure 1.1: Schematic picture of the cell membrane: The membrane contains different types of proteins. In addition, the inside and outside of the cell are decorated by filaments. The figure is taken from [10].

1.2 Lipid bilayers

Chemically, the lipids are composed of a small hydrophilic head group and two large hydrophobic hydrocarbon tails. At an oil-water interface, the lipids form a monolayer in which the tails are located in the oil-phase and the head-group is inside the water-phase. In an aqueous environment, one possible configuration is the bilayer. In the experimental situation, one finds in general closed bilayers called vesicles. This is favorable since for a membrane of finite size the closed geometry is the easiest way to avoid boundaries where the hydrophobic lipid tails at the edges of the membrane are exposed to the surrounding water. Vesicles are important experimental objects, with which one can study the properties of lipid membranes and the influence of attached polymers.

Vesicles are also important from the point of view of pharmacological applications [17, 18, 19]. Inside a vesicle it is possible to transport drugs in order to avoid direct injection. A prominent example is insulin. The vesicles can penetrate the skin and inside the body release their cargo. Since the immune system would recognize them as invadors, it is necessary to protect their surface by decoration with specific polymers and consequently avoid the attack [20, 21, 22]. The polymers (glycolipids) hinder proteins and antibodies to adsorb on the vesicles.

We will in the following focus on the physical properties of the membrane [24, 25, 16]. The thickness of the bilayer is about $4nm$. The lateral size can extend up to the μm-range. It is therefore justified to neglect the thickness and to model the membrane mesoscopically as a two-dimensional surface. This is even more justified, since we are not interested in the molecular properties of the membrane but in the shape profile and the curvature. However, in order to find out which quantities are crucial to describe the membrane on the mesoscopic scale one has to return to the molecular level.

Above a certain temperature the membrane is in the fluid state in which the hydrophobic chains of the lipid are disordered and the lipids can freely move inside their monolayer. There is little friction between both monolayers. In the simplest model the lipids move independently in each layer.

In principle, the lipids can change from one monolayer to the other. However it turns out that the time scale for these so-called flip-flops is large and in a range between minutes and days [26], since the lipid has to cross the hydrophobic part of the bilayer with its hydrophilic head group. In the

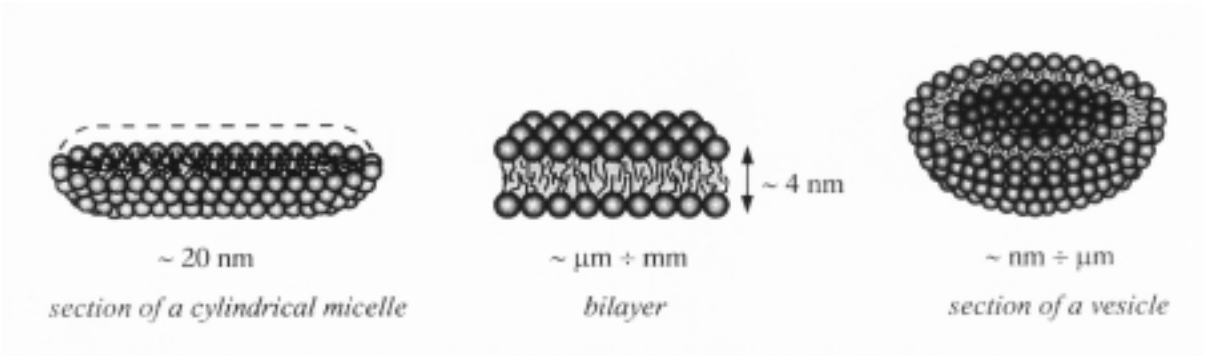

Figure 1.2: Different types of lipid aggregates: micelle, bilayer and vesicle (cut in a half sphere). Thanks to [23].

following we will neglect the possibility of such flip-flops.

The membrane is energetically described by a local energy functional, which takes into account the spatial position of the surface, the gradients and the curvature. This is, in fact, an expansion in gradients which can be extended further. Nevertheless, it turns out that these three observables are sufficient to describe the membrane energy.

As long as we consider the environment of the membrane as homogeneous and isotropic we expect the membrane to be translationally invariant. Thus, the spatial position of the membrane does not influence the energy which is attributed to the membrane and will not enter the Hamiltonian explicitly.

Since in the fluid state the membrane lipids form a two-dimensional fluid, it is not possible to change the area of the membrane. No work is done in increasing the area, which would correspond to a surface tension. For fluid membranes, the crucial quantity which governs their physical properties is the curvature. This is intuitive from a molecular point of view, since the long tails of the lipids are squeezed if the membrane is curved. Due to the steric repulsion they tend to avoid curved configurations of the surface. Furthermore, if the membrane is symmetric, i.e. if there is no difference between the half space above and below it, and if the two monolayers have the same composition, the curvature will enter the Hamiltonian in a quadratic term. The energy of the whole membrane will be given by the integral of the curvature, where the integration extends over the membrane surface. Thus, this term will be dimensionless. The prefactor, which relates the integrated curvature to the energy of the membrane, is called the bending rigidity κ, which has the dimension of an energy. The simplest Hamiltonian to describe a symmetric membrane is therefore given by

$$\mathcal{H}_{me} \quad = \quad \int d\mathcal{A}\, 2\kappa\, M^2 \tag{1.1}$$

where M is the (mean) curvature and the factor two is of conventional reasons.

In general the curvature of a two-dimensional surface is defined via two principal curvature axes and the two corresponding principal curvature radii denoted by R_1 and R_2, which mathematically are given by the two eigenvalues of the curvature tensor [27]. There are two invariant measures of the curvature [28] which describe the surface, namely the above mentioned mean curvature given by

$$M \quad = \quad \frac{1}{2}\left(\frac{1}{R_1} + \frac{1}{R_2}\right) \tag{1.2}$$

and the Gaussian curvature

$$G = \frac{1}{R_1}\frac{1}{R_2} \tag{1.3}$$

which is related to the topology of the surface. In the case of an asymmetric membrane, i.e. a membrane where both half-spaces, which are separated by the surface, are not identical, one could think of a spontaneous induced curvature of the membrane. This curvature is called the spontaneous curvature of the membrane, denoted by M_{sp}. Including the spontaneous curvature leads us to a quite complete description of the membrane energy. The corresponding Hamiltonian was suggested by Helfrich [29] and is given by

$$\mathcal{H}_{me} = \int d\mathcal{A}\; 2\kappa\; (M - M_{sp})^2 \; + \; \int d\mathcal{A}\; \kappa_G\; G \tag{1.4}$$

where κ_G is the Gaussian bending rigidity. Both κ and κ_G can be measured experimentally. For phospholipid membranes one finds $\kappa \approx 10 - 20 k_B T$, which is high compared to the thermal energy $k_B T$. The Gaussian bending rigidity κ_G is difficult to measure since the second integral in eq. (1.4) is a topological invariant, which is a consequence of the Gauß-Bonnet theorem [30]. The elastic parameter κ_G measures the energy for the formation of handles.

The most important experimental objects with which one can study the curvature of lipid membranes are vesicles in aqueous solution [31]. The physics of vesicles is governed by the fact that their volume and area are constant. The volume is fixed, since once a vesicle has formed there is no driving force for water to enter or to leave the vesicle. The area of the vesicles is constant, since the concentration of lipid monomers in the water is very small and thus the interchange of lipids between membrane and solution is negligible.

The shape of the vesicles is given by minimizing the energy in the spontaneous curvature model for given values of volume, area and curvature [32].

The two remaining parameters in case of the spontaneous-curvature-model are the reduced volume and the reduced spontaneous curvature. Both quantities are dimensionless and normalized with respect to the area of the vesicle in such a way, that one defines the radius R_A, which corresponds to the unique sphere of surface area A. Consequently the reduced volume is given by

$$v = \frac{V}{4\pi R_A^3/3} \tag{1.5}$$

and the reduced spontaneous curvature is given by

$$m_{sp} = R_A M_{sp}\ . \tag{1.6}$$

One ends up with a phase diagram of different vesicle shapes [32, 33, 34] depending on both parameters. We will later refer to these results in order to see whether or not the anchoring of polymers has an observable influence on the shape of the decorated vesicles.

It turns out that the spontaneous curvature-model is not able to predict the richness of shapes which one observes in experiments. The main reason for this deficit is due to neglect of the bilayer structure. A vesicle with surface area $\mathcal{A}$ has in fact an area $2\mathcal{A}$ of lipid surface. There might be an initial difference between the areas of the outer and the inner monolayer $\Delta\mathcal{A}_0$ which provides an additional parameter for the vesicle shapes. The corresponding theory which includes the difference $\Delta\mathcal{A}$ uses

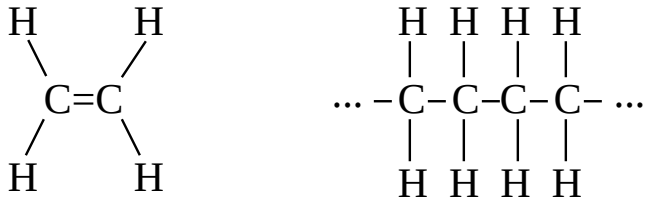

Figure 1.3: Ethylene and polyethylene.

the so called area-difference-model [35], in which the vesicle shape is obtained by minimization of the Hamiltonian

$$\mathcal{H}_{ADE} \;=\; \int d\mathcal{A}\, 2\kappa\, (M - M_{sp})^2 \;+\; \frac{\bar{\kappa}}{2}\frac{\pi}{\mathcal{A} l_{me}^2}(\Delta\mathcal{A} - \Delta\mathcal{A}_0)^2 \tag{1.7}$$

with respect to the area-difference between the monolayers and the curvature for given volume V, area $\mathcal{A}$, preferred area difference $\Delta\mathcal{A}_0$ and preferred (spontaneous) curvature M_{sp}. l_{me} denotes the thickness of the bilayer, which is about $4\mathrm{nm}$. The parameter $\bar{\kappa}$ is called the non-local bending rigidity, since the area difference is related to the integrated (non-local) curvature of the membrane

$$\Delta\mathcal{A} \;=\; 2 l_{me} \int d\mathcal{A}\; M\;. \tag{1.8}$$

The parameters κ and $\bar{\kappa}$ have similar values for phospholipid membranes. The minimization is in general done numerically [36]. Finally, one obtains a corresponding phase diagram of the area-difference-elasticity model [32].

The lipid bilayer which we discussed so far represents one component of our system. The other important component is the polymer which will be attached to the membrane. In the following, we will give a brief introduction to polymer physics.

1.3 Introductory remarks to polymers

Polymers consist of a large number of molecular units, monomers, which are covalently linked. In general the backbone structure is provided by carbon atoms $\mathrm{C}-\mathrm{C}$. The simplest example of a polymer is polyethylene, which is usually formed by polymerization of ethylene. The chemical structure is shown in figure 1.3. The large variety of organic chemistry arises from the infinite possibilities to link different types of monomers together. The chains which emerge from these polymerization processes are not necessarily linear. Possible configurations are long chains with small side chains, star polymers or cross-linked polymers, which form networks. Furthermore, one distinguishes polymers which are basically neutral and polymers which carry charges, called polyelectrolytes.

One of the simplest theoretical models to describe polymer chains is the freely jointed chain [37, 38, 39]. Each monomer is considered pointlike and linked by a straight bond of fixed length a_p, the so-called Kuhn length. The bonds have total rotational freedom. The probability distribution of one single bond is given by

$$p(\mathbf{r}_n - \mathbf{r}_{n-1}) \;\;=:\;\; p(\mathbf{R}_n) = \frac{\delta(|\mathbf{R}_n| - a_p)}{4\pi a_p^2}\;, \tag{1.9}$$

where $\mathbf{r}_n$ is the spatial position of the n-th monomer. An important quantity is the end-to-end vector of the chain, measuring the relative spatial position of the first and the last bead of the polymer. It is clear that the average end-to-end vector vanishes, since it points into all directions with equal probability. The interesting measure is the average of the squared end-to-end vector as given by

$$\langle \mathbf{R}^2 \rangle \;=\; \langle (\sum_n \mathbf{R}_n)^2 \rangle \;=\; N a_p^2 \,. \tag{1.10}$$

This leads to the end-to-end distance

$$R_p \;\equiv\; \sqrt{\langle \mathbf{R}^2 \rangle} \;=\; a_p \sqrt{N} \,, \tag{1.11}$$

which is a measure of the polymer size. This result is identical to the time-dependence of the average displacement of a Brownian particle from the original starting point, if N is identified with time. The corresponding probability distribution for the distance of the Brownian particle is Gaussian. In fact, if we choose the step size between neighboring beads larger than the Kuhn length a_p of the polymer, the spatial positions of the beads are uncorrelated and thus fulfill the properties of a random walk. Consequently one expects the probability distribution of the polymer end-to-end vector to become Gaussian in the limit of small a_p. Mathematically, the Gaussian distribution is reached in the limit of small a_p and large N in such a way that $R_p = a_p \sqrt{N}$ is constant. This is the continuum limit for the polymer chain. One ends up with the probability distribution

$$p(\mathbf{R}) \;=\; \left(2\pi \frac{R_p^2}{3} \right)^{-3/2} \exp\left(-\frac{3}{2} \frac{\mathbf{R}^2}{R_p^2} \right) \tag{1.12}$$

of the end-to-end vector $\mathbf{R}$. Because of the Gaussian character of the chain, the same distribution function holds for each bond with average bond length a_p. This implies that the Gaussian chain is self-similar on all length scales resulting in a fractal structure with the fractal dimension $d = 2$. This is due to the relation between the number of monomers and the mean displacement $N \sim r^2$. The fractal dimension d, which relates the mass of an object to its diameter is defined as the exponent in the relation $N \sim r^d$ and thus in case of the Gaussian chain $d = 2$ [39].

It is clear that the ideal polymer model can not predict the properties of real polymers in all details. The model applies to a certain range of $\mathbf{R}$-values which are large compared to the Kuhn length a_p and smaller or in a range of R_p. Below the lower limit, the polymer stiffness cannot be neglected anymore. Above the upper limit, the finite bond lengths of real chains forbid configurations which are strongly overstretched. In the Gaussian model itself there is no upper limit for the stretching of the polymer.

The Gaussian distribution function suggests a model of the polymer in which the pointlike beads are linked by harmonic springs, known as the bead-spring-model. The (effective) energy of the chain in discretized form is given by

$$\mathcal{E} \;=\; \frac{D}{2} \sum_{n=1}^{N} (\mathbf{r}_n - \mathbf{r}_{n-1})^2 \,, \tag{1.13}$$

which in the continuum limit yields

$$\mathcal{E} \;=\; \frac{D}{2} \int_0^N \mathrm{d}s \, \left(\frac{\mathrm{d}\mathbf{r}(s)}{\mathrm{d}s} \right)^2 \,, \tag{1.14}$$

where s is the internal length of the polymer. The equilibrium of the chain is described by the distribution function given by the Boltzmann factor $\exp(-\mathcal{E}/k_BT)$. In order to recover the form according to eq. (1.12) one identifies the spring constant D as

$$D = \frac{3k_BT}{a_p^2} . \tag{1.15}$$

The basic ingredient of the Gaussian chain is the free random walk of the polymer beads with respect to the internal length N, corresponding to the number of beads. Thus, the chain can freely intersect and different pointlike beads can occupy the same spatial positions. Because of this behavior one calls the Gaussian model also the ideal chain model.

A more realistic model is provided by the self-avoiding walk where the polymer beads have a certain volume, the so-called excluded volume, in which no other bead can enter. It is intuitively clear that the overall size of the polymer will be enlarged due to this steric interaction. An estimate for the size of the polymer which turns out to be very good in comparison to experiments and computer simulations is given by the Flory radius

$$R_F \sim N^{3/5} \tag{1.16}$$

where the exponent $1/2$ of the ideal chain is enlarged to $3/5$ for the excluded-volume chain [40, 41].

Whether the polymer can be considered as ideal or not mainly depends on the energies between polymer and solvent. In a good solvent, the polymer likes to have solvent molecules in the neighborhood of its beads and thus spreads out in order to increase the contact area with the solvent. This is the case where excluded-volume effects are important. If the solvent is bad, the polymer monomers prefer to shrink together in order to avoid contacts with the solvent. Then the van der Waals attraction between the polymer beads is dominant and the polymer forms a globular configuration. In between, where the excluded-volume interaction is balanced by the van der Waals attraction the polymer ca be considered to be ideal. Since the energetic interactions are fixed by the polymer and the solvent, the temperature governs the polymer behavior. The temperature at which the polymer is ideal is called the θ-temperature. Below, the size of the polymer is smaller and above this temperature it is larger than the ideal chain.

In most cases the ideal chain serves as a starting point, from which excluded-volume-effects are considered perturbatively.

We will now discuss the properties of polymers anchored on surfaces which are impenetrable for the polymers. It is intuitively clear that the configuration of the polymer beads will be perturbed by the wall and lead to an anisotropic polymer shape which differs from the spherical configuration of the free chain.

1.4 Anchored polymer

Anchoring a polymer to a surface involves a loss of entropy of the chain. In fig. 1.4 we show an experimental situation where DNA is linked to a phospholipid membrane via a big anchoring molecule called streptavidin. In the idealized situation of a flat substrate, the polymer is confined to the half-space and thus looses entropy since it can no longer explore the half-space on the other side of the substrate[42]. In order to anchor the polymer on the surface it is thus necessary to compensate the entropic effect by a chemically induced energy gain due to the anchoring. If this energy is smaller

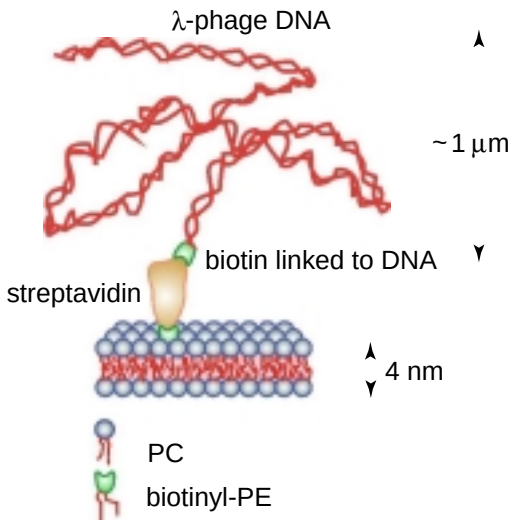

Figure 1.4: Schematic picture of an experimental situation: DNA anchored to a lipid bilayer. The anchor molecule is streptavidin, a protein, which enters the membrane with a small connected molecule. The DNA is linked to the anchor using biotin. Thanks to [23].

than the entropy loss, the polymers will not stay at the surface. If the energy is large compared to the entropy decrease, polymers will stay at the surface for a long time. For a large reservoir of polymers, in principle, this anchoring will lead to very large coverage densities. However, for large densities the steric interaction of the polymer chains provides an additional entropy decrease which balances the anchoring energy and leads to an equilibrium coverage density of polymers on the surface. The situation is similar if the polymers are anchored on the membrane. If the membrane is initially flat, the anchoring energy in the phospholipid bilayer has to overcome the entropy decrease. Since the membrane is a flexible object, the anchoring of the polymer leads to a change in the membrane shape in such a way that the membrane bends away from the polymer. Consequently the polymer gains configuration space. If one considers the curvature of the membrane to be small one can expand the polymer's entropy difference of the curved geometry and the flat situation in powers of the membrane curvature up to second order, which leads to [43]

$$\Delta S_p \quad = \quad b_1 R_p M + b_2 (R_p M)^2 + b_3 R_p^2 G \; . \tag{1.17}$$

If one solves the problem for a polymer anchored on a flat surface, on a sphere and on a cylinder, one ends up with the prefactors [44]

$$b_1 = \sqrt{\frac{\pi}{6}} \; , \quad b_2 = -\left(\frac{\pi}{12} + \frac{1}{6}\right) \; , \quad b_3 = \frac{1}{6} \; . \tag{1.18}$$

Since the first coefficient b_1 is positive the polymer gains entropy if the membrane bends away from it. Calculation of the spontaneous curvature leads to

$$M_{sp} \quad \approx \quad T \frac{b_1}{4 \kappa R_p} \approx 0.18 \frac{T}{\kappa R_p} \tag{1.19}$$

where the temperature is measured in energy units and the curvature is defined as positive if the membrane bends away from the polymer.

In addition, the anchoring of the polymer suppresses membrane fluctuations and leads to an entropic contribution to the bending rigidity κ. Thus one defines an effective bending rigidity κ_{eff} which is larger than κ. The Gaussian bending rigidity is decreases due to the anchored polymer and therefore the formation of holes and handles in the membrane surfaces becomes easier [44]. Similar results have been obtained in [45] for the situation of so-called Siamese lipid-polymers, where two polymers are connected via their anchor molecules, having chains which due to the presence of an artificial hard wall between them do not penetrate each other.

1.5 Overview

Anchored polymers are considered in chapter 2 and 3 both in a perturbative approach and in a Monte Carlo simulation. We consider the pressure of the polymers exerted on the membrane, as well as the resulting shape profile and the curvature of the membrane.

Another aspect is presented in chapter 4 where the polymer interaction due to membrane curvature is calculated. The results lead to predictions on experiments with polymer covered vesicles.

In chapters 5 and 6, we investigate different geometries such as polymers which are anchored with both ends and polymers which translocate the membrane. External forces are considered, which in the case of lateral forces acting on the membrane lead to surface tension, and in the case of perpendicular forces acting on the polymer lead to changes in the polymer configuration and the membrane shape profile.

In chapters 7 and 8, we include adsorption due to short range interaction between the membrane surface and the polymer. First we investigate a pure contact potential, which only acts directly on the membrane surface, and generalize the calculation to a square-well potential. The results are compared with Monte Carlo simulations. Finally, we extend the work to free polymers in the solution above the membrane. Here we consider the curvature for different sizes of the interaction potential and compare with the results obtained in the case of anchored polymers.

In the last chapter we summarize the major results of the thesis and conclude with an outlook considering future work.

Chapter 2

Anchored Polymers: Perturbative Approach

Membranes which are decorated by polymers on one side bend away from the polymers [43, 46]. The induced spontaneous curvature can be calculated by comparing the configuration of polymers on curved surfaces with those on a flat substrate. The basic simplification in these calculations is due to the replacement of the fluctuating membrane by fixed membrane shapes.

We will now change the starting point of the calculation. Both polymer and membrane fluctuations are taken into account in the initial partition function of the compound system. In order to simplify the situation we start with a single polymer which is attached to an infinitely extended membrane.

Further simplifications arise from the assumption of neglecting the membrane thickness l_{me}, i.e. the membrane is a two-dimensional surface. In addition the anchor is a pointlike segment of the polymer which enters the membrane in the anchor segment without any changes in the conformation of the membrane surface. Furthermore the beads of the polymer are pointlike and the polymer can freely intersect. Mathematically, the polymer is described by a Gaussian chain, in which the weight of each bond is distributed Gaussian around an average bond length given by the Kuhn length a.

We do not take into account any interaction between polymer and membrane except the steric repulsion of polymer and membrane surface: Polymer and membrane cannot penetrate each other.

Since we do not fix the geometries of the curved surface, our approach allows us to calculate explicitly the membrane shape which arises from the interactions with the anchored polymer.

In the following section we will introduce the mathematical description of the compound polymer/membrane system.

2.1 Parameterization of the system

2.1.1 Membrane

The membrane is regarded as a two-dimensional surface, which moves freely in the three-dimensional space, i.e. we neglect any effects due to the thickness of the bilayer. In addition, we only take look at equilibrium states, which implies, that we do not describe the membrane by the equations of motion of its lipids in the bilayer.

A simple model for the membrane is given by the curvature Hamiltonian presented in the introduction. In the following we will continue this description. First, we introduce our system of

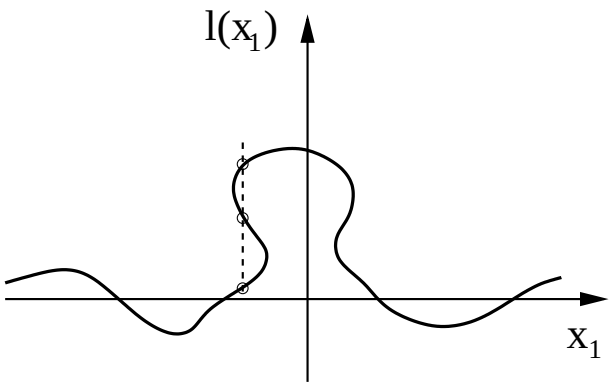

Figure 2.1: Schematic picture of a membrane configuration, which is not represented by the membrane Hamiltonian. The snapshot shows a cut in the $\underline{x}$-plane along the x_1-direction for fixed x_2. Here, l is not a unique function of x_1.

reference (x_1, x_2, z). Each membrane segment will be described by its height l above the (x_1, x_2)-plane. This so-called Monge parameterization implies that the topology of the membrane does not change. Consequently, the integrated Gaussian curvature stays constant. Since each reference point x_1, x_2 is attributed to one unique membrane height $l(x_1, x_2)$ we also neglect configurations, in which the membrane forms overhangs as shown in the schematic figure 2.1. This is true as long as the lateral size L of the membrane is small compared to the membrane persistence length [47]. If L is increased towards the latter length scale, the bending rigidity is reduced by the shape fluctuations, which become larger [48, 49]. In case of most lipid bilayers, the bending rigidity typically is found in a range of $\kappa \approx 10 - 20\ k_BT$ and the persistence length, which is $\sim \exp(4\pi\kappa/3k_BT)$ is large. This justifies the above introduced parametrization.

The Hamiltonian, which describes the membrane, arises from a gradient expansion in the membrane height l. Since the free membrane is symmetric with respect to its upper and lower half space, each term in this expansion is quadratic. We find

$$\mathcal{H}_{me} = \int \mathrm{d}^2x \left[\frac{\kappa}{2}\left(\nabla^2 l(\underline{x})\right)^2 + \frac{\Sigma}{2}\left(\nabla l(\underline{x})\right)^2 + \frac{v_2}{2} l(\underline{x})^2\right] \tag{2.1}$$

with bending rigidity κ, surface tension Σ and additional harmonic potential v_2 which confines the membrane around the plane of reference. The potential takes into account the effect of neighboring membranes or external potentials. In addition, it turns out to be useful to introduce v_2 in order to avoid, if necessary, divergences in our calculations. The limit of vanishing v_2 is obtained by adequate subtraction of these divergences.

A lateral tension Σ introduces the additional crossover length scale $\xi_* = (\kappa/\Sigma)^{1/2}$. The membrane can be regarded as tensionless on length scales $x \ll \xi_*$. However, for fluid membranes the surface tension Σ is a small quantity and hence ξ_* very large. It is therefore reasonable to neglect the surface tension Σ and only take into account the bending rigidity κ.

The Hamiltonian which we use for the following calculation is consequently given by

$$\mathcal{H}_{me} = \int_{-\infty}^{\infty} \mathrm{d}x_1 \int_{-\infty}^{\infty} \mathrm{d}x_2 \left(\frac{\kappa}{2}\left[\nabla^2 l(x_1, x_2)\right]^2 + \frac{v_2}{2}[l(x_1, x_2)]^2\right) . \tag{2.2}$$

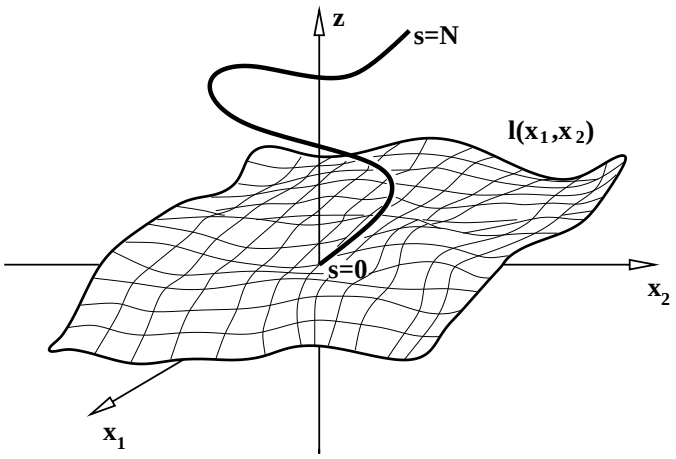

Figure 2.2: Schematic picture for the system parameterization

2.1.2 Polymer

The polymer which is anchored on the membrane is Gaussian. The spatial positions of the polymer beads are given by $\mathbf{r} = (r_1(s), r_2(s), r_3(s))$ where s denotes the internal length of the polymer, starting from the internal coordinate of the anchor bead $s = 0$, and ending at $s = N$, which corresponds to the position of the free polymer end. The simplest equivalent picture to describe the Gaussian polymer is a chain composed of pointlike beads which are connected by harmonic springs. Due to the equipartition theorem each spring constant is proportional to temperature. The mean distance of the beads, i.e. the average length of a bond, is denoted by the Kuhn length a_p.

The corresponding Hamiltonian reads

$$\mathcal{H}_p \;=\; \frac{3T}{2a_p^2}\int_0^N \mathrm{d}s' \,\left(\frac{\mathrm{d}\mathbf{r}(s')}{\mathrm{d}s'}\right)^2 \;=\; \frac{3T}{2R_p^2}\int_0^1 \mathrm{d}s \,\left(\frac{\mathrm{d}\mathbf{r}(s)}{\mathrm{d}s}\right)^2 . \tag{2.3}$$

Here and in the following we measure the temperature T in energy units. In case of an ideal chain, the average end-to-end-distance R_p of the polymer, which serves as a measure for the polymer size, is proportional to $\sqrt{N}$ as expected for a random walk of a particle, whose time coordinate corresponds to the internal length N:

$$R_p = a_p\sqrt{N} \,. \tag{2.4}$$

The Gaussian Hamiltonian describes an ideal chain. In the ideal chain model one neglects excluded volume effects between the monomer beads. Thus, the bonds can intersect each other without steric repulsion. This is only possible, if the solvent is close to the θ-temperature, where the excluded volume effect is balanced by the van der Waals attraction of the polymer beads [37]. The partition function of a polymer starting at position $\mathbf{r}_a$ and ending at position $\mathbf{r}_e$ is given by

$$\begin{aligned}\mathcal{Z}_p \;&=\; \int_{-\infty}^{\infty}\mathcal{D}\{\mathbf{r}\}\;\delta[\mathbf{r}(0)-\mathbf{r}_a]\delta[\mathbf{r}(1)-\mathbf{r}_e]\;\exp\left(-\frac{3}{2R_p^2}\int_0^1 \mathrm{d}s\;[\mathrm{d}\mathbf{r}(s)/\mathrm{d}s]^2\right)\\ &=:\; \mathcal{Z}(\mathbf{r}_a,\mathbf{r}_e|1)\end{aligned} \tag{2.5}$$

representing the statistical weight of all possible configurations with fixed end points. As shown in Appendix A, partition functions of Gaussian type are solutions of a Schrödinger-type equation. $\mathcal{Z}$ is a function of the starting point, the end point and the internal length of the polymer or the polymer piece, respectively. The path integral which is introduced in the partition function is defined as the continuous limit of the discretized integration

$$\prod_i \int_{-\infty}^{\infty} \mathrm{d}r_i \to \int_{-\infty}^{\infty} \mathcal{D}\{r\} \; . \tag{2.6}$$

It is a crucial property of the Gaussian weights, i.e. the solutions of the corresponding Schrödinger-type equation, that they fulfill the equation

$$\mathcal{Z}(\mathbf{r}_a, \mathbf{r}_e|1) \;\; = \;\; \int_{-\infty}^{\infty} \mathrm{d}^3 r \; \mathcal{Z}(\mathbf{r}_a, \mathbf{r}|s)\mathcal{Z}(\mathbf{r}, \mathbf{r}_e|1-s) \; . \tag{2.7}$$

2.1.3 Compound system

Since we already introduced both the Hamiltonian for a membrane and for a polymer, we now have to write down the partition functions for each of them and the compound partition function. For simplicity, the anchor of the polymer is put on the membrane at location $(x_{a,1}, x_{a,2}) = \underline{0}$.

The partition function of the membrane is given by

$$\mathcal{Z}_{me} \;\; = \;\; \int \mathcal{D}\{l\} \exp\left(-\frac{1}{T}\mathcal{H}_{me}\{l\}\right) \; . \tag{2.8}$$

The partition function of the polymer on top of the membrane is given by

$$\mathcal{Z}_p\{l\} \;\; = \;\; \int_{-\infty}^{\infty} \mathcal{D}\{\underline{r}\} \int_{l(\underline{r})}^{\infty} \mathcal{D}\{r_3\} \; \delta[\underline{r}(0)] \, \delta[r_3(0) - l(\underline{0})] \exp\left(-\frac{3}{2R_p^2}\int_0^1 \mathrm{d}s \; \left[\frac{\mathrm{d}}{\mathrm{d}s}\mathbf{r}(s)\right]^2\right) \; . \tag{2.9}$$

In order to simplify the notation the lateral positions are denoted by $\underline{r} = (r_1, r_2)$. The δ-functions ensure that the polymer stays anchored on the membrane. The structure of 2.9 allows us to separate the partition function into a lateral and a perpendicular part $\mathcal{Z}_p\{l\} = Z_{\parallel} \cdot Z_{\perp}\{l\}$ with

$$Z_{\parallel} \;\; = \;\; \int_{-\infty}^{\infty} \mathcal{D}\{\underline{r}\} \; \delta[\underline{r}(0)] \exp\left(-\frac{3}{2R_p^2}\int_0^1 \mathrm{d}s \; \left[\frac{\mathrm{d}}{\mathrm{d}s}\underline{r}(s)\right]^2\right) \tag{2.10}$$

and

$$Z_{\perp}\{l\} \;\; = \;\; \int_{l(\underline{r})}^{\infty} \mathcal{D}\{r_3\} \; \delta[r_3(0) - l(\underline{0})] \exp\left(-\frac{3}{2R_p^2}\int_0^1 \mathrm{d}s \; \left[\frac{\mathrm{d}}{\mathrm{d}s}r_3(s)\right]^2\right) \; . \tag{2.11}$$

The partition function of the compound system is given by

$$\mathcal{Z}_{\mathrm{c}} \;\; = \;\; \int \mathcal{D}\{l\} \; \exp(-\frac{\mathcal{H}_{me}\{l\}}{T})\mathcal{Z}_p\{l\} \; . \tag{2.12}$$

The problem, which is immediately striking, is due to the integration boundary in the z-path-integration of eq. (2.11) for the polymer bead position in z-direction. This restriction arises from the fact that

the polymer bead can not penetrate the membrane, i.e. the membrane position beneath the bead at $(r_1(s), r_2(s))$ indicates the lower integration boundary. It is clear that the corresponding Schrödinger equation to this path integral problem can not be solved because of this complicated boundary condition. To reduce the problem we start to expand the polymer partition function in functional powers of l. We will later show that this expansion only depends on gradients of l such that it is not restricted to small values of l. However, it is assumed that the effect, which the polymer induces on the membrane, is small in comparison to the average flat geometry of an unperturbed membrane.

2.2 Perturbative calculation

The task of the following calculation is to integrate out the polymer part in the compound partition function (2.12). We start with a formal expansion of the partition function $\mathcal{Z}_p$ given in eq. (2.9). Expanding around the flat membrane configuration, we find

$$\frac{\mathcal{Z}_p\{l\}}{\mathcal{Z}_p\{0\}} = 1 \; + \; \int_{-\infty}^{\infty} \mathrm{d}^2x \;\; \frac{1}{\mathcal{Z}_p\{0\}} \frac{\delta \mathcal{Z}_p\{l\}}{\delta l(\underline{x})}\bigg|_{l=0} \cdot l(\underline{x}) \; + \; \mathcal{O}(l^2) \; . \tag{2.13}$$

The functional expansion only acts on $Z_\perp\{l\}$. We will therefore and for reasons of notation in the following restrict on the perpendicular part.

To start the expansion we first shift the integration in the r_3-direction by substituting $r_3(s) \to r_3(s) + l(\underline{r}(s))$, which yields

$$\mathcal{Z}_\perp\{l\} \;\; = \;\; \int_0^\infty \mathcal{D}\{r_3\} \; \delta[r_3(0)] \exp\left(-\frac{3}{2R_p^2} \int_0^1 \mathrm{d}s \left([\dot{r}_3(s)]^2 + 2\dot{r}_3(s)\dot{l}(s) + [\dot{l}(s)]^2 \right) \right) \tag{2.14}$$

with $\dot{r} = \mathrm{d}r/\mathrm{d}s$ and the short notation $l(s) := l(\underline{r}(s))$.

The functional derivative $\delta \mathcal{Z}_\perp\{l\}/\delta l(\underline{x})$ can only be evaluated correctly, if one discretizes the polymer partition function.

$$\begin{aligned} \mathcal{Z}_\perp^{(D)}\{l\} = \int_0^\infty \mathcal{D}\{r_3\} \delta[r_3(0)] \;\; \exp\Bigg(-\frac{3}{2R_p^2} \sum_i \Delta s \Bigg[\left(\frac{r_3(s_i + \Delta s) - r_3(s_i)}{\Delta s} \right)^2 + \\ + 2 \frac{r_3(s_i + \Delta s) - r_3(s_i)}{\Delta s} \cdot \frac{l(s_i + \Delta s) - l(s_i)}{\Delta s} + \left(\frac{l(s_i + \Delta s) - l(s_i)}{\Delta s} \right)^2 \Bigg] \Bigg) \; . \end{aligned} \tag{2.15}$$

The reason why only gradient terms in l appear is due to the identity $\mathrm{d}l/\mathrm{d}s = \mathrm{d}l/\mathrm{d}r \cdot \mathrm{d}r/\mathrm{d}s$.

We now use the relation

$$\frac{\delta l(\underline{r}(s))}{\delta l(\underline{x})} = \frac{\delta l(s)}{\delta l(\underline{x})} \;\; = \;\; \delta[\underline{r}(s) - \underline{x}] \tag{2.16}$$

in order to expand the perpendicular part

$$\begin{aligned} \frac{\delta \mathcal{Z}_\perp^{(D)}\{l\}}{\delta l(\underline{x})}\bigg|_{l=0} = & - \frac{3}{R_p^2} \sum_i \Delta s \int_0^\infty \mathcal{D}\{r_3\} \; \delta[r_3(0)] \frac{r_3(s_i + \Delta s) - r_3(s_i)}{\Delta s} \cdot \\ & \cdot \frac{1}{\Delta s} \Big(\delta[\underline{r}(s_i + \Delta s] - \underline{x}) - \delta[\underline{r}(s_i) - \underline{x}] \Big) \exp\left(-\frac{3}{2R_p^2} \int_0^1 \mathrm{d}s \, [\dot{r}_3(s)]^2 \right) \; . \end{aligned} \tag{2.17}$$

So far we have calculated the functional derivative of the perpendicular part with respect to l. Since we initially separated the polymer partition function into the l-independent lateral part $Z_{\parallel}$ and the l-dependent $Z_{\perp}$ it is now easy to put both parts together in the derivative,

$$\left.\frac{\delta \mathcal{Z}_p^{(D)}\{l\}}{\delta l(\underline{x})}\right|_{l=0} = Z_{\parallel} \cdot \left.\frac{\delta Z_{\perp}^{(D)}\{l\}}{\delta l(\underline{x})}\right|_{l=0} . \tag{2.18}$$

For convenience it is reasonable to put (2.18) and (2.17) together in the following way:

$$\left.\frac{\delta \mathcal{Z}_p^{(D)}\{l\}}{\delta l(\underline{x})}\right|_{l=0} = -\frac{3}{R_p^2}\sum_i \Delta s \, \frac{\Delta Z_{\parallel}}{\Delta s}\cdot\frac{\Delta Z_{\perp}}{\Delta s} \tag{2.19}$$

with

$$\frac{\Delta Z_{\parallel}}{\Delta s} := \int_{-\infty}^{\infty} \mathcal{D}\{\underline{r}\}\, \delta[\underline{r}(0)] \frac{1}{\Delta s}\Big(\delta[\underline{r}(s_i+\Delta s)-\underline{x}] - \delta[\underline{r}(s_i)-\underline{x}]\Big) \exp\left(-\frac{3}{2R_p^2}\int_0^1 \mathrm{d}s\, [\dot{\underline{r}}(s)]^2\right)$$

and

$$\frac{\Delta Z_{\perp}}{\Delta s} := \int_0^{\infty} \mathcal{D}\{r_3\}\, \delta[r_3(0)] \frac{r_3(s_i+\Delta s)-r_3(s_i)}{\Delta s} \exp\left(-\frac{3}{2R_p^2}\int_0^1 \mathrm{d}s\, [\dot{r}_3(s)]^2\right) . \tag{2.20}$$

Before we perform the continuum limit with respect to s we will integrate out the spatial path integrals, which are equivalent to the corresponding solution of the Schrödinger-type equation. Starting with the lateral directions the first equation of eq. (2.20) leads to

$$\begin{aligned}\int_{-\infty}^{\infty} \mathcal{D}\{\underline{r}\}\, \delta[\underline{r}(0)]\, \delta[\underline{r}(s)-\underline{x}]\, \exp\left(-\frac{3}{2R_p^2}\int_0^1 \mathrm{d}s\, \left[\frac{\mathrm{d}\underline{r}(s)}{\mathrm{d}s}\right]^2\right) &= \\ = \int_{-\infty}^{\infty} \mathrm{d}\underline{x}_e\, \mathcal{Z}(0,\underline{x}|s)\, \mathcal{Z}(\underline{x},\underline{x}_e|1-s) . &\end{aligned} \tag{2.21}$$

Because the path integrations in the two lateral directions extend from $-\infty$ to $+\infty$ the $\mathcal{Z}$'s are solutions of the Schrödinger-type equation for the free polymer:

$$\mathcal{Z}(\underline{x}_a,\underline{x}_e|s) = \frac{3}{2\pi s}\frac{1}{R_p^2}\exp\left(-\frac{3}{2s}\frac{(x_{1,e}-x_{1,a})^2+(x_{2,e}-x_{2,a})^2}{R_p^2}\right) . \tag{2.22}$$

The integral over the end point of the polymer $(x_{1,e}; x_{2,e})$ can be evaluated and yields 1 due to normalization.

The remaining task is to calculate the r_3-direction. In this direction the polymer is confined to the half space above the surface. The solution of the corresponding Schrödinger-type equation is denoted by the index hs. The second equation of (2.20) yields

$$\begin{aligned}\int \mathcal{D}\{r_3\}\, \delta[r_3(0)]\, r_3(s) \exp\left(-\frac{3}{2R_p^2}\int_0^1 \mathrm{d}s\, \left[\frac{\mathrm{d}r_3(s)}{\mathrm{d}s}\right]^2\right) & \\ = \int_0^{\infty}\mathrm{d}z_e \int_0^{\infty}\mathrm{d}z\; z\; \mathcal{Z}_{hs}(0,z|s)\; \mathcal{Z}_{hs}(z,z_e|1-s) . &\end{aligned} \tag{2.23}$$

Note that for reasons of convention we introduced different notations for the coordinates and the fields in the corresponding direction in order to clearly separate both. The half space solution is [50, 51, 52, 53]

$$\mathcal{Z}_{hs}(z_a, z_e|s) \;=\; \sqrt{\frac{3}{2\pi s}}\frac{1}{R_p}\left[\exp\left(-\frac{3}{2s}\frac{(z_e-z_a)^2}{R_p^2}\right) - \exp\left(-\frac{3}{2s}\frac{(z_e+z_a)^2}{R_p^2}\right)\right] \tag{2.24}$$

where the forbidden path, in which the starting point is on the other side of the surface, is subtracted. Thus, the partition function takes into account the restriction of the configuration space. Mathematically, one can immediately conclude, that the partition function $\mathcal{Z}_{hs}(0, z|s)$ of a polymer which is anchored on the surface at $z = 0$ vanishes. However, we can easily avoid this problem by introducing a cutoff l_{an} which, due to normalization, cancels again if one expands for small l_{an}. We define

$$\tilde{\mathcal{Z}}_{hs}(l_{an}, z|s) \;:=\; \frac{\mathcal{Z}_{hs}(l_{an}, z|s)}{\int_0^\infty \mathrm{d}z\; \mathcal{Z}_{hs}(l_{an}, z|s)}\,. \tag{2.25}$$

In the limit of small l_{an} one obtains

$$\tilde{\mathcal{Z}}_{hs}(0, z|s) \;=\; \frac{3}{s}\frac{1}{R_p}\left(\frac{z}{R_p}\right)\exp\left(-\frac{3}{2s}\frac{z^2}{R_p^2}\right)\,. \tag{2.26}$$

Coming back to the initial expansion eq. (2.13) the normalization with respect to the half-space partition function $\mathcal{Z}_p\{0\}$ leads to the continuum limit

$$\frac{1}{\mathcal{Z}_p\{0\}}\left.\frac{\delta\mathcal{Z}_p\{l\}}{\delta l(\underline{x})}\right|_{l=0} \;=\; -\frac{3}{R_p^2}\int_0^1 \mathrm{d}s\;\left(\frac{\mathrm{d}}{\mathrm{d}s}\langle z(s)\rangle_{hs}\right)\left(\frac{\mathrm{d}}{\mathrm{d}s}\mathcal{Z}(\underline{0}, \underline{x}|s)\right) \;\equiv\; -\int_0^1 \mathrm{d}s\; P(s, \underline{x})\,. \tag{2.27}$$

for the prefactor of the linear term in l.

The function P we defined above contains the polymer part, which is integrate out. The remaining task is to calculate the derivatives of the z-expectation value and of the free polymer partition function in the (x_1, x_2)-directions.

If one inserts eq. (2.27) back into the full expansion of eq. (2.13) one ends up with

$$\frac{\mathcal{Z}_p\{l\}}{\mathcal{Z}_p\{0\}} \;=\; 1 \;-\; \int_0^1 \mathrm{d}s\int_{-\infty}^{\infty}\mathrm{d}^2x\; P(s, \underline{x})\; l(\underline{x}) \;=\; \exp\left(-\int_0^1 \mathrm{d}s\int_{-\infty}^{\infty}\mathrm{d}^2x\; P(s, \underline{x})\; l(\underline{x})\right) \tag{2.28}$$

to first order in l. The last step we wrote down above is correct in linear order of our l-expansion. The remaining term in the exponent of the partition function is nothing but an additional Hamiltonian which adds to the membrane Hamiltonian. If we furthermore define $P(\underline{x}) = \int_0^1 \mathrm{d}s\; P(s, \underline{x})$ this function couples linearly to the membrane height $l(\underline{x})$. Since it contains the polymer part one concludes that $P(\underline{x})$ is the pressure which the polymer exerts on the membrane [54]. The pressure will be calculated explicitly in section 2.4.

2.3 Polymer shape

The expectation value of the polymer in the z-direction, which we have to calculate in eq. (2.27) contains information on the shape structure of the polymer [51]. Let us start with the expectation

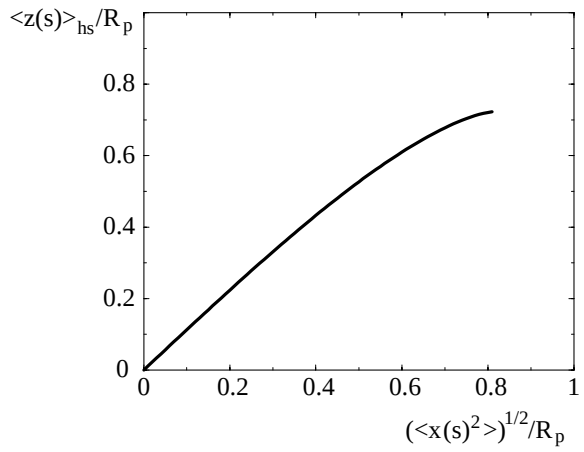

Figure 2.3: The average z-position of the polymer beads plotted versus their corresponding x-position, i.e. their radial distance from the anchor. Note that the polymer is anchored on a flat substrate.

value $\langle z(s)\rangle_{hs}$ which as usual is defined by

$$\langle z(s)\rangle_{hs} = \frac{\int_0^\infty dz_e \int_0^\infty dz\ \tilde{\mathcal{Z}}_{hs}(0,z|s)\ z\ \mathcal{Z}_{hs}(z,z_e|1-s)}{\int_0^\infty dz_e \int_0^\infty dz\ \tilde{\mathcal{Z}}_{hs}(0,z|s)\mathcal{Z}_{hs}(z,z_e|1-s)} \tag{2.29}$$

$$= R_p\sqrt{\frac{2}{3\pi}}\left(\arctan\left(\frac{\sqrt{s}}{\sqrt{1-s}}\right) + \sqrt{s(1-s)}\right) \tag{2.30}$$

where $\mathcal{Z}_{hs}$ and $\tilde{\mathcal{Z}}_{hs}$ are the half-space partition functions of the polymer as given by eq. (2.24) and eq. (2.26). The limiting positions for the first and the last monomer of the chain are $\langle z(0)\rangle_{hs} = 0$ and $\langle z(1)\rangle_{hs} = \sqrt{\pi/6}R_p$, respectively.

Let us investigate the average polymer position in a more detailed way. A brief calculation shows that the average squared distance in the lateral directions leads to

$$\langle x^2\rangle = \langle x_1^2\rangle + \langle x_2^2\rangle = \frac{2}{3}sR_p^2\ . \tag{2.31}$$

By inserting of eq. (2.31) into the average distance $\langle z(s)\rangle_{hs}$ of eq. (2.29) we can express the average z-position as a function of the average radial position $\sqrt{\langle x^2\rangle}$, which is displayed in figure 2.3. The profile grows linearly for small distances from the anchor bead and reaches the maximal average distance, which corresponds to the position of the last chain bead, with zero slope. Another interesting quantity concerning the polymer configuration is the segment density. The segment density measures the probability $\mathrm{w}(x_1,x_2,z)$ of one bead (we do not count which one of the beads) being located at a certain spatial position (x_1,x_2,z). The probability distribution is given by

$$\mathrm{w}(x_1,x_2,z) = \frac{1}{\mathcal{N}}\int_0^1 \mathrm{d}s \int_0^\infty \mathrm{d}z_e\ \mathcal{Z}(0,x_1|s)\mathcal{Z}(0,x_2|s)\tilde{\mathcal{Z}}_{hs}(0,z|s)\mathcal{Z}_{hs}(z,z_e|1-s)\ . \tag{2.32}$$

The normalization constant $\mathcal{N}$ is calculated by evaluation of

$$\mathcal{N} = \int_0^1 \mathrm{d}s \int_{-\infty}^\infty \mathrm{d}x_1 \int_{-\infty}^\infty \mathrm{d}x_2 \int_0^\infty \mathrm{d}z \int_0^\infty \mathrm{d}z_e\ \mathcal{Z}(0,x_1|s)\mathcal{Z}(0,x_2|s) \times$$

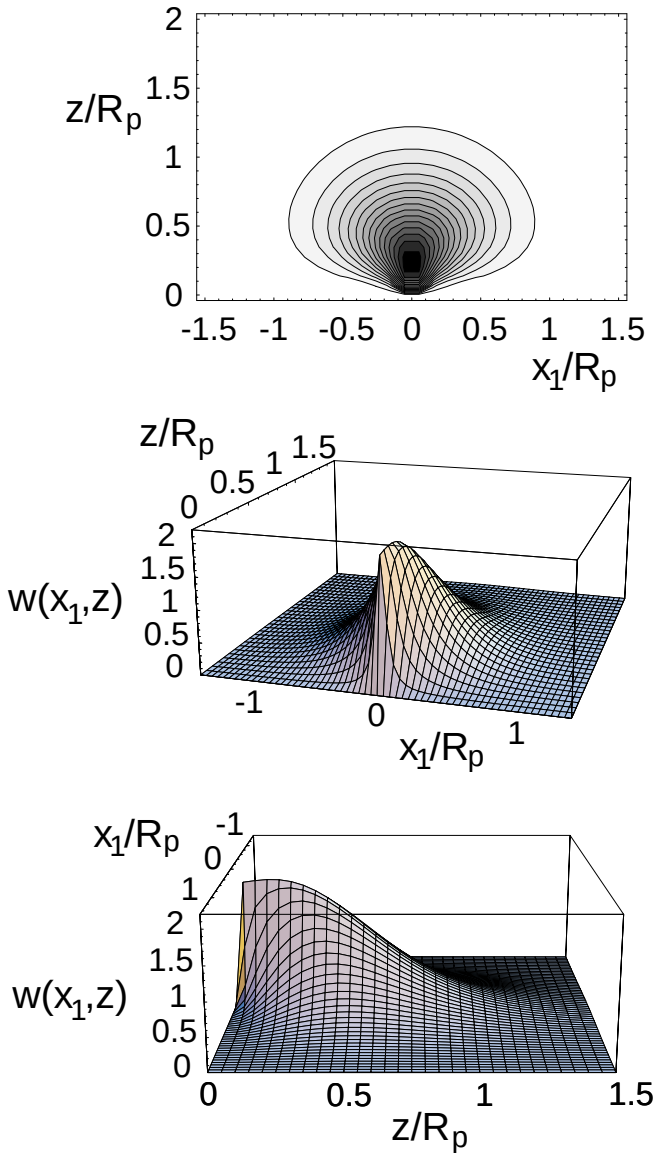

Figure 2.4: The polymer segment density: (a) Contour plot in the (x_1, z)-plane. Due to the presence of the wall the polymer is squeezed in the z-direction and strongly deviates from the spherical shape of the free polymer. The shape profile justifies the term mushroom to characterize the polymer form. (b)+(c) Surface plot in the (x_1, z)-plane from different view angles. The profile in this diagram resembles a shark fin.

$$\times \tilde{\mathcal{Z}}_{hs}(0, z|s)\mathcal{Z}_{hs}(z, z_e|1-s)\,. \tag{2.33}$$

This leads to

$$\mathrm{w}(x_1, x_2, z) \;=\; \frac{27}{4\pi}\frac{1}{R_p^3}\frac{z}{R_p}\int_0^1 \mathrm{d}s\;\frac{1}{s^2}\exp\left(\frac{3}{2s}\frac{x^2+y^2}{R_p^2}\right)\exp\left(-\frac{3}{2s}\frac{z^2}{R_p^2}\right)\mathrm{erf}\left(\sqrt{\frac{3}{2(1-s)}}\frac{z}{R_p}\right)\,. \tag{2.34}$$

In figure 2.4 we display the segment density in the (x_1, z)-plane, which corresponds to $\mathrm{w}(x_1, x_2 = 0, z)$. The segment density gives an estimate of the shape of the polymer anchored on a flat surface. If one compares with the density profile obtained in case of a free polymer, which leads to a circle in the (x_1, z)-plane, one can easily see the deformation in the vicinity of the surface. It is important that the segment density vanishes on the surface. The polymer is never located on the surface, which is a known property of continous polymer models.

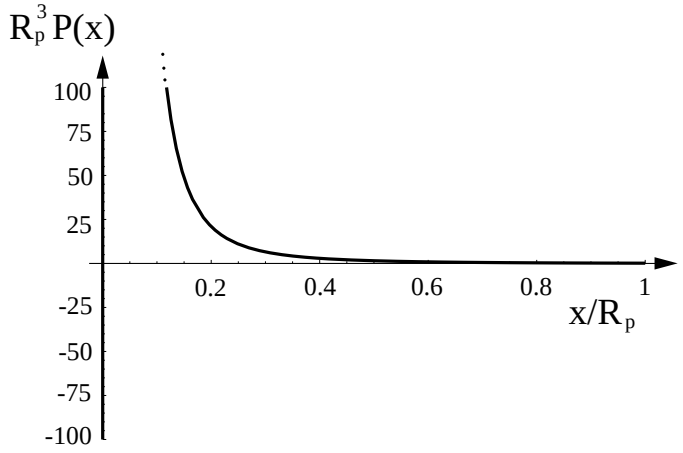

Figure 2.5: The total polymer pressure plotted versus the anchor distance. The pressure is positive for all $x/R_p > 0$. It decays exponentially for large distances x/R_p and diverges for small x/R_p. The pressure is negative infinity in the anchor point at $x/R_p = 0$.

2.4 Polymer pressure

We will now continue with the calculation of the local polymer pressure $P(\underline{x})$ given by (2.27). The derivative of $\langle z(s)\rangle_{hs}$ is given by

$$\frac{\mathrm{d}}{\mathrm{d}s}\langle z(s)\rangle_{hs} \;=\; R_p\sqrt{\frac{2}{3\pi}}\sqrt{\frac{1-s}{s}}\,. \tag{2.35}$$

The derivative of $\mathcal{Z}(\underline{0},\underline{x}|s)$ with respect to s is

$$\frac{\mathrm{d}}{\mathrm{d}s}\mathcal{Z}(\underline{0},\underline{x}|s) \;=\; \frac{3}{2\pi R_p^2}\left(\frac{3}{2}\frac{x^2}{R_p^2}\frac{1}{s^3}-\frac{1}{s^2}\right)\exp\left(-\frac{3}{2s}\frac{x^2}{R_p^2}\right)\,. \tag{2.36}$$

Inserting both derivatives into the expression for the polymer pressure eq. (2.27) leads to

$$P(\underline{x}) \;=\; \int_0^1 \mathrm{d}s\; P(s,\underline{x}) \tag{2.37}$$

with

$$P(s,\underline{x}) \;=\; \frac{2}{{R_p}^3}\left(\frac{3}{2\pi}\right)^{3/2}\left(\frac{1-s}{s}\right)^{1/2}\left(\frac{3}{2}\frac{x^2}{{R_p}^2}\frac{1}{s^3}-\frac{1}{s^2}\right)\exp\left(-\frac{3}{2}\frac{x^2}{{R_p}^2 s}\right)\,. \tag{2.38}$$

Note that the pressure is measured in units of T.

Since we have put the anchor point of the polymer into the origin of the (x_1,x_2)-plane, the pressure is rotationally symmetric and depends only on the distance $x=|\underline{x}|$ to the anchor.

Let us now discuss the result which we obtained. First of all, we can analytically perform the s-integral. However, it is important to note the divergence of the integral at $x=0$.

The total pressure is

$$P(\underline{x}) \;=\; \int_0^1 \mathrm{d}s\; P(s,\underline{x}) \;=\; \begin{cases} \frac{1}{2\pi x^3}\left(1+3\frac{x^2}{R_p^2}\right)\exp\left(-\frac{3}{2}\frac{x^2}{R_p^2}\right) & \text{for } x>0 \\ -\infty & \text{for } x=0 \end{cases}\,. \tag{2.39}$$

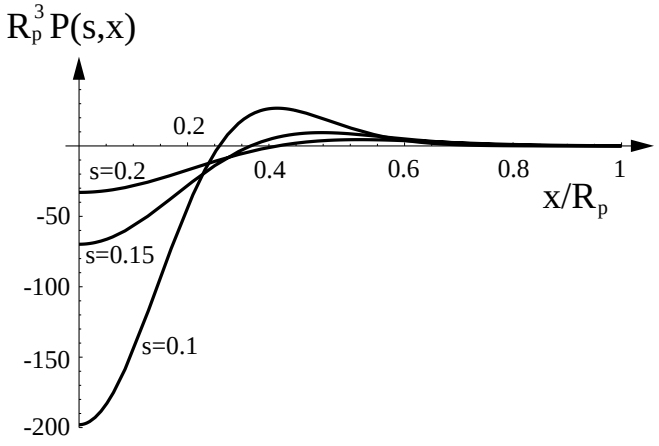

Figure 2.6: The function $P(s,x)$ plotted versus the anchor distance for different internal lengths s. It is negative for small distances x/R_p from the anchor point and positive for large x/R_p. In this limit $P(s,x)$ is exponentially decreasing.

The plot in figure 2.5 shows according to the analytic formula that for $x > 0$ the pressure is positive, indicating that the polymer pushes the membrane away from it. For large distances this pressure decays exponentially (with a prefactor $\sim 1/x$). For small distances the pressure diverges, i.e. the polymer pushes the membrane stronger and stronger. At the origin $x = 0$, the pressure is infinite, but with opposite sign, i.e. in the anchor point the polymer pulls the membrane. Additionally, we plot $P(s,x)$ in figure 2.6, which is negative for small and positive for large distances from the anchor. $P(s,x)$ is a function which one could call an effective monomer pressure, namely the pressure which is exerted by the monomer at internal position s. As one can see in the diagram, the monomer pulling increases, if one goes to smaller internal length s. The smaller s the closer the monomer is neighbored to the anchor bead. According to the intuitive picture, the main pressure contribution is due to the polymer beads in the vicinity of the anchor bead.

However note, that $P(s,x)$ is not a real pressure in the physical sense, since it does not correspond to real forces on the membrane (therefore we call it effective). The only bead, with which the polymer can exert a negative force (pulling the membrane), is the anchor segment at $x = 0$.

The behavior of the total pressure is in agreement with Newton's third law. Each bead of the chain, which exerts a force on the membrane due to collision, leads due to the connectivity of the chain to an equally sized force of opposite direction on the membrane. The only bead which is connected to the membrane is the anchor point. Since the area there, on which the force is acting, is zero, the pressure is infinite.

We additionally have to check, if the integrated pressure is zero, since in total, the polymer cannot exert a net-force on the membrane, which would lead to a center-of-mass motion of the whole polymer-membrane system. In fact, a brief calculation shows that

$$\int_0^1 \mathrm{d}s \int \mathrm{d}^2x \; P(s,\underline{x}) = 0 \; . \tag{2.40}$$

The vanishing of the integrated pressure is also a consequence of the fact, that in the expansion we used here only gradients of l, namely $\partial l/\partial x_1$ and $\partial l/\partial x_2$ occur, which implies that the pressure term

is invariant under the transformation $l(\underline{x}) \to l(\underline{x}) + \Delta l$ of the shape profile.

2.5 Membrane shape profile

In this section we derive the shape profile. The corresponding calculation is divided into numerous parts. First, we start with the general case of a membrane with bending rigidity κ, confined in a harmonic potential with corresponding parameter v_2. The potential might arise from van der Waals interaction of the membrane with a substrate or with neighboring membranes. As we already pointed out, the potential will regularize our calculation, enforcing the membrane to be located on average at zero height for large distances from the polymer anchoring point. In this first part we derive the general solution for the shape profile.

In the following part we consider the limiting case of the free membrane. We first calculate a general expression for the membrane curvature. Using the curvature we afterwards derive the free shape profile.

2.5.1 Membrane in a confining potential

In order to perform the calculation we will formally rewrite the partition function of the compound system. So far we have calculated the pressure. For the partition function of the polymer on the membrane related to the flat substrate we found via eq. (2.13) that

$$\frac{\mathcal{Z}_p\{l\}}{\mathcal{Z}_p\{0\}} = 1 \; - \; \int_0^1 \mathrm{d}s \int_{-\infty}^{\infty} \mathrm{d}^2x \; P(s,\underline{x}) \; l(\underline{x}) \; + \; \mathcal{O}(l^2) \; . \tag{2.41}$$

In linear order it is therefore correct to put the pressure term back into the exponential

$$\frac{\mathcal{Z}_p\{l\}}{\mathcal{Z}_p\{0\}} \quad = \quad \exp\left(- \int_0^1 \mathrm{d}s \int_{-\infty}^{\infty} \mathrm{d}^2x \; P(s,\underline{x}) \; l(\underline{x}) \right) \; . \tag{2.42}$$

Since we are dealing with Gaussian membranes it is possible to rewrite the Hamiltonian in terms of the Gaussian bilinear kernel K^{-1} which we introduce here. One finds

$$\frac{\mathcal{H}_{me}}{T} = \frac{1}{2} \int \mathrm{d}^2x' \left[\frac{\kappa}{T} \left(\nabla^2 l \right)^2 + \frac{v_2}{T} l^2 \right] = \frac{1}{2} \int \mathrm{d}^2x' \int \mathrm{d}^2x'' \; l(\underline{x}') K^{-1}(\underline{x}' - \underline{x}'') l(\underline{x}'') \; . \tag{2.43}$$

Integrating by parts yields the form of the Gaussian bilinear kernel

$$K^{-1} \quad = \quad \frac{\kappa}{T} \, \delta(\underline{x}' - \underline{x}'') \left[\frac{\mathrm{d}^4}{\mathrm{d}\underline{x}''^4} + \frac{v_2}{\kappa} \right] \; . \tag{2.44}$$

In order to calculate the average profile $\langle l(\underline{x}) \rangle$ we introduce a generating field $\gamma(\underline{x})$, which couples linearly to the membrane height $l(\underline{x})$ and leads to the partition function

$$\begin{aligned} \mathcal{Z}\{\gamma\} \quad &= \quad \int \mathcal{D}\{l\} \; \exp\left(-\frac{\mathcal{H}_{me}}{T} \right) \; \left[\frac{\mathcal{Z}_p\{l\}}{\mathcal{Z}_p\{0\}} \right] \; \exp\left(\int \mathrm{d}^2x' \; \gamma(\underline{x}') l(\underline{x}') \right) \\ &= \quad \int \mathcal{D}\{l\} \; \exp\left(-\frac{1}{2} \int \mathrm{d}^2x' \int \mathrm{d}^2x'' \; l(\underline{x}') K^{-1}(\underline{x}' - \underline{x}'') l(\underline{x}'') \right. \\ &\qquad \left. - \int_0^1 \mathrm{d}s \int \mathrm{d}^2x' \; P(s,\underline{x}') l(\underline{x}') + \int \mathrm{d}^2x' \; \gamma(\underline{x}') l(\underline{x}') \right) \; . \end{aligned} \tag{2.45}$$

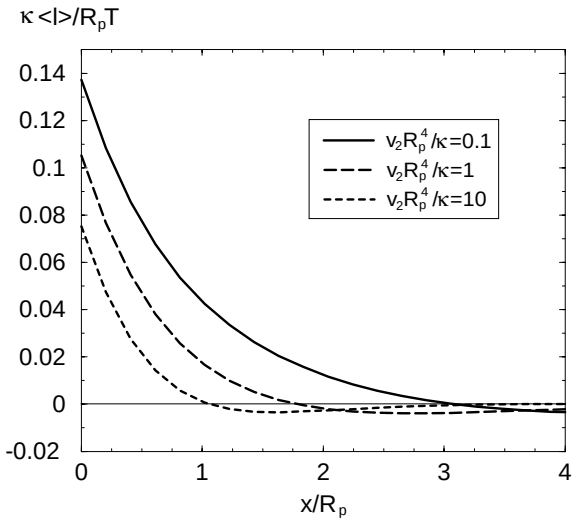

Figure 2.7: The profile of the membrane as obtained by the perturbative calculation for different non-vanishing values of $v_2 {R_p}^4/\kappa$.

The average shape profile is now given by

$$\langle l(\underline{x})\rangle \;=\; \left.\frac{\delta\ \ln \mathcal{Z}\{\gamma\}}{\delta\gamma(\underline{x})}\right|_{\gamma=0} . \tag{2.46}$$

Using the properties of Gaussian integrals one finds

$$\langle l(\underline{x})\rangle \;=\; -\int_0^1 \mathrm{d}s \int \mathrm{d}^2x' K(\underline{x}-\underline{x}')P(s,\underline{x}') \; . \tag{2.47}$$

The equation can be solved by Fourier transformation which leads to

$$\begin{aligned}
\langle l(\underline{x})\rangle \;&=\; -\int \mathrm{d}\underline{x}' \left\{\int \frac{\mathrm{d}\underline{q}}{(2\pi)^2}\ \tilde{K}(\underline{q})\exp(-i\underline{q}(\underline{x}-\underline{x}'))\right\}\ \left\{\int \frac{\mathrm{d}\underline{q}'}{(2\pi)^2}\ \tilde{P}(\underline{q}')\exp(-i\underline{q}'\underline{x}')\right\} \\
&=\; -\int \frac{\mathrm{d}\underline{q}}{(2\pi)^2}\int \mathrm{d}\underline{q}'\ \tilde{K}(\underline{q})\tilde{P}(\underline{q}')\delta(\underline{q}-\underline{q}')\exp(-i\underline{q}\underline{x}) \\
&=\; -\int \frac{\mathrm{d}\underline{q}}{(2\pi)^2}\ \tilde{K}(\underline{q})\tilde{P}(\underline{q})\exp(-i\underline{q}\underline{x}) \;=\; -\int_0^\infty \frac{\mathrm{d}q}{2\pi} q\ \tilde{K}(q)\tilde{P}(q)\ J_0(qx) \; ,
\end{aligned} \tag{2.48}$$

where J_0 is a Bessel function of integer order [55].

Consequently we have to calculate the Fourier transforms of the membrane propagator and the polymer pressure. The Fourier transformed membrane propagator is given by

$$\tilde{K}(\underline{q}) \;=\; \frac{T}{\kappa\left(\underline{q}^4 + v_2/\kappa\right)} \; . \tag{2.49}$$

The Fourier transform of the pressure yields

$$\begin{aligned}\tilde{P}(\underline{q}) &= \frac{3}{R_p^2}\int_0^1 \mathrm{d}s\,\left(\frac{\mathrm{d}}{\mathrm{d}s}\langle z(s)\rangle_{hs}\right)\int_{-\infty}^{\infty}\mathrm{d}^2x\left(\frac{\mathrm{d}}{\mathrm{d}s}\mathcal{Z}(\underline{0},\underline{x}|s)\right)\exp(i\underline{q}\underline{x}) \\ &= -\sqrt{\frac{\pi}{6}}R_p\frac{q^2}{2}\exp\left(-\frac{R_p^2}{12}q^2\right)\left(I_0\left(\frac{R_p^2}{12}q^2\right)+I_1\left(\frac{R_p^2}{12}q^2\right)\right) \qquad (2.50)\end{aligned}$$

where I_0 and I_1 are Bessel functions of integer order [55].

The average membrane profile is now given by

$$\langle l(x)\rangle = \frac{R_pT}{4\sqrt{6\pi}\kappa}\int_0^\infty \mathrm{d}q\,\frac{q^3}{q^4+v_2/\kappa}\exp\left(-\frac{R_p^2}{12}q^2\right)\left(I_0\left(\frac{R_p^2}{12}q^2\right)+I_1\left(\frac{R_p^2}{12}q^2\right)\right)J_0(qx)\ . \qquad (2.51)$$

If we consider non-vanishing v_2 the final integration is performed numerically using Mathematica [56]. The convergence behavior is studied in the subsequent section.

The resulting shape profile is displayed in figure 2.7. As we will show in the following the profile is a cone in the vicinity of the anchor. In case of non-vanishing potential strength v_2 the membrane approaches a flat configuration far away from the anchor. The approach is given by exponentially damped oscillations with a wavelength proportional to R_p, which depends on v_2 and κ.

2.5.2 Free membrane

An important case is the limit of vanishing harmonic potential, i.e. $v_2 = 0$. As we already pointed out, the integral of eq. (2.51) is divergent in this case. The physical origin of this divergence arises from the translational invariance of the membrane in the z-direction, since it is not confined around zero by the harmonic potential anymore.

To study the convergence behavior of the integral we have to concentrate on the asymptotic properties of the Bessel functions (see Appendix B).

The difference in the integration for non-vanishing and vanishing v_2 arises from the behavior for small q, i. e. at the lower bound of the integral.

For non-vanishing potential v_2 we find that

$$\langle l(x)\rangle \sim \frac{R_pT}{4\sqrt{6\pi}\kappa}\int_0^\varepsilon \mathrm{d}q\,q^3 \qquad (2.52)$$

with small $\varepsilon > 0$. The integral is finite for small q.

In case of vanishing v_2 the limiting behavior is changed into

$$\langle l(x)\rangle \sim \frac{R_pT}{4\sqrt{6\pi}\kappa}\int_0^\varepsilon \mathrm{d}q\,\frac{1}{q}\ , \qquad (2.53)$$

i.e. the integral is logarithmically divergent for small q. This infrared divergence corresponds to the center-of-mass motion of the membrane due to free diffusion. The divergence can be subtracted by the following integration:

$$\langle l(x)\rangle - \langle l(\underline{0})\rangle = \frac{R_pT}{4\sqrt{6\pi}\kappa}\int_0^\infty \mathrm{d}q\,\frac{1}{q}\exp\left(-\frac{R_p^2}{12}q^2\right)\left(I_0\left(\frac{R_p^2}{12}q^2\right)+I_1\left(\frac{R_p^2}{12}q^2\right)\right)\left[J_0(qx)-1\right]\ , \qquad (2.54)$$

which subtracts the position of the anchor segment. Now, this segment is located in the origin of our system of reference.

For large q the asymptotic behavior in both cases is given by

$$\langle l(x)\rangle \quad = \quad \frac{R_p T}{4\sqrt{6\pi}\kappa}\int_{1/\varepsilon}^{\infty} \mathrm{d}q\, \frac{1}{q}\frac{2}{\sqrt{2\pi}}\sqrt{\frac{12}{R_p^2 q^2}}\sqrt{\frac{2}{\pi}}\frac{1}{\sqrt{qx}}\cos\left(qx-\frac{\pi}{4}\right)\ . \tag{2.55}$$

It is easy to verify that this integral is finite. Thus, we have shown, that our Fourier transformed shape profile is integrable.

Let us briefly derive an equivalent integral to eq. (2.55) using (2.50) and eq. (2.48). Both lead to the expression

$$\langle l(x)\rangle - \langle l(\underline{0})\rangle = -\frac{1}{8\pi}\frac{T}{\kappa}\int_0^1 \mathrm{d}s\ \left(\frac{\mathrm{d}}{\mathrm{d}s}\langle z(s)\rangle_{hs}\right)\left[\gamma+\Gamma\left(0,\frac{3}{2s}\frac{x^2}{R_p^2}\right)+\ln\left(\frac{3}{2s}\frac{x^2}{R_p^2}\right)\right] \tag{2.56}$$

where γ is the Euler constant and Γ is an incomplete Gamma-function [57]. This formula is very helpful since it allows us to calculate easily an equation for the membrane curvature. The curvature is given by

$$M(\underline{x}) \quad = \quad -\frac{1}{2}\nabla^2_{\underline{x}}\langle l(\underline{x})\rangle = -\frac{1}{2}\frac{1}{x}\frac{\partial}{\partial x}\left(x\frac{\partial}{\partial x}\langle l(x)\rangle\right)\ . \tag{2.57}$$

Here we use the negative sign convention, which leads to a positive curvature if the membrane bends away from the polymer and a negative curvature if the membrane bends towards it.

Applying the spatial derivatives to the shape profile of the free membrane one immediately finds

$$M(x) = \frac{T}{4\pi\kappa}\frac{1}{x}\left[\exp\left(-\frac{3}{2}\frac{x^2}{R_p^2}\right)-\sqrt{\frac{3\pi}{2}}\frac{x}{R_p}\left(1-\mathrm{erf}\left(\sqrt{\frac{3}{2}}\frac{x}{R_p}\right)\right)\right]\ . \tag{2.58}$$

The profile of the curvature is displayed in the inset of figure 2.10.

The limiting behavior of the curvature attains for small distances x from the anchor point

$$M(x) \quad \sim \quad \frac{T}{4\pi\kappa}\frac{1}{x} \tag{2.59}$$

and for large distances from the anchor

$$M(x) \quad \sim \quad \frac{T}{12\pi\kappa}\frac{1}{x}\left(\frac{R_p}{x}\right)^2\exp\left(-\frac{3}{2}\frac{x^2}{R_p^2}\right)\ . \tag{2.60}$$

We have shown, that the curvature for small distances is logarithmically divergent. However, this divergence is cured, if we integrate over the plane of reference.

It is of general importance, that the curvature for large distances vanishes exponentially. Therefore, if we study the situation of several anchored polymers on a membrane, we expect, that the total curvature stays finite. In fact, it is easy to realize that the total curvature of N_p polymers is just the sum of all N_p single curvature contributions. This is due to the linearity of our calculation.

In order to calculate the spontaneous curvature of the whole membrane induced by an anchored polymer one has to integrate over the lateral plane. Using eq. (2.56) one ends up with a simple

equation for the integrated curvature, which relates it to the average z-distance of the polymer end in the half-space. One finds $\mathcal{A}\overline{M} = \int \mathrm{d}^2x\ M(\underline{x})$

$$\mathcal{A}\overline{M} \quad = \quad \frac{T}{4\kappa}\langle z(1)\rangle_{hs}\ . \tag{2.61}$$

We introduced the lateral area $\mathcal{A}$ in order to garantee the correct units of the mean (spontaneous) curvature $\overline{M}$. It is not necessary for the integration to introduce this area, since the integral over $M(\underline{x})$ is finite. The mean curvature we obtained is the integrated curvature of the infinite membrane.

Since $\langle z(1)\rangle_{hs} = \sqrt{\pi/6}R_p$ the integrated spontaneous curvature of the free membrane is given by

$$\mathcal{A}\overline{M} \quad = \quad \frac{T}{4\kappa}\sqrt{\frac{\pi}{6}}R_p\ . \tag{2.62}$$

We can compare our results on the membrane curvature with results obtained for the spontaneous curvature where one does not explicitly know the exact membrane shape, but compares the free energies of the polymer which is anchored on fixed geometries with the situation of the flat substrate. The basic idea is to expand the entropy gain of the polymer and its free energy loss respectively for small curvatures, assuming that the bending in the anchor point is smooth and sufficiently small.

For practical reasons it is sufficient to put the polymer on a cylinder and a sphere [46]. The corresponding partition sum for these geometries is derived and expanded in powers of the curvature.

This approach is different from our perturbative approach, since it initially fixes the geometries of the membrane. Therefore, it is not necessarily obvious from the beginning that both calculations end up in the same result for the membrane curvature. However, we can insert the fixed geometries into the original partition function (2.9). The integration boundary in the perpendicular direction leads to

$$l_{sp}[\underline{r}(s)] \quad = \quad \begin{cases} R\sqrt{1-\frac{r^2}{R^2}} & , r \leq R \\ 0 & , r > R \end{cases} \tag{2.63}$$

where r is the lateral distance from the origin. Shifting the origin of the system of reference by $r_3(s) \mapsto r_3(s) + R$ (see figure 2.8) and expanding for large radii R leads to

$$l_{sp}[\underline{r}(s)] \quad = \quad -\frac{r(s)^2}{2R} \tag{2.64}$$

Insertion into the integration boundary of (2.9) and expanding the integral yields the limiting partition function

$$\frac{\mathcal{Z}_p\{l\}}{\mathcal{Z}_p\{0\}} = 1\ +\ \sqrt{\frac{\pi}{6}}\frac{R_p}{R} + \mathcal{O}\left(\frac{R_p^2}{R^2}\right)\ . \tag{2.65}$$

Since the curvature of the sphere is $M = 1/R$ one finds

$$\frac{\mathcal{Z}_p\{l\}}{\mathcal{Z}_p\{0\}} = 1\ +\ \sqrt{\frac{\pi}{6}}R_pM + \mathcal{O}((R_pM)^2)\ . \tag{2.66}$$

The same holds for the cylinder with curvature $M = 1/2R$. The free energy difference $\Delta\mathcal{F}_p =$

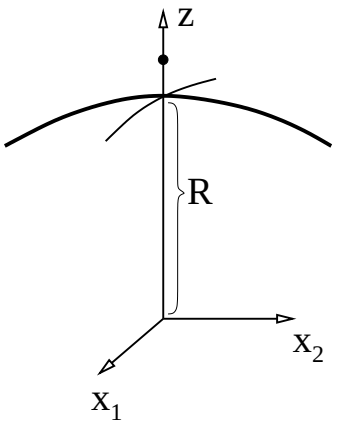

Figure 2.8: The system of reference used to derive $l(\underline{x})$. The polymer bead (η_1, r_2, r_3) which is located outside the sphere, must fulfill the equation ${\eta_1}^2 + {r_2}^2 + (R+r_3)^2 \geq R^2$. Solving the equation in linear order in $1/R$ yields the equation (2.64).

$-T\ln(\mathcal{Z}_p\{l\}/\mathcal{Z}_p\{0\})$ is now given by

$$\Delta\mathcal{F}_p = -\sqrt{\frac{\pi}{6}}TR_pM + \mathcal{O}((R_pM)^2)\ . \tag{2.67}$$

Considering the curvature energy of the membrane

$$\Delta E_{me} \;=\; 2\kappa\int \mathrm{d}^2x\ M^2 = 2\kappa\mathcal{A}M^2 \tag{2.68}$$

we add both contributions (neglecting the M^2 term of the polymer free energy) to obtain the free energy of the compound polymer/membrane system

$$\Delta\mathcal{F}(M) \;=\; \Delta\mathcal{F}_p(M) + \Delta E_{me}(M) \;=\; -\sqrt{\frac{\pi}{6}}TR_pM + 2\kappa\mathcal{A}M^2\ . \tag{2.69}$$

Minimizing the total free energy with respect to the curvature leads to

$$\mathcal{A}\overline{M} = \frac{T}{4\kappa}\sqrt{\frac{\pi}{6}}R_p\ . \tag{2.70}$$

If one compares this result for the integrated curvature $\mathcal{A}\overline{M}$ with our result in equation (2.62) obtained by the perturbative calculation, both are identical.

An expression for $\overline{M}$ can only be obtained if one inserts an effective area, in which the polymer interacts with the membrane and induces a spontanous curvature. This area will be determined by the polymer end-to-end distance: $\mathcal{A} = c_A R_p^2$, where c_A is a parameter of order 1, see fig. 2.9.

However, it is not necessary to introduce this parameter in the perturbative approach, since the latter calculation leads us to the exact $\underline{x}$-dependent expression for the membrane curvature $M(\underline{x})$ as given by eq. (2.58).

This explicit expression allows us to derive a closed expression for the shape profile by integration. Since our problem is circular symmetric the Laplace operator in polar coordinates is given by

$$\Delta \;=\; \frac{1}{x}\frac{\partial}{\partial x}\left(x\frac{\partial}{\partial x}\right)\ . \tag{2.71}$$

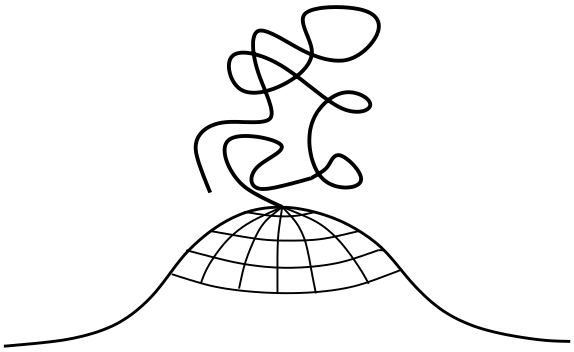

Figure 2.9: The form of the membrane, in a rough estimation, is influenced on an area determined by the polymer end-to-end distance R_p.

We find

$$l_1(x') = -2\int_0^{x'} \mathrm{d}x\; x\; m(x) \;=\; -\frac{1}{8\pi}\frac{T}{\kappa}R_p\left\{2\frac{x}{R_p}\left(\exp\left(-\frac{3}{2}\frac{x^2}{R_p^2}\right) - \sqrt{\frac{3}{2}}\sqrt{\pi}\frac{x}{R_p}\right) + \right.$$
$$\left. + \sqrt{\frac{2}{3}}\sqrt{\pi}R_p\left(1+3\frac{x^2}{R_p^2}\right)\mathrm{erf}\left(\sqrt{\frac{3}{2}}\frac{x}{R_p}\right)\right\}\,. \qquad (2.72)$$

Note that $l_1(0)$ vanishes. Thus, the integration constant is zero.

The membrane shape profile is now obtained by

$$\langle l(x)\rangle - \langle l(0)\rangle \;=\; \int_0^x \mathrm{d}x'\frac{1}{x'}l(x') \qquad (2.73)$$

which leads to [54] the final expression

$$\langle l(x)\rangle - \langle l(0)\rangle \;=\; -\frac{R_p}{8\pi}\frac{T}{\kappa}\left\{\frac{x}{R_p}\exp\left(-\frac{3}{2}\frac{x^2}{{R_p}^2}\right) + \sqrt{\frac{\pi}{6}}\left[\left(1+3\frac{x^2}{{R_p}^2}\right)\mathrm{erf}\left(\sqrt{\frac{3}{2}}\frac{x}{R_p}\right) - 3\frac{x^2}{{R_p}^2}\right]\right.$$
$$\left. + 2\left(\frac{x}{R_p}\right){}_2\mathrm{F}_2\left(\{\frac{1}{2},\frac{1}{2}\},\{\frac{3}{2},\frac{3}{2}\},-\frac{3}{2}\frac{x^2}{{R_p}^2}\right)\right\} \qquad (2.74)$$

where ${}_2\mathrm{F}_2$ is a generalized hypergeometric function [57, 55]. The profile as given by (2.74) attains the cone-like shape given by

$$\langle l(\underline{x})\rangle - \langle l(\underline{0})\rangle \approx -(T/2\pi\kappa)x \qquad (2.75)$$

for small x and the catenoid-like shape given by

$$\langle l(\underline{x})\rangle - \langle l(\underline{0})\rangle \approx -(T/\kappa)(R_p/4\sqrt{6\pi})\ln(x/R_p)\,. \qquad (2.76)$$

for large x. The profile for $v_2 = 0$ and intermediate x-values is displayed in figure 2.10. The analytical formula for the shape profile proofs, that the polymer induces a sharp bend at the anchor. Far away from the anchor point the profile approaches a minimal surface shape, i.e. a shape with vanishing curvature as given by the catenoid.

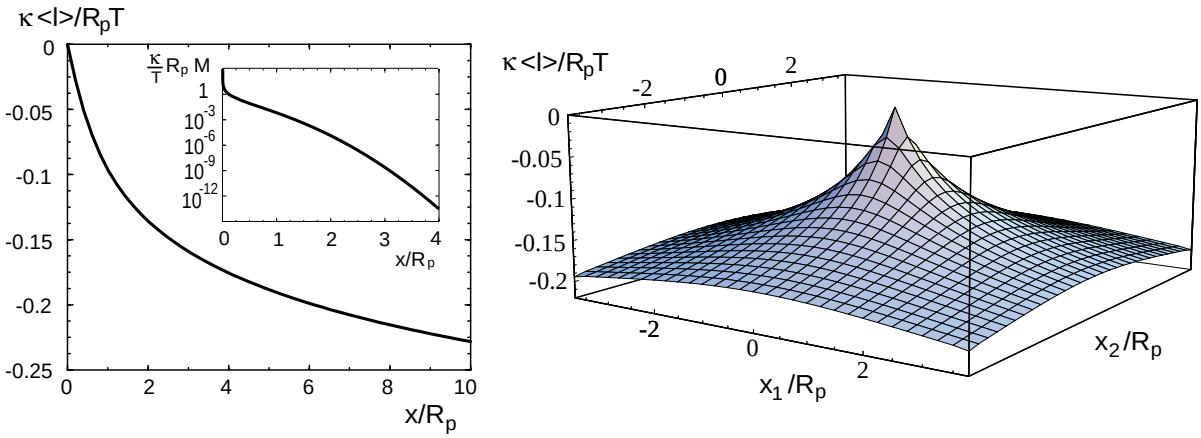

Figure 2.10: The profile of the membrane as obtained by the perturbative calculation for vanishing potential parameter v_2. In the inset the corresponding curvature is plotted as a function of x. On the right side the shape profile is displayed in a surface plot.

The only length scale, which remained in our calculation, is the polymer end-to-end distance R_p. Therefore, if we want to separate both regimes, it is legitimate to assume that the polymer influences the membrane on an area corresponding to a distance of R_p. The approach towards the catenoid can be considered as a long range correction of the perturbation around the anchor point.

Since the shape of the free membrane is logarithmically divergent for large distances, it is still an interesting question, what happens if many polymers are anchored on the membrane. This situation is much more important from the experimental point of view, since it is difficult to anchor only one polymer on top of a large membrane.

2.5.3 Polymer covered membranes

So far, we considered the effect of a single polymer which is anchored on a membrane. From an experimental point of view it is important to generalize this situation to one, where several polymers are anchored on the membrane [58, 59], also on both sides. In the case of a large anchor-distance, the situation is referred to as the mushroom regime. If one decreases the anchor distance of the polymers, the mushrooms will start to intersect and perturb each other. This will lead to a laterally squeezed mushroom shapes, because the steric hinderence will become stronger and the polymers will avoid to intersect. This high coverage regime is called brush regime [60, 61, 62, 63]. Due to the excluded volume interaction, the initial mushroom shape will be deformed into a strongly stretched configuration.

What happens now, if several polymers are anchored on the membrane? Since our expansion we did in the derivation of the shape and curvature profile is nothing but an expansion up to linear order in l, the problem of N_p anchored polymers can be reduced to the problem of a linear superposition of the effect of N_p single polymers [1].

Let us therefore consider a membrane of area $\mathcal{A}$ which is covered by N_p anchored polymers in the dilute regime. Up to first order in the surface height l, we may simply superimpose the separate

[1] A similar superposition of membrane deformations has been considered in the so-called hat model in [64, 65]

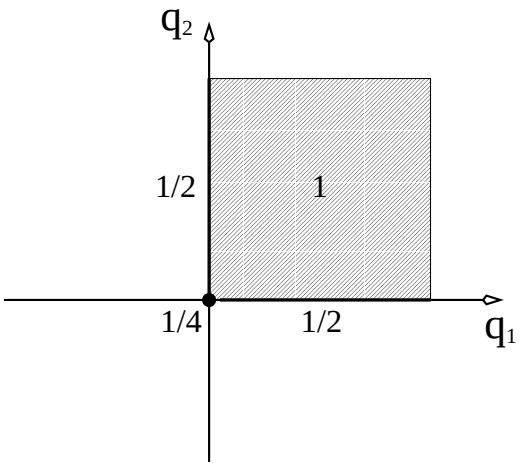

Figure 2.11: The weights for a symmetric Fourier transform: The origin, which belongs to all four quadrants, has weight $1/4$, the border lines $1/2$ and the bulk has weight 1.

shape deformations arising from these polymers. Thus, for the coverage $\Gamma_p = N_p/\mathcal{A}$ one obtains the mean (spontaneous) curvature $M_{sp} = \sqrt{\pi/6}(T/4\kappa)\Gamma_p R_p$. Thus, the polymer induced spontaneous curvature is proportional to the coverage density.

It is of special interest to study the situation of membranes which are covered by polymers in such a way, that the anchors form a regular lattice in the plane of reference. This situation corresponds to a polymer anchored on a membrane of lateral size L with periodic boundary conditions in both lateral directions. Thus, the anchor distance of such a rectangular lattice is L.

The situation is easily calculated by changing the continuous Fourier transformation into a discrete one. In one dimension the periodic Fourier transform is given by

$$\langle l(x)\rangle = \frac{a_0}{2} + \sum_{q=1}^{\infty}\left(a_q \cos\left(\frac{2\pi}{L}qx\right) + b_q \sin\left(\frac{2\pi}{L}qx\right)\right) \tag{2.77}$$

with the coefficients

$$a_q = \frac{2}{L}\int_{-L/2}^{L/2} l(x)\cos\left(\frac{2\pi}{L}qx\right)\mathrm{d}x\,, \tag{2.78}$$

$$b_q = \frac{2}{L}\int_{-L/2}^{L/2} l(x)\sin\left(\frac{2\pi}{L}qx\right)\mathrm{d}x\,. \tag{2.79}$$

We assume that the membrane extends from $x \in [-L/2, L/2]$. Using the axial symmetry (which in two dimensions corresponds to the spherical symmetry) $l(x) = l(-x)$ the system reduces to

$$a_q = \frac{4}{L}\int_{0}^{L/2} l(x)\cos\left(\frac{2\pi}{L}qx\right)\mathrm{d}x\,, \tag{2.80}$$

$$b_q = 0\,. \tag{2.81}$$

Generalizing to two dimensions one finds

$$\langle l(x_1,x_2)\rangle = \frac{a_{0,0}}{4} + \frac{1}{2}\sum_{q_1=1}^{\infty} a_{q_1,0}\cos\left(\frac{2\pi}{L}q_1x_1\right) + \frac{1}{2}\sum_{q_2=1}^{\infty} a_{0,q_2}\cos\left(\frac{2\pi}{L}q_2x_2\right) +$$

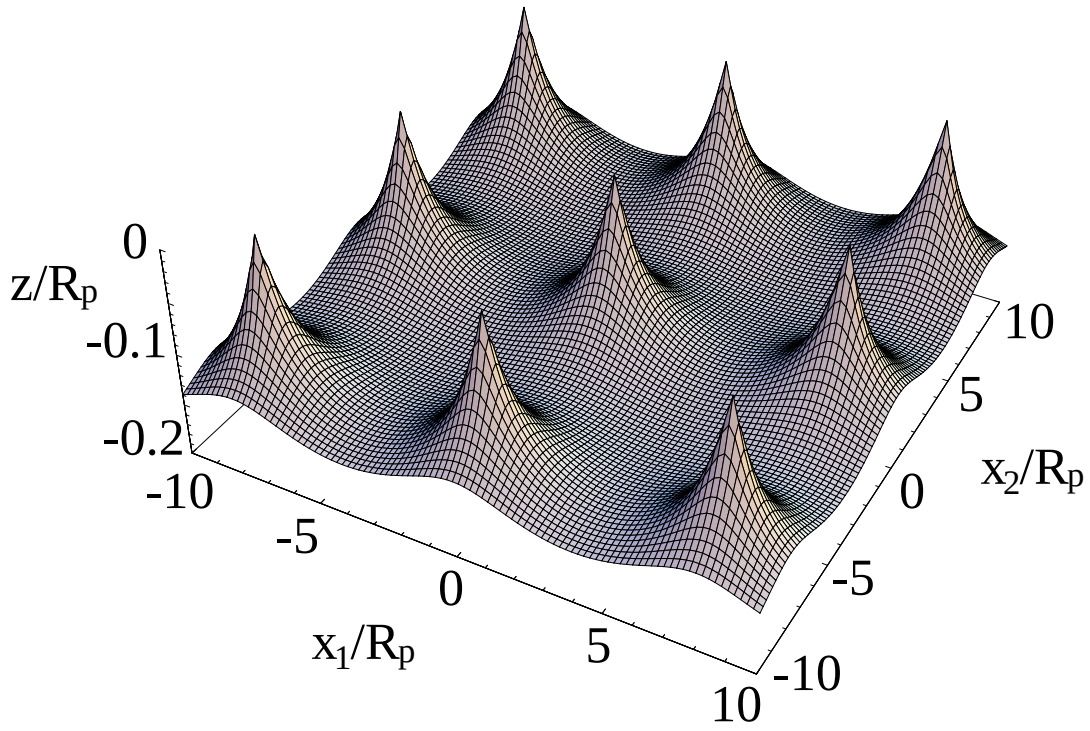

Figure 2.12: The membrane shape using periodic boundary conditions. The lateral size of one elementary unit is $8R_p$. The discrete Fourier transformation was done numerically with Mathematica [56], taking into account the first 30 Fourier modes.The membrane is not confined by a potential.

$$+\sum_{q_1=1}^{\infty}\sum_{q_2=1}^{\infty} a_{q_1,q_2}\cos\left(\frac{2\pi}{L}q_1x_1\right)\cos\left(\frac{2\pi}{L}q_2x_2\right)\ . \tag{2.82}$$

In order to find the Fourier coefficients we will start from eq. (2.47),

$$\langle l(\underline{x})\rangle \;=\; -\int_0^1 \mathrm{d}s\int \mathrm{d}^2x' K(\underline{x}-\underline{x}')P(s,\underline{x}')\ . \tag{2.83}$$

which is equal to

$$\langle l(x_1,x_2)\rangle \;=\; -\left(\frac{4}{L}\right)^2\sum_{q_1}\sum_{q_2}\tilde{K}(q_x,q_y)\tilde{P}(q_x,q_y)\cos\left(\frac{2\pi}{L}q_1x_1\right)\cos\left(\frac{2\pi}{L}q_2x_2\right) \tag{2.84}$$

where we respect the above introduced weights inside the sum. The Fourier transformed (continuous) membrane propagator is

$$\begin{aligned}\tilde{K}^{-1}(q_1,q_2) \;=\;& \frac{\kappa}{T}\int_0^{L/2}\mathrm{d}x_1\int_0^{L/2}\mathrm{d}x_2\;\delta(x_1)\;\delta(x_2)\left[\Delta^2_{\underline{x}'}+\frac{v_2}{\kappa}\right]\times\\ &\times\cos\left(\frac{2\pi}{L}q_1(x_1-x_1')\right)\cos\left(\frac{2\pi}{L}q_2(x_2-x_2')\right)\Big|_{\underline{x}'=0}\end{aligned} \tag{2.85}$$

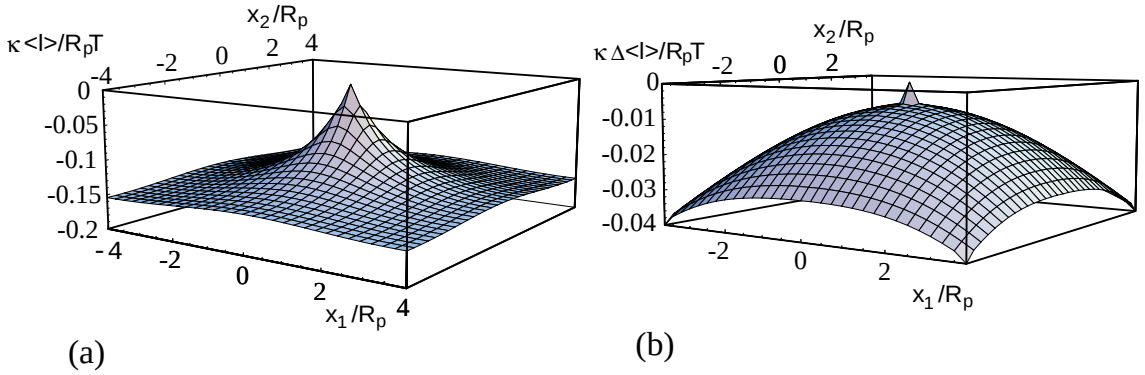

Figure 2.13: Membrane shape: (a) The shape of a freely diffusing membrane without confining potential in a periodic potential. Compare with the shape in fig. 2.10, where the membrane boundaries are free. (b) The difference between the membrane in periodic boundaries and the membrane in free boundaries. The difference in the anchor region is not a boundary effect but due to the finite amount of Fourier modes, namely 30 modes, which were taken into account in the discrete Fourier transformation performed with Mathematica [56].

which leads to

$$\tilde{K}^{-1}(q_1, q_2) \;=\; \frac{\kappa}{T}\left[\left(\frac{2\pi}{L}\right)^4 (q_1^2+q_2^2)^2 + \frac{v_2}{\kappa}\right] . \tag{2.86}$$

The Fourier transformed polymer pressure is more complicated and will be calculated numerically [56].

$$\tilde{P}(q_1, q_2) \;=\; \int_0^{L/2} \mathrm{d}x_1 \int_0^{L/2} \mathrm{d}x_2 \; P(x_1, x_2) \; \cos\left(\frac{2\pi}{L} q_1 x_1\right) \cos\left(\frac{2\pi}{L} q_2 x_2\right) . \tag{2.87}$$

Evaluating eq. (2.84) gives the membrane shape with a lattice of anchored polymers as displayed in figure 2.12. In this figure we show a free membrane, i.e. a membrane which is not confined by a harmonic potential. As we have already calculated, the membrane shape profile which arises from one anchored polymer is a cone close to the anchor and a catenoid far away from it. The catenoid logarithmically diverges and is only possible as long as the lateral boundaries of the membrane are free. Here, we consider the effect of periodic boundaries. In consequence of this, several polymers regularly cover the membrane and lead to a non-diverging shape profile with clearly visible cone-regions. In figure 2.13 we show an elementary cell with one polymer. In addition we plot the difference between the membrane inside this cell and the membrane with free boundary conditions. The difference increases close to the boundaries. The difference of both profiles in the anchor region is not a boundary effect but due to the finite number of Fourier modes which were taken into account in the calculation (since the transform is done numerically we take into account 30 Fourier modes). The number of Fourier modes correspond to the number of discretization points of the membrane in the lateral direction. Consequently, one can use these results to compare later with the Monte Carlo simulation where one uses periodic boundary conditions and where the membrane is discretized, see chapter 3 and figure 3.4 and for the adsorption-simulations in chapter 8. Therefore, we use the same parameters in the

above calculation as in our Monte Carlo simulations, especially the lateral size of the elementary cell, which is $8R_p$.

Chapter 3

Anchored Polymers: Monte Carlo Simulation

In the previous chapters, we have introduced our system and a method to calculate analytically the physically important quantities which characterize the membrane and the polymer. We have seen that the expansion we made in our calculation is linear in the membrane profile $l(\underline{x})$. In order to check, if the expansion is in fact justified and gives correct results we confirm the analytical calculation by a Monte Carlo simulation.

In order to give an overview we start with a description of the simulation algorithm.

3.1 Simulation method

The crucial point which we have to take into account is the discrete representations of membrane and polymer, respectively. The continuous membrane Hamiltonian has been introduced in eq. (2.2). The parametrization of the membrane as a surface with height l above the plane of reference $\underline{x} = (x_1, x_2)$ implies that the membrane cannot undergo any changes in its topology. Thus, the Gaussian curvature term stays constant and can be ignored in our energy expression. Furthermore, we neglect configurations with overhangs as shown in fig. 2.1. The two-dimensional coordinate system $\underline{x}$ is represented by a lattice $x^{(i,j)}$ with lattice constant a_m. The configuration of the membrane is determined by $l^{(i,j)}$ indicating the membrane height at position $x^{(i,j)}$. The discretized Laplace operator is

$$\nabla_d^2 l^{(i,j)} \;=\; l^{(i+1,j)} + l^{(i-1,j)} + l^{(i,j+1)} + l^{(i,j-1)} - 4l^{(i,j)} \; . \tag{3.1}$$

We use a single-site-move algorithm, in which we compare the energies of two configurations: $\{\tilde{l}_N\}$, the new one, and the old one, $\{l_N\}$. Both configurations differ in the value of l at position (i,j). As long as the energy difference is negative, i.e. the new configuration has lower energy than the new one, the move is accepted. If the energy difference is positive, the probability of acceptance is given by $\exp(-\Delta\mathcal{H}/T)$. This method is known as the Metropolis-algorithm. Via this accepting procedure, we ensure thermodynamic equilibrium and in particular detailed balance.
We can now write down the energy difference of the elastic part of the membrane.

$$\begin{aligned}\Delta\mathcal{H}_{me} \;&=\; \mathcal{H}^{el}(\{\tilde{l}_N\}) - \mathcal{H}^{el}(\{l_N\}) \;= \\ &= \frac{\kappa}{2}\Big((\nabla_d^2\tilde{l}^{(i,j)})^2 + (\nabla_d^2\tilde{l}^{(i+1,j)})^2 + (\nabla_d^2\tilde{l}^{(i-1,j)})^2 + (\nabla_d^2\tilde{l}^{(i,j+1)})^2 + (\nabla_d^2\tilde{l}^{(i,j-1)})^2 -\end{aligned}$$

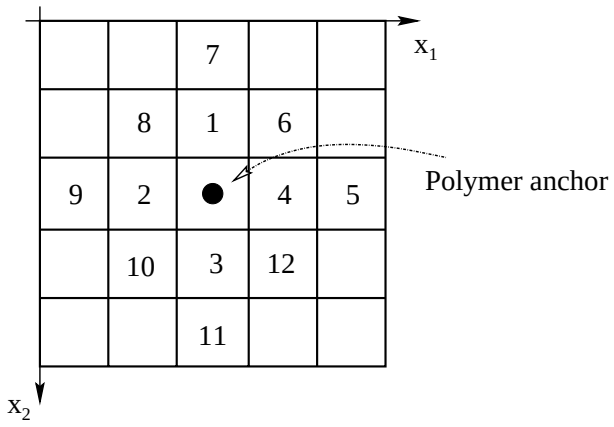

Figure 3.1: The discretization of a 5×5-membrane in the x_1, x_2-plane. The anchor bead of the polymer is located in the middle of the anchor segment. In addition we plotted the 12 next neighbors which are taken into account in the energy difference.

$$-(\nabla_d^2 l^{(i,j)})^2 - (\nabla_d^2 l^{(i+1,j)})^2 - (\nabla_d^2 l^{(i-1,j)})^2 - (\nabla_d^2 l^{(i,j+1)})^2 - (\nabla_d^2 l^{(i,j-1)})^2\Big) \quad . (3.2)$$

Inserting the discretized Laplace operator leads to

$$\begin{aligned}\Delta\mathcal{H}_{me} &= \kappa\Big\{\Big(\tilde{l}^{(i,j)} - l^{(i,j)}\Big)\Big(l^{(i+2,j)} + l^{(i-2,j)} + l^{(i,j+2)} + l^{(i,j-2)} + \\ &\quad +2\Big[l^{(i+1,j+1)} + l^{(i-1,j+1)} + l^{(i+1,j-1)} + l^{(i-1,j-1)}\Big] - \\ &\quad -8\Big[l^{(i+1,j)} + l^{(i-1,j)} + l^{(i,j+1)} + l^{(i,j-1)}\Big] + 10\Big[\tilde{l}^{(i,j)} + l^{(i,j)}\Big]\Big)\Big\} \quad . \qquad (3.3)\end{aligned}$$

The energy difference takes into account twelve next neighbors. We use periodic boundary conditions. The harmonic potential and tension terms can easily be included into the discretized Hamiltonian.

We choose the lateral size of the membrane lattice $L = (8 + a_m)R_p$, which ensures, that the membrane is always much larger than the polymer end-to-end distance. This is important in order to avoid disturbances due to the membrane boundaries. The membrane discretization varies from $a_m = R_p$ to $a_m = 0.125R_p$. The anchored polymer is treated as a chain of springs with $N + 1$ beads and consequently N bonds. The zero bead stays on the membrane segment (i_0, j_0), which is referred to as the anchor segment. Moving the membrane at this position enforces us to take into account the position of the neighboring polymer bead. Note that the polymer beads are point-like as long as we do not take into account excluded volume effects. Since our polymer is ideal it can freely intersect.

The internal polymer length s is discretized by $\Delta s = 1$. To adjust the discretization of the polymer to the lattice constant a_m of the membrane, one uses the Kuhn length a_p. In general, a_p is of the order of the membrane discretization a_m. Thus, we vary a_p in a range of $a_p = R_p$ to $a_p = 0.125R_p$. If we change the Kuhn length of the polymer we consequently have to change the number of beads N in such a way that the end-to-end distance $R_p = a_p\sqrt{N}$ stays constant. For example, if we bisect a_p we end up with $4N$ polymer beads.

Changing the i-th bead inside the polymer from position $\mathbf{r}$ to position $\tilde{\mathbf{r}}$ yields an energy change

$$\Delta\mathcal{H}_p = \frac{3}{2a_p^2}\Big\{(\mathbf{r}_{i+1} - \tilde{\mathbf{r}}_i)^2 + (\tilde{\mathbf{r}}_i - \mathbf{r}_{i-1})^2 - (\mathbf{r}_{i+1} - \mathbf{r}_i)^2 - (\mathbf{r}_i - \mathbf{r}_{i-1})^2\Big\} \quad . \qquad (3.4)$$

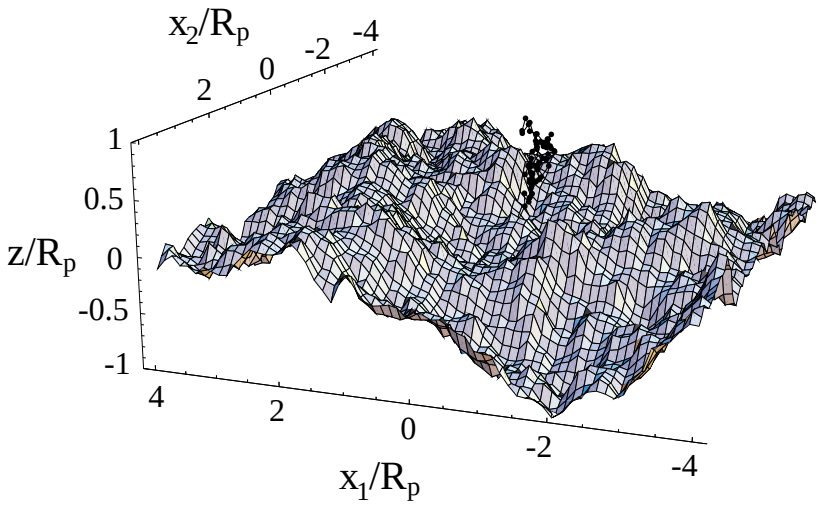

Figure 3.2: Snapshot of the polymer and membrane configuration, as obtained by the Monte Carlo simulation after 10^7 Monte Carlo steps. The influence of the polymer is not visible in the snapshots due to membrane roughness.

In figure 3.1 we have shown the discretization of a 5×5-membrane and the position of the polymer anchor in the middle of the anchor segment. Each membrane segment can move continuously in the z-direction. The important restriction for the move of the segment is the impenetrability of polymer and membrane. Therefore, if there are polymer beads on top of the membrane segment, the segment can only move in such a way that it stays below the lowest polymer bead above it. All beads are moved according to the Hamiltonian 3.3 and the hard core repulsion on the surface. There is only one exception, namely the membrane anchor segment, which has to take into account the neighboring bead of the polymer chain. The same restriction of impenetrability holds, of course, for the move of the polymer beads above the membrane. Each bead can move continuously in three dimensions.

After each membrane move, i.e. after having moved each lattice site once, we perform the polymer move, in which we change each bead position once. Merging both, we have performed one Monte Carlo step of our compound system. Most of the runs are extended over 10^7 Monte Carlo steps.

3.2 Theoretical background

In our analytic calculation, we introduced a harmonic potential which acts on the membrane and confines it around $z = 0$. Using this trick one avoids the free diffusion of the membrane, which leads to a divergence in the calculation. However, it is possible to subtract the divergent part in case of the limit of vanishing potential. This subtraction is equivalent to a change in our coordinate system in such a way that the anchor segment is put in the origin. The resulting shape profile is displayed in figure 2.10. The same properties hold for the simulation. We start to simulate the polymer-membrane system by introducing a harmonic potential with potential parameter $\mathfrak{v}_2$. This ensures that the membrane approaches a flat profile for large distances of the anchor point. If the lateral size of the membrane, which is equal to the polymer anchor distance, is sufficiently large compared to the polymer end-to-end distance we expect to obtain a good agreement between the analytic prediction and the simulation,

because the effect of the periodic boundary conditions is expected to be small. However, our analytic calculation for a periodic system also allows us to compare both, including the periodic boundary conditions.

In figure 3.2, we present a snapshot configuration of the membrane with anchored polymer after 10^7 Monte Carlo steps.

3.2.1 Gaussian membranes

In this section, we briefly investigate some basic properties of Gaussian membranes, which are not perturbed by an anchored polymer. The membrane is influenced by its bending rigidity and the strength of the confining potential. The first quantity we are interested in is the correlation function

$$C(\underline{x}) \quad = \quad \langle l(\underline{x}) l(\underline{0}) \rangle \; . \tag{3.5}$$

This definition makes use of the translational symmetry of the membrane. In order to derive the formula we again introduce the generating field $\gamma(\underline{x})$ in the membrane Hamiltonian, which leads to the partition function

$$\mathcal{Z}\{\gamma\} \quad = \quad \int \mathcal{D}\{l\} \; \exp\left(-\frac{1}{2} \int \mathrm{d}^2x' \int \mathrm{d}^2x'' \; l(\underline{x}') K^{-1}(\underline{x}' - \underline{x}'') l(\underline{x}'') + \int \mathrm{d}^2x' \; \gamma(\underline{x}') l(\underline{x}') \right) \; . \tag{3.6}$$

The membrane bilinear kernel is defined as in eq. (2.44). Dividing the partition function by the unperturbed membrane system

$$\mathcal{Z}_0 \quad = \quad \int \mathcal{D}\{l\} \; \exp\left(-\frac{1}{2} \int \mathrm{d}^2x' \int \mathrm{d}^2x'' \; l(\underline{x}') K^{-1}(\underline{x}' - \underline{x}'') l(\underline{x}'') \right) \tag{3.7}$$

one ends up with

$$\frac{\mathcal{Z}\{\gamma\}}{\mathcal{Z}_0} \quad = \quad \exp\left(\frac{1}{2} \int \mathrm{d}^2x' \int \mathrm{d}\underline{x}'' \; \gamma(\underline{x}') K(\underline{x}' - \underline{x}'') \gamma(\underline{x}'') \right) \; . \tag{3.8}$$

The correlation function is now given by

$$C(\underline{x}) \quad = \quad \frac{\delta^2 \ln(\mathcal{Z}\{\gamma\}/\mathcal{Z}_0)}{\delta\gamma(\underline{x}) \delta\gamma(\underline{0})} \tag{3.9}$$

which leads to the simple identity

$$C(\underline{x}) = K(\underline{x}) = \int \frac{\mathrm{d}^2q}{(2\pi)^2} \tilde{K}(\underline{q}) \exp(i\underline{q}\underline{x}) = -\frac{T\xi_{||}^2}{4\pi\kappa} \mathrm{kei}(\sqrt{2}\mathrm{x}/\xi_{||}) \; . \tag{3.10}$$

In the final step we made use of the isotropy of the system which allows us to shift into polar coordinates. In addition, we introduced the parallel (because it refers to the lateral direction) correlation length $\xi_{||}$ given by

$$\xi_{||} \quad = \quad (4\kappa/v_2)^{1/4} \; . \tag{3.11}$$

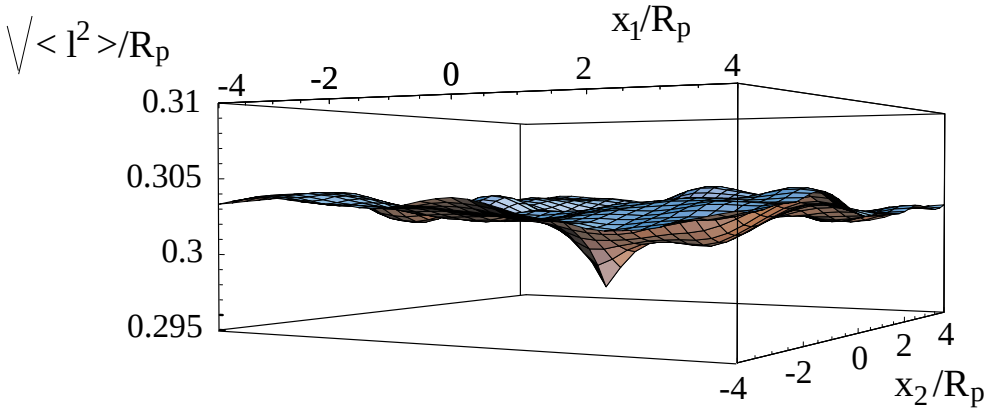

Figure 3.3: The roughness of the membrane after 10^7 MC-steps. For large distances from the anchor point the roughness approaches the analytical value for the unperturbed case. In the vicinity of the anchor, where the polymer suppresses fluctuations, the roughness decreases.

kei is the Thomson function. If one inserts the asymptotic behavior of this function, see appendix B, one obtains

$$C(x) \quad \sim \quad \frac{T}{\kappa} \frac{\xi_{||}^{5/2}}{4\sqrt{\sqrt{2}\pi x}} \exp\left(-\frac{x}{\xi_{||}}\right) \sin\left(\frac{x}{\xi_{||}} + \frac{\pi}{8}\right) \ . \tag{3.12}$$

One sees immediately that our definition of the correlation length is justified, since it determines the exponential decay of the correlation function for large distances. The correlation function, which determines the roughness of the membrane, i.e. the average squared size of the fluctuations, is given by

$$\xi_\perp^2 = C(0) = \langle l^2 \rangle = \frac{T}{\kappa} \frac{\xi_{||}^2}{16}. \tag{3.13}$$

Both quantities are important for our simulation.

The parallel correlation length determines the choices of reasonable values for both the membrane discretization a_m and the lateral membrane size L. Both values should be chosen such that

$$a_m \ \ll \ \xi_{||} \ \ll \ L \tag{3.14}$$

in order to ensure that boundary effects are sufficiently small and to ensure that the discretization is fine enough to resolve all physically important length-scales. From another point of view, relation (3.14) helps us to determine a reasonable ratio between the bending rigidity κ and the strength of the harmonic potential v_2. In most simulations we take a ratio of $v_2 R_p^4/\kappa = 2$, which corresponds to a value of the parallel correlation length $\xi_{||} = 1.1892 R_p$. This is always in between our membrane discretization and the lateral size of the membrane. The perpendicular correlation length, the roughness of the membrane, measures the fluctuation size and contains important information of the polymer effect on the membrane. We expect the polymer to suppress membrane fluctuations in the vicinity of the anchor point, since the membrane is restricted in its movements by the presence of the polymer

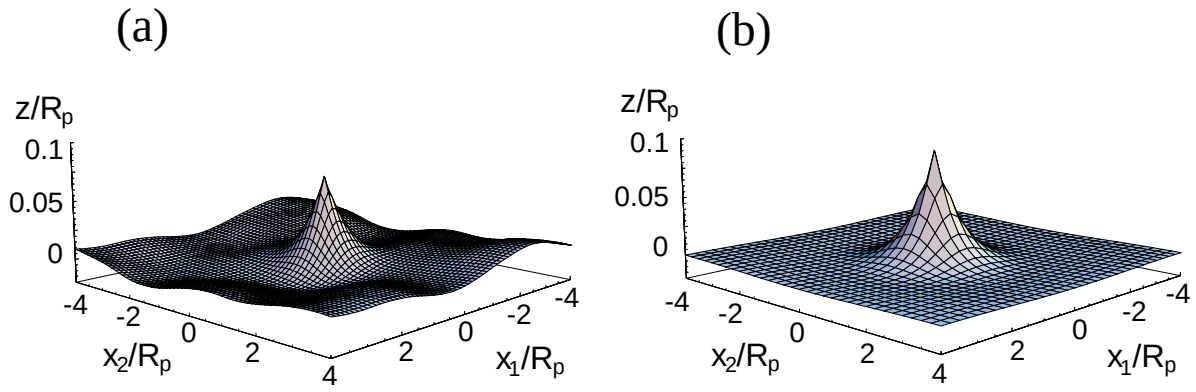

Figure 3.4: a) Membrane profile averaged over 10^7 MC-steps with bending rigidity $\kappa/T = 1$ and harmonic potential parameter $v_2 {R_p}^4/T = 2$. The membrane contains $65 \times 65 = 4225$ lattice sites, the polymer has 65 beads. (b) Perturbative calculation of the shape using periodic boundary conditions and 32 Fourier modes; same parameters as in (a).

beads. As we have seen in eq. (3.13) the roughness is related to the bending rigidity. If in our simulation we measure the change of the roughness we can thus define an effective rigidity κ_{eff}, which takes into account the effect due to the polymer. If the fluctuations are smaller, the effective bending rigidity will be higher as in case of the unperturbed membrane.

An analytic estimation for the change of the bending rigidity [46] gives

$$\kappa_{\text{eff}} \quad = \quad \kappa + \frac{1+\pi/2}{12} T \simeq \kappa + 0.21T \ . \tag{3.15}$$

If we assume reasonable experimental values for the bending rigidity of $10 - 20T$ we conclude that the effect is in the percent regime.

In figure 3.3 the roughness of the simulated membrane is plotted along the lateral directions. The limiting value for large distances from the polymer anchor is close to the theoretical prediction for the unperturbed Gaussian membrane, namely $\sqrt{\langle l^2 \rangle / R_p^2} \approx 0.30$. In the vicinity of the anchor bead, the roughness decreases due to the polymer, which suppresses the fluctuations of the membrane. The comparison with the theoretical result of eq. (3.15) leads to the qualitatively correct result, i.e. the bending rigidity is effectively increased in the anchoring region. However, it is not possible to compare both results quantitatively, since in contrary to the result of (3.15) in the simulation and in the membrane Hamiltonian the polymer leads to an $\underline{x}$-dependent contribution $\delta\kappa(\underline{x})$ which adds to the bending rigidity κ. This yields a complicated coupling between the total bending rigidity $\kappa + \delta\kappa(\underline{x})$ and the membrane height $l(\underline{x})$.

3.3 Comparison with the perturbative calculation

In the snapshot configuration shown in figure 3.2 the membrane appears crumpled as one expects for a curvature governed fluctuating membrane. Due to the fluctuations the polymer effect is not visible.

Only if one displays the averaged profile of the membrane, see fig. 3.4, one can clearly see the induced bending due to the anchored polymer. 10^7 Monte Carlo steps are taken into account in the

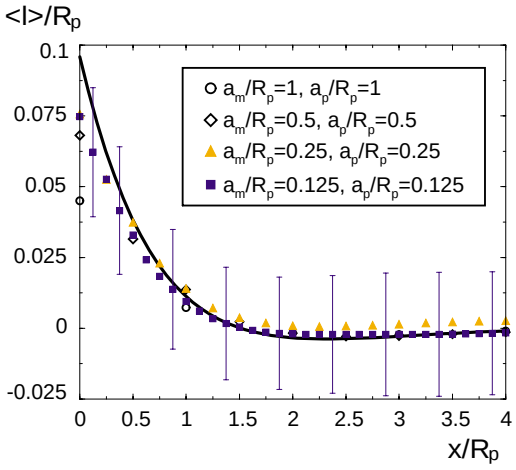

Figure 3.5: Membrane profile: Comparison of analytical calculation (solid line) and Monte Carlo data for different polymer and membrane discretizations a_p/R_p and a_m/R_p, respectively, and $\kappa/T = 1$, $v_2 {R_p}^4/T = 2$. The shape profiles are averaged over 10^7 MC-steps.

averaging. The lattice constant in the (x_1, x_2)-plane is $a_m = 0.125 R_p$, which is equal to the used polymer discretization a_p. In consequence, the membrane contains $65 \times 65 = 4225$ segments and the polymer contains 65 beads. This is our largest simulated system. As one can see in the shape profile the membrane is still not equilibrated. But we can clearly identify the polymer effect on the averaged shape, namely the cone in the vicinity of the anchor point. As one expects, the membrane becomes flat for larger distances from the anchor point. Note that the scale of the axes is different for the plane of reference and for the height in the z-direction. Therefore the effect on the membrane is exaggerated. Additionally we in fig. 3.4 plot the analytically calculated shape profile for the same parameter values as used in the simulation. Apart from the small deviation in the cone region the agreement is good. Note that the fluctuations in the simulated membrane are still visible since it is not completely equilibrated.

In order to investigate the comparison quantitatively we show in fig. 3.5 both the analytic prediction and the simulation data for different discretizations of polymer and membrane. In the displayed simulation data a_m and a_p are always equal. By simultaneously decreasing both lengths scales we approach the continuous limit.

One can clearly see the improvement when the discretization is made finer. However there is still a difference between both curves in the vicinity of the anchor such that the tip of the profile in the simulation is slightly beneath the analytical shape.

As one can see in the discrete Fourier transformation this difference arises from the finite number of Fourier modes which is related to the number of discretization points, which is clearly visible in figure 2.13, where the difference in the anchor region of plot (b) is due to the finite amount of Fourier modes, which corresponds to the amount of discretization points of the membrane.

The fluctuations which are included in the simulation up to a length scale of the membrane discretization a_m have an additional influence on the membrane shape, which might lead to differences in the continuum limit, compared to the analytic prediction obtained by the perturbative approach.

In fig. 3.6 we present the polymer segment density, which we already calculated analytically

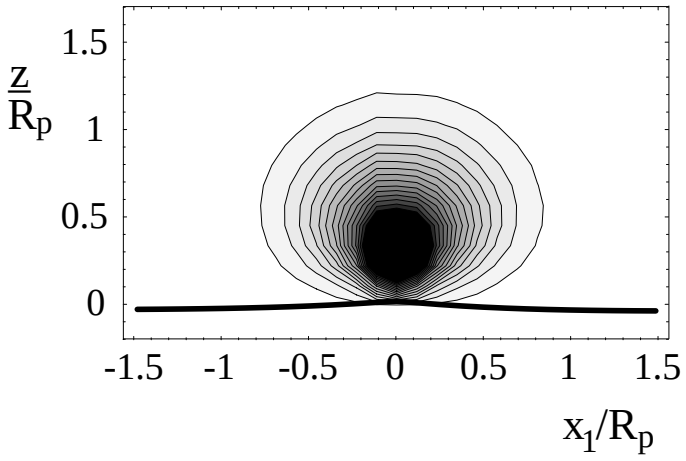

Figure 3.6: Segment density of the polymer on top of the membrane cut in the x_1 direction. The density is obtained by counting the probability of polymer beads to be localized at position $(x_1/R_p, z/R_p)$ in the cut-plane. The parameters have the same values as in fig. 3.4.

in eq. (2.34) for the half-space situation. Now, we in addition see the effect due to the bending of the membrane, which increases the spatial freedom of the polymer in the vicinity of the anchor point compared to the flat geometry. This leads to a higher segment density of the polymer close to the anchor. If one compares with the analytic results for the half-space polymer anchored on a flat substrate, see fig. 2.4, one can clearly see the difference.

Chapter 4

Polymer Interaction and Experiments

In the previous chapters, we integrated over the polymer degrees of freedom in order to focus on the membrane degrees of freedom, which implied to integrate out the polymer degrees of freedom. We started the investigation by studying a single polymer on an idealized infinite membrane. Later we generalized the calculation to the case of several polymers anchored to the membrane. Since we perform a gradient expansion up to linear order the latter situation follows from the initial one by linear superposition of single polymer effects. We will now focus on the polymers and study the membrane induced interaction energy due to membrane curvature. This problem is related to the interaction between inclusions in fluctuating membranes. There is an extensive literature studying the effect of fluctuations and curvature of the membrane on inclusions, such as rods [66, 67], which are attracted due to the membrane. Other authors study the influence of inclusions on the thickness of the membrane [68] and self-assembly of inclusions [69]. Additionally, the presence of inclusions leads to changes in the local stiffness of the membrane and might induce a spontaneous curvature [70, 71, 72].

4.1 Interaction energy of anchored polymers

Polymers are regarded as a special type of three-dimensional inclusion [73]. We start by anchoring N_p polymers on top of the membrane, each of them located at the spatial position $\underline{x}_i$ The partition function of the polymers is given by

$$\mathcal{Z}_p\{l\} \;=\; \exp\left[-\sum_{i=1}^{N_p}\int \mathrm{d}^2x\, P(\underline{x}-\underline{x}_i)\, l(\underline{x})\right]\,, \tag{4.1}$$

Insertion into the partition function of the compound system yields

$$\mathcal{Z} \;=\; \int \mathcal{D}\{l\}\; \exp\left(-\frac{1}{2}\int \mathrm{d}^2x \int \mathrm{d}^2x'\; l(\mathbf{x})K^{-1}(\mathbf{x}-\mathbf{x}')l(\mathbf{x}') - \sum_{i=1}^{N_p}\int \mathrm{d}^2x\; P(\mathbf{x}-\mathbf{x}_i)\, l(\mathbf{x})\right)\,. \tag{4.2}$$

The Gaussian integral leads to

$$\mathcal{Z} \;=\; \exp\left(\frac{1}{2}\sum_{i=1}^{N_p}\sum_{j=1}^{N_p}\int \mathrm{d}^2x \int \mathrm{d}^2x'\; P(\mathbf{x}-\mathbf{x}_i)K(\mathbf{x}-\mathbf{x}')P(\mathbf{x}'-\mathbf{x}_j)\right)\times$$

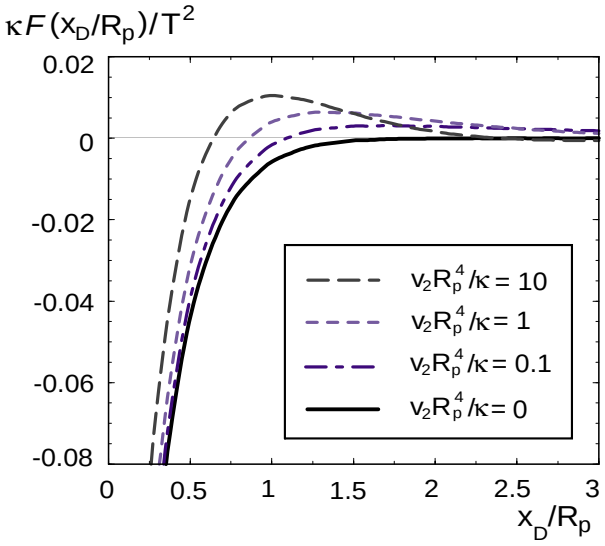

Figure 4.1: The pairwise polymer interaction energy due to membrane curvature for different values of the harmonic potential parameter v_2 which confines the membrane. For vanishing v_2 the membrane is free. The membrane induced polymer interaction is always attractive in this limit.

$$\times \int \mathcal{D}\{l\}\ \exp\left(-\frac{1}{2}\int \mathrm{d}^2x \int \mathrm{d}^2x'\ l(\mathbf{x})K^{-1}(\mathbf{x}-\mathbf{x}')\,l(\mathbf{x}')\right)\ . \qquad (4.3)$$

The free energy difference to the unperturbed membrane system with partition function $\mathcal{Z}_0$ is given by $\Delta\mathcal{F} = -T\ln(\mathcal{Z}/\mathcal{Z}_0)$ which gives

$$\begin{aligned}\Delta\mathcal{F} &= -\frac{T}{2}\sum_i\sum_j \int \mathrm{d}^2x \int \mathrm{d}^2x'\ P(\mathbf{x}-\mathbf{x}_i)K(\mathbf{x}-\mathbf{x}')P(\mathbf{x}'-\mathbf{x}_j)\\ &= \frac{N_p}{2}\mathcal{F}_{self} + \sum_{i>j}\mathcal{F}(\mathbf{x}_i-\mathbf{x}_j)\ . \end{aligned} \qquad (4.4)$$

The free energy is the sum of the self energy of each polymer and the pairwise interaction energy. In the following the pairwise interaction $\mathcal{F}(\mathbf{x}_1-\mathbf{x}_2)$ will be calculated. For simplicity we set $\mathbf{x}_1$ to zero and denote $\mathbf{x}_2$ by $\mathbf{x}_D$.

$$\begin{aligned}\mathcal{F}(\mathbf{x}_D) &= -T\int \mathrm{d}^2x \int \mathrm{d}^2x'\ P(\mathbf{x})K(\mathbf{x}-\mathbf{x}')P(\mathbf{x}'-\mathbf{x}_D)\\ &= -T\int \mathrm{d}^2x \int \mathrm{d}^2x' \int \frac{\mathrm{d}^2q}{(2\pi)^2}\int \frac{\mathrm{d}^2q'}{(2\pi)^2}\int \frac{\mathrm{d}^2q''}{(2\pi)^2}\,\tilde{g}(\mathbf{q})\tilde{P}(\mathbf{q}')\tilde{K}(\mathbf{q}'')\ \times\\ &\quad \times\ \exp(-i(\mathbf{q}+\mathbf{q}'')\mathbf{x})\exp(-i(\mathbf{q}'-\mathbf{q}'')\mathbf{x}')\exp(i\mathbf{q}'\mathbf{x}_D) \end{aligned} \qquad (4.5)$$

which leads to

$$\mathcal{F}(\mathbf{x}_D) = -T\int_0^\infty \frac{\mathrm{d}q}{2\pi}\,q\tilde{K}(q)[\tilde{P}(q)]^2 J_0(qx_D)\ . \qquad (4.6)$$

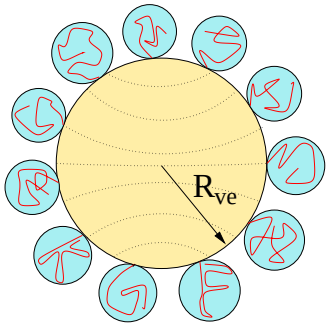

Figure 4.2: Schematic picture of polymers, which are anchored on top of the vesicle: For an estimate of the interaction energy between the polymers, we consider them as spheres of radius R_p, which repel each other.

Inserting the pressure and the membrane propagator finally yields the interaction energy

$$\mathcal{F}(x_D) = -\frac{R_p^2}{48}\frac{T^2}{\kappa}\int_0^\infty \mathrm{d}q\ \frac{q^5}{(q^4 + v_2/\kappa)}\exp\left(-\frac{R_p^2}{6}q^2\right)\left[I_0\left(\frac{R_p^2}{12}q^2\right) + I_1\left(\frac{R_p^2}{12}q^2\right)\right]^2 J_0(qx_D) \tag{4.7}$$

between two polymers at separation x_D. In Fig. 4.1 the interaction energy is shown for different values of $v_2 {R_p}^4/\kappa$. For small distances, it is always attractive. As long as v_2 does not vanish, one also finds regions with repulsive interaction due to damped oscillations in $\mathcal{F}$. For vanishing v_2, the interaction energy is monotonic and attractive for all values of x_D. The interaction vanishes for stiff membranes because of $\mathcal{F}(x_D)/T \sim T/\kappa$, as we expect for this fluctuation induced phenomenon. However, the attractive tail in $\mathcal{F}(x_D)$ occurs for distances of the order of R_p and smaller, where the polymers intersect. Therefore, if we include excluded volume effects between the polymers, the attraction interaction will be strongly suppressed.

4.2 Experimental investigations

In order to compare our previous results on the spontaneous curvature of membranes with experiments we will now focus on vesicles with attached polymers, see figure 4.2, since it is possible to deduce changes in the spontaneous curvature of vesicles by examining their shape transformations. We will consider three contributions to the spontaneous curvature of vesicles. The first contribution is given by the interaction between the polymer and the membrane due to the pressure which the polymer exerts on it. We already calculated the spontaneous curvature $M_{sp}^{(pm)} = \sqrt{\pi/6}(T/4\kappa)\Gamma_p R_p$ from this mushroom/membrane interactions. The contribution is linear in the coverage density Γ_p. A second contribution, which is also linear in Γ_p, arises from the size and geometry of the anchor molecules inserted into the membrane. If there is no exchange of molecules between both monolayers (flip-flops) a simple geometric argument leads to $M_{sp}^{(an)} = \Gamma_p A_{an}/2l_{me}$, where A_{an} is the lateral anchor area ($\approx 0.7\mathrm{nm}^2$) and l_{me} is the thickness of the bilayer ($\approx 4\mathrm{nm}$).

The last contribution arises from the interaction between the anchored polymers due to their steric repulsion. This contribution becomes important, if the mushrooms start to squeeze each other because of excluded volume effects. Even if we consider polymers at the θ-point there is excluded volume in-

teraction because of three-point-interactions between different chains. In a low density approximation the repulsive polymer/polymer interaction is characterized by the second virial coefficient b_2, which in this case is given by $b_2 = 4\pi {R_p}^2$. The free energy contains the repulsive interaction as well as the translational entropy of the N_p polymers, which leads to

$$\mathcal{F} \;=\; N_p \ln \Gamma_p \;+\; \frac{b_2}{2} N_p \Gamma \; . \tag{4.8}$$

The translation of the polymer spheres is described by their center of mass movement. Since the spheres are located on the vesicle surface, the center of mass moves on a sphere of radius $R + R_p$ and the densitity is

$$\Gamma \;=\; \frac{N_p}{4\pi (R+R_p)^2} \;=\; \underbrace{\frac{N_p}{4\pi R^2}}_{=\Gamma_p} \left(1 + \frac{R_p}{R}\right)^{-2} \; . \tag{4.9}$$

Expanding for large curvature radius R (for small curvatures $M = 1/R$ respectively) one finds the free energy per vesicle surface, including the curvature energy per area

$$\frac{\mathcal{F}}{4\pi R^2} \;=\; 2\kappa M^2 + \Gamma_p \ln \Gamma_p - b_2 \Gamma_p^2 R_p M + \frac{b_2}{2} \Gamma_p^2 \; . \tag{4.10}$$

Minimizing the compound free energy leads to the spontaneous curvature

$$M_{sp}^{(pp)} = \frac{T}{4\kappa} b_2 {\Gamma_p}^2 R_p \; , \tag{4.11}$$

which is induced by the polymer/polymer interaction. This contribution is quadratic in the coverage density Γ_p.

Equating the spontaneous curvature contributions from polymer/membrane and polymer/polymer interactions gives an estimated crossover coverage $\Gamma_p^* \simeq 1/4\sqrt{6\pi}{R_p}^2$, which is proportional to but smaller than the overlap concentration $\Gamma_p^{(ov)} = 1/\pi R_p^2$. In this way, one can identify two different mushroom regimes 1 and 2. Regime 1 with $\Gamma_p < \Gamma_p^*$ is dominated by the entropically induced polymer/membrane interaction. Regime 2 with $\Gamma_p > \Gamma_p^*$ is governed by the polymer/polymer interaction arising from the excluded volume.

For a typical polymer end-to-end distance $R_p = 10^{-2}\mu\mathrm{m}$ and a giant vesicle radius $R_{ve} = 10\mu\mathrm{m}$, a coverage density Γ_p of about ten percent of the overlap coverage and a bending rigidity of $\kappa/T = 10$ all three contributions discussed above are of comparable size. We find $M_{sp}^{(pm)} \approx 0.06\mu\mathrm{m}^{-1}$, $M_{sp}^{(an)} \approx 0.03\mu\mathrm{m}^{-1}$ and $M_{sp}^{(pp)} \approx 0.03\mu\mathrm{m}^{-1}$. For the total reduced curvature $(M_{sp}^{(pm)} + M_{sp}^{(an)} + M_{sp}^{(pp)})R_{ve}$, which determines the equilibrium shape of the vesicle, we find a value of about 1.2, which according to the spontaneous curvature model (and the area-difference-elasticity model) presented in the introduction [35] leads to a measurable change in the shape of vesicles.

An experimental result is shown in figure 4.3. Initially, the vesicle is a so called stomatocyte. There is no polymer solution outside the vesicle. In picture (b) polymers with a chemical anchor segment are added to the outside. The curvature of the vesicle is decreased, which can be deduced from the shape transformation. A possible explanation are the polymers which are not yet anchored to the vesicle. As long as they are in solution, the depletion effect is dominant and leads to a decrease of the membrane curvature, see chapter 9.

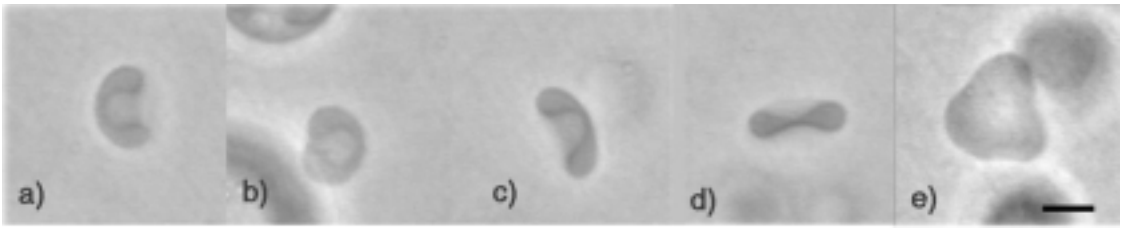

Figure 4.3: Shape change of a vesicle induced by adding polymers which anchor into the membrane: The spontaneous curvature is first decreased (a to b) and than increased. a) vesicle without polymer solution. b) After adding the polymers. c) 4 min. after (b). d) 6 min. after (b). e) 10 min. after (b). The bar denotes 5 μm. Taken from [74]

In the subsequent pictures, the curvature is increased which is in accord with the theoretical prediction for the effect of anchored polymers. In the last picture one ends up with a starfish-like vesicle [74].

Another system, which allows to study the effect of polymers on membranes is given by microemulsions in a ternary system of water, oil and surfactant [14]. If one adds block copolymers to the microemulsion, which are part of the monolayer and have loose ends which extend from the membrane to one subspace (for example the oil-phase in case of a hydrophobic tail), the one-phase microemulsion is rapidly growing. This effect is possibly explained by the interaction between the tails and the membrane, which lead to an increase in the spontaneous curvature and an increase of the membrane rigidity.

Chapter 5

Different Anchoring Geometries

In this short chapter, we will generalize the method introduced in the previous chapters to polymers, which are anchored with both of their ends and to polymers which translocate the membrane. In the first case we consider freely diffusing ends and anchors with fixed distances. The latter situation is motivated by the biological process of DNA translocation through the cell membrane.

5.1 Polymer anchored with both ends

An interesting generalization of the previous calculations, in which the polymer has been anchored to the membrane with one of its ends, is the case where both ends of the polymer are attached to the membrane. There are two situations, namely fixed and freely diffusing ends, which we are going to study. In the latter case the distance of the two ends is variable. It is easy to show that a polymer with free ends does not induce any spontaneous curvature on the membrane [75, 76]. We fix the first end of the polymer in the origin of our system of reference at $x_1 = x_2 = 0$. The last monomer will be located at $\mathbf{x}_e = (x_d, 0)$. Without loss of generality we put the second anchor on the x_1-axis. Thus, x_d is the lateral distance of the anchor points.

If one calculates the polymer pressure integrating over the last monomer one finds

$$\begin{aligned}\frac{1}{\mathcal{Z}_p\{0\}}\,\frac{\delta\mathcal{Z}_p}{\delta l(\mathbf{x})}\Big|_{l=0} &= -\frac{3}{R_p^2}\int_{-\infty}^{\infty}\mathrm{d}^2x_0\int_{-\infty}^{\infty}\mathrm{d}^2x_d\;\frac{\mathrm{d}}{\mathrm{d}s}\langle z(s)\rangle_{hs}\;\frac{\mathrm{d}}{\mathrm{d}s}\left(\mathcal{Z}(\mathbf{x}_0,\mathbf{x}|s)\;\mathcal{Z}(\mathbf{x},\mathbf{x}_d|1-s)\right)\\ &= -\frac{3}{R_p^2}\frac{\mathrm{d}}{\mathrm{d}s}\langle z(s)\rangle_{hs}\;\frac{\mathrm{d}}{\mathrm{d}s}\Big(1\Big) = 0 \qquad (5.1)\end{aligned}$$

with the partition functions in the lateral directions

$$\begin{aligned}\mathcal{Z}(0,x_1;0,x_2|s) &= \frac{3}{2\pi s R_p^2}\exp\left(-\frac{3}{2s}\frac{x_1^2+x_2^2}{R_p^2}\right),\\ \mathcal{Z}(x_1,x_{e,1};x_2,0|1-s) &= \frac{3}{2\pi(1-s)R_p^2}\exp\left(-\frac{3}{2(1-s)}\frac{(x_{e,1}-x_1)^2+x_2^2}{R_p^2}\right) \qquad (5.2)\end{aligned}$$

and in the perpendicular direction

$$\tilde{\mathcal{Z}}_{hs}(0,z|s) = \frac{3}{sR_p^2}\;z\;\exp\left(-\frac{3}{2s}\frac{z^2}{R_p^2}\right)\;,$$

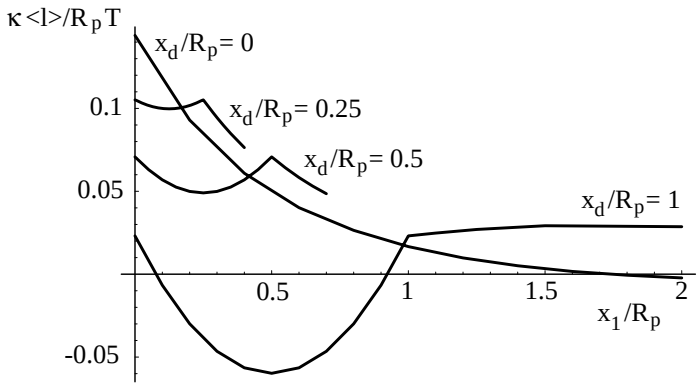

Figure 5.1: The membrane shape profile for a polymer which is anchored on the membrane with both ends for different anchor distances x_d. Additionally, the membrane is confined in a harmonic potential of strength $v_2 R_p^4/\kappa$. The profile is displayed in the anchor plane. In between the anchors, the polymer acts as a spring which pulls the membrane upwards.

$$\tilde{\mathcal{Z}}_{hs}(z,0|1-s) \quad = \quad \frac{3}{(1-s)R_p^2}\, z\, \exp\left(-\frac{3}{2(1-s)}\frac{z^2}{R_p^2}\right). \tag{5.3}$$

The result shows, that for small anchor distances the polymer effectively acts as if it was anchored by one end and bends the membrane away from it. For large anchor distances the polymer acts as a spring which pulls the membrane up. In average, both effects cancel, when integrating over both anchors. The pressure vanishes and the resulting shape profile of the membrane is flat. In the following calculation the anchors will be fixed. The calculation is more complicated, since we break the radial symmetry.
We start again with (5.1). Calculation of the derivative of the average path in z-direction yields

$$\frac{\mathrm{d}}{\mathrm{d}s}\langle z(s)\rangle_{hs} \quad = \quad \sqrt{\frac{2}{3\pi}}\frac{1-2s}{\sqrt{s(1-s)}}R_p\,. \tag{5.4}$$

In order to simplify the calculation it is necessary to restrict the investigation to the profile along the x-axis. Using the same methods as in the previous chapters the membrane profile, which depends on the anchor distance x_d yields

$$\begin{aligned}\langle l(x)\rangle_{x_d} \quad = \quad & \frac{R_p}{2\sqrt{6}\pi^{3/2}}\frac{T}{\kappa}\int_0^1 \mathrm{d}s \int_0^\infty \mathrm{d}q\, \frac{1-2s}{\sqrt{s(1-s)}}\frac{q^2}{q^4+v_2/\kappa}\,(q(1-2s)J_0(q(x-sx_d))- \\ & -\frac{6}{R_p^2}x_d J_1(q(x-sx_d))\Big)\exp\left(-s(1-s)\frac{q^2}{6}R_p^2\right) \quad .\end{aligned} \tag{5.5}$$

It is easy to proof that the profile is symmetric with respect to $x_d/2$.

There are two limiting cases, namely for small and for large anchor distances. In case of vanishing anchor distance $x_d = 0$ one ends up with a ring polymer which is anchored on the membrane. The resulting shape profile is given by

$$\langle l(x)\rangle_0 \quad = \quad \frac{R_p}{4\sqrt{6\pi}}\frac{T}{\kappa}\int_0^\infty \mathrm{d}q\, \frac{q^3}{q^4+v_2/\kappa}\left(I_0\left(\frac{q^2}{48}R_p^2\right)+I_1\left(\frac{q^2}{48}R_p^2\right)\right)J_0(qx)\,. \tag{5.6}$$

In this limit the dependence on x is the same as in case of the single anchored polymer. Consequently the resulting profile is qualitatively identical to this case, which is also clear from an intuitive point of view, since the ring corresponds to a polymer anchored with one end and smaller amount of monomers due to the closed configuration.

However, if one increases the anchor distance the profile along the x-axis is changed. In between the anchors the membrane is always bend upwards. Far away from the two anchors the membrane profile decreases via damped oscillations, as in case of the single anchored polymer and the ring polymer, respectively. The profiles for different x_d are shown in Figure 5.1. The integrations are done numerically [56].

5.2 Polymer passing through a membrane

Figure 5.2: Polymer which is transported through the membrane.
The pictures are taken from a Monte Carlo simulation and show subsequent steps of the translocation process.

The perturbative calculation allows us to generalize the previous calculations of polymers anchored on one side to the situation of polymers which are anchored on both sides of the membrane. The induced curvature is given by the sum of all single polymer contributions. Especially there is no net effect on the membrane curvature if there is an equal number of polymers anchored on both sides.

An important biological system where the method can be applied is provided by the translocation of DNA through the cell membrane. Recently models have been studied in which the DNA passes through a pore in the membrane [77, 78]. The pore represents an entropic barrier, which the polymer has to pass. Once a pore has formed there is a certain probability that one end of the polymer/DNA enters. The simplest driving force which now pulls the polymer into the cell would be a concentration gradient between DNA outside and inside the cell. Another possible mechanism is due to diffusion of the polymer through the pore. Those parts which are already inside the cell are decorated by larger molecules such that it is not possible for the chain to step back to the outside and the diffusion becomes directed. Another mechanism might be a molecular motor inside the membrane which threads the polymer through it.

It is still not clear, if the DNA is translocated linearly through a small pore. An alternative process would be a packing of the DNA such that the molecule can enter the cell as a compact object. One can estimate the passage time for this process theoretically [79, 80]. The translocation time τ for large polymers is found to scale as $\tau \sim N^2$ if there is no concentration gradient. The translocation time scales linear with N if there is a small concentration gradient on both sides of the impenetrable wall. This is in agreement with experimental results [81] in which single-stranded RNA and DNA molecules pass through a 2.6-nm diameter ion channel in a lipid bilayer membrane.

In the following we are not going to study the dynamics of such a process, but the single steps of the translocation. In each equilibrated step the polymer influences the membrane shape and curvature and due to its pres-

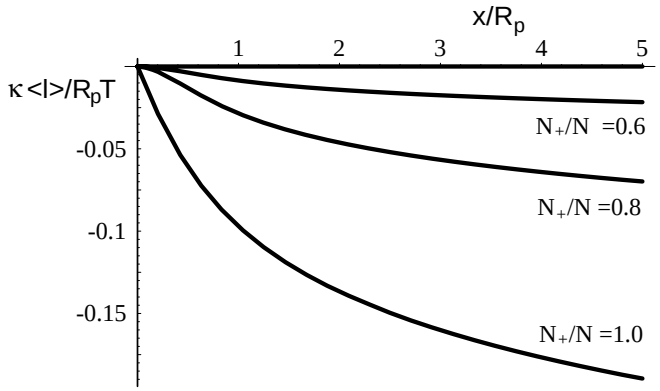

Figure 5.3: The shape profile for a polymer which threads through the membrane. Initially, all monomers are on top of the membrane, corresponding to $N_+/N = 1$. If half of the polymer is on top and half below the membrane, the average profile is flat. Of course, the diagram is continued by mirroring the profiles if more monomers are below the membrane, corresponding to $N_+/N < 0.5$.

ence suppresses membrane fluctuations in the vicinity of the pore. This might lead to additional effect which influence the translocation dynamics.

If the total number of monomers of the polymer is N we start with a configuration where all the monomers are on one membrane side. The intermediate steps are given by configurations where N_+ monomers are above and N_- monomers are below the membrane, such that $N_+ + N_- = N$. The configuration can be decomposed in two polymers anchored on top and below, respectively. The position of the anchor is identical. As a simple consequence, if half of the polymer passed the membrane, the membrane profile is flat, since the effects of both polymers cancel identically. The end configuration, where the DNA passed through, induces, of course, a shape profile of opposite sign.

The free membrane profiles for different values of N_+/N are shown in figure 5.3.

Chapter 6

External Force Fields

In this chapter, we will investigate the behavior of the polymer/membrane system influenced by external forces. There are two cases which we are going to study.

In the first section we include a membrane surface tension Σ , which might arise from lateral forces applied to the membrane, as depicted in figure 6.1. Without such forces the surface tension of lipid bilayers is negligible in comparison to the bending rigidity.

The second section deals with perpendicular forces applied locally both to the membrane and to the polymer. One can explicitly calculate the membrane shape which arises from a force applied in one point. Furthermore, we study forces which act on the end bead of the anchored polymer.

6.1 Membranes under surface tension

Figure 6.1: Schematic picture of the a membrane under the influence of lateral forces, which leads to a surface tension Σ.

It is relatively simple to include surface tension in the theory. The only part which is changed is, of course, the membrane kernel as given by eq. (2.44) which we immediately write down in Fourier space

$$\tilde{K}(q) \;=\; \frac{T}{\kappa q^4 + \Sigma q^2 + v_2}\,. \tag{6.1}$$

In the following investigations the confining potential can be neglected, thus $v_2 = 0$.

The membrane shape profile is again given by eq. (2.48) with the Fourier transformed pressure as derived in eq. (2.50). The kernel $\tilde{K}(q) = T/(\kappa q^4 + \Sigma q^2)$ includes the surface tension. The shape changes for increasing Σ compared to the surface free membrane are shown in fig. 6.2. In the limit of small anchoring distance the shape always approaches a cone, whereas far away from the anchor point the profile is exponentially damped for non-vanishing values of Σ and thus becomes flat for large distances of x. Contrary to the case of a confining membrane potential, which previously regularized

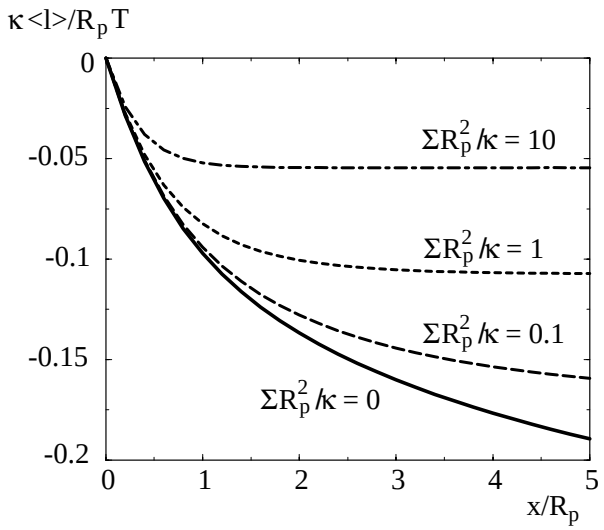

Figure 6.2: The membrane profile for non-vanishing bending rigidity κ and different values of the surface tension Σ. There is no confining potential acting on the membrane.

the shape and lead to an exponentially damped oscillation, is case of surface tension the damping is monotonous.

For $\Sigma = 0$ the asymptotic profile is a catenoid, as already calculated in chapter 2.

6.2 Locally applied forces

In this section we will consider the situation of a force acting on the polymer/membrane system. There are various situations, one can think of. For example we can apply a force which pinches the membrane in one point. In a first step we will calculate the membrane shape, which arises from such a single point perturbation on the membrane. In the following step we consider the additional effect of the anchored polymer.

If the force acts on the anchor point of the polymer the situation is rather easy, since both, the force effect and the polymer effect on the membrane add up in a linear superposition. The resulting shape profile is a linear superposition of the force induced membrane shape and the shape related to polymer pressure which we calculated in the previous chapter.

This changes if we consider forces which act on any other bead of the polymer than the anchor bead. In this case, due to the presence of the force, the whole configuration of the polymer will be changed and consequently the pressure of the polymer differs from the situation of the unperturbed system.

From the experimental point of view the latter situation is of special interest. One could anchor a latex sphere to the free end of the chain and move the latex sphere by optical tweezers. Using this method it is easy to apply a force in the perpendicular direction to the membrane surface. The resulting shape profile and membrane curvature as well as the distribution of the polymer segments can be measured.

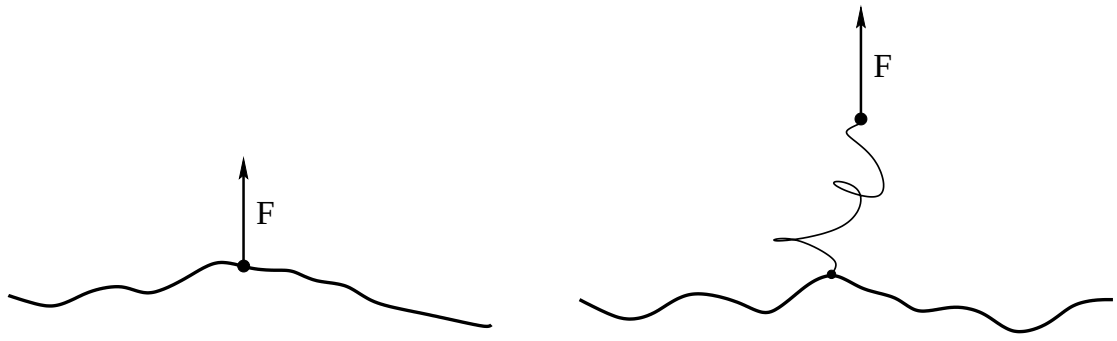

Figure 6.3: Schematic picture: (a) Force, which acts directly on the membrane. (b) Force acting on the free end of the anchored polymer. The displayed figures correspond to a snapshot configuration. Experimentally, the force can be induced by optical tweezers.

6.2.1 Membrane

A force F which is applied to the membrane in the positive z-direction represents a pull on the membrane and leads to the x-dependent pressure term

$$P(\underline{x}) \quad = \quad -\frac{F}{T}\delta(\underline{x}) \tag{6.2}$$

where $F > 0$. The Fourier transform is given by $\tilde{P}(\underline{q}) = -F/T$. Inserting into the expression for the shape profile one finds

$$\langle l(x)\rangle \quad = \quad \frac{F}{T}\int_0^\infty \frac{\mathrm{d}q}{2\pi}\, q\tilde{K}(q)J_0(qx)\,. \tag{6.3}$$

Since we apply a constant outer force on the membrane it is necessary to confine the membrane by a harmonic potential or to fix the membrane at a boundary in order to ensure a counteracting force. If we introduce the potential parameter v_2 in order to locate the membrane around 0 we find the shape profile

$$\langle l(x)\rangle \quad = \quad \frac{1}{4\pi}\frac{F}{\kappa}\xi_{||}^2\,\mathrm{kei}\left(\frac{\sqrt{2}x}{\xi_{||}}\right) \tag{6.4}$$

with the Thomson function kei. In this formula we use the parallel correlation length of the membrane $\xi_{||} = (4\kappa/v_2)^{1/4}$, see eq. (3.11) in chapter 3. For large arguments the limiting behavior of kei is given by an exponentially damped oscillation, see appendix B. The wavelength of the oscillations is determined by $\xi_{||}$, which is the only remaining length scale in this problem. For small distances from the origin the profile attains a paraboloid-like shape. The profile, which interpolates between both regions is displayed in figure 6.4.

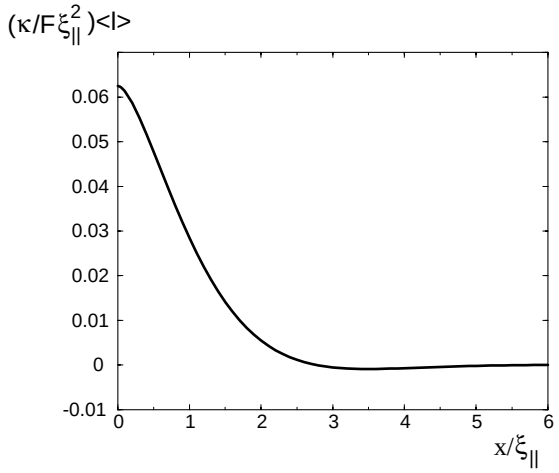

Figure 6.4: Shape profile of a membrane with force acting in the origin.

6.2.2 Polymer end point

In the following we consider the geometry of a force pulling at the free end of the polymer. If the force pulls in the positive z-direction the discretized Hamiltonian for $F > 0$ is

$$\mathcal{H} = \frac{3T}{2R_p^2} \sum_{i=1}^{N} \Delta s \left(\frac{z_i - z_{i-1}}{\Delta s} \right)^2 - F z_N \ . \tag{6.5}$$

We can rewrite this Hamiltonian

$$\mathcal{H} = \frac{3T}{2R_p^2} \sum_{i=1}^{N} \left\{ \Delta s \left(\frac{z_i - z_{i-1}}{\Delta s} \right)^2 - F(z_i - z_{i-1}) \right\} \tag{6.6}$$

which shows that the force applied to the end point distributes uniformly to each bond, i.e. the same force acts on each single monomer of the chain. Thus we can immediately write down the partition function for the polymer starting at z_0 and ending at z and take into account the half space solution which we need in the z-direction. We end up with

$$\mathcal{Z}_F(z_0, z|s) = \sqrt{\frac{3}{2\pi s}} \frac{1}{R_p} \left[\exp\left(-\frac{3}{2s} \frac{(z - z_0)^2}{R_p^2} \right) - \exp\left(-\frac{3}{2s} \frac{(z + z_0)^2}{R_p^2} \right) \right] \exp\left(\frac{F}{T} z \right) \ . \tag{6.7}$$

Due to the Gaussian weights, the configuration of the polymer in the x_1- and in the x_2-direction is not affected by a force in the z-direction.

Analogous to the previous investigations we can now calculate the membrane shape. In order to control the calculation it is necessary to expand for small forces F, since several integrations are not solvable analytically. We end up with a linear correction term in F which adds to the unperturbed profile, i.e. the profile without acting force. The total shape is the sum of the unperturbed shape and the force induced perturbation, i.e. $\langle l(x) \rangle = \langle l(x) \rangle_0 + \langle l(x) \rangle_F$. For small distances x from the anchor

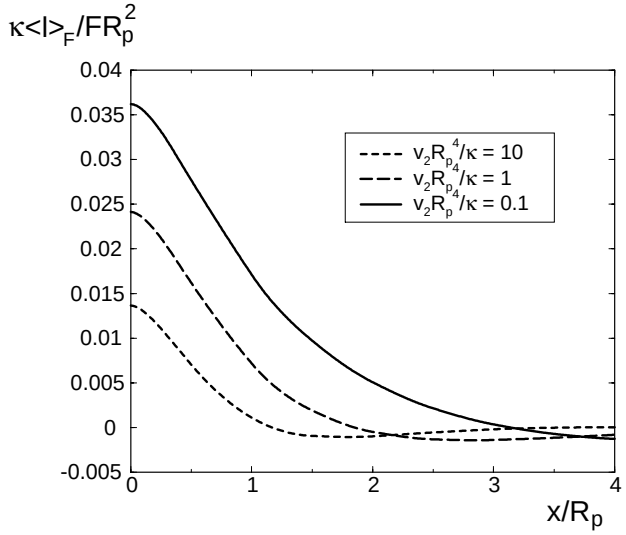

Figure 6.5: Correction term to the shape profile for various values of the confining membrane potential. The profile is obtained numerically [82, 56].

one finds the following limiting behavior of the profile correction:

$$\begin{aligned}\langle l(x)\rangle_F &= \frac{FR_p^2}{\kappa}\left[\left|c_0\left(\frac{v_2}{\kappa}R_p^4\right)\right| + \right. \\ &\left. + \frac{1}{16\pi^2}\left(\frac{x^2}{R_p^2}\right)\left(12-2\pi-\pi^2+(3\pi-8)\gamma+(3\pi-8)\ln\left(\frac{3}{2}\frac{x^2}{R_p^2}\right)\right)\right] \quad (6.8)\end{aligned}$$

where γ denotes the Euler constant and c_0 is a constant which depends on the potential parameter v_2. c_0 is the height of the profile correction in the anchor point. As one would expect, the correction is large in the anchor point and decreases by damped oscillations for large distances.

The limit of high forces is trivial, since it corresponds to the situation of a force pulling directly at the anchor segment of the membrane. Because the polymer is totally stretched in the direction of the force the polymer pressure does not have any effect in this limit. Thus, we obtain the same profile as in the case we previously studied in section 6.2.1.

Chapter 7

Adsorbed Polymers: Contact Potential

In this chapter, we focus on the adsorption behavior of polymers, which are attached to the membrane by one end. In addition to the situation of a purely repulsive hard core interaction between the membrane and the polymer segments, we will now take into account short-ranged attractive interactions between membrane and polymer [83, 84, 85]. The origin of these short-ranged interactions might for example be a screened electrostatic interaction between membrane and polymer.

In general, the adsorption problem is treated for polymers in solutions [86], which are influenced by an attractive or repulsive surface [83]. There is a controversial discussion about the adsorption behavior on curved surfaces [87, 88] and consequently on the induced spontaneous curvature of fluctuating surfaces, which are influenced by the solution. We will investigate the latter problem in chapter 9.

For simplicity, we will restrict ourselves, as we did in the previous calculations, to θ-solvents, where the excluded volume contribution of the polymer segments is balanced by their van der Waals interaction. This justifies to consider our polymer as an ideal chain with Gaussian weights.

In the following, we will come back to the formalism which we introduced in the previous chapter to derive shape profiles, spontaneous curvature and related quantities of the compound polymer-membrane system. We will generalize these calculations taking into account the attractive interaction potential, which allows us to study the desorption/adsorption behavior of the polymer on the fluctuating membrane, as we change the strength of the potential.

7.1 Interaction potential

It is shown in Appendix A that the path integral, which one can write down for the ideal chain partition function $\mathcal{Z}(\mathbf{r}_0, \mathbf{r}|s)$ of a polymer which starts at the spatial position $\mathbf{r}_0$ and ends at $\mathbf{r}$ with internal length $s \in [0, 1]$ corresponding to the number of monomers in the chain, is the solution of the Schrödinger-type equation

$$\left[\frac{\partial}{\partial s} - \frac{R_p^2}{6}\Delta_{\mathbf{r}} + \frac{V(\mathbf{r})}{T}\right] \mathcal{Z}(\mathbf{r}_0, \mathbf{r}|s) \quad = \quad 0 \,, \tag{7.1}$$

with $V(\mathbf{r}) = Nv(\mathbf{r})$ and $v(\mathbf{r})$ denoting the potential per bond. The corresponding initial condition for the partition function is given by

$$\mathcal{Z}(\mathbf{r}_0, \mathbf{r}|s \equiv 0) = \delta(\mathbf{r}_0 - \mathbf{r}) \,. \tag{7.2}$$

In the calculations we did so far, the only interaction between polymer and membrane was given by their impenetrability. The corresponding boundary condition for the polymer on the membrane surface, namely

$$\mathcal{Z}(\mathbf{r}_0, \mathbf{r}|s) = 0 \quad \text{for all } \mathbf{r} \text{ on the membrane.} \tag{7.3}$$

transfers into the potential

$$V(\mathbf{r}) = \begin{cases} \infty & \text{for all } \mathbf{r} \text{ on and below the membrane,} \\ 0 & \text{for all other } \mathbf{r}. \end{cases} \tag{7.4}$$

It is not possible to solve the Schrödinger-type equation with such an $\mathbf{r}$-dependent potential given by the fluctuating membrane.

The major simplification of our calculation in the previous chapters is due to the expansion in the membrane height $l(\underline{x})$, with which we could map the problem of anchoring on the membrane to the related situation of a polymer anchored on a flat surface, i.e. a polymer in the half space.

In the following we will take into account an additional short-range interaction given by

$$V(\mathbf{r}) = \begin{cases} \infty & \text{for all } \mathbf{r} \text{ on and below the membrane,} \\ V_I(\mathbf{r}) & \text{for all } \mathbf{r} \text{ with distance above the membrane surface smaller than } x_V, \\ 0 & \text{for all other } \mathbf{r}. \end{cases} \tag{7.5}$$

Since the potential is short-ranged the polymer bonds only interact with those membrane segments which are closest to them.

It is not clear from the beginning, that the included potential is also transferred into a potential which only acts in the z-direction perpendicular to the surface. In order to proof this, we briefly have a closer look at the original calculation.

7.1.1 Spatial dependence of interaction potential

The important quantity is the polymer partition function, see eq. (2.5) where we now include the potential V:

$$\mathcal{Z}_p\{l\} \;=\; \int' \mathcal{D}\{\mathbf{r}\}\; \delta[\underline{r}(0)]\, \delta[r_3(0) - l(\underline{0})] \exp\left(-\frac{3}{2R_p^2} \int_0^1 \mathrm{d}s \; \left[\frac{\mathrm{d}\mathbf{r}(s)}{\mathrm{d}s}\right]^2 - \int_0^1 \mathrm{d}s \; \frac{V(\mathbf{r}(s))}{T} \right) \tag{7.6}$$

where the prime at the path integral indicates, that the polymer beads in the z-direction are restricted by the membrane. The potential is determined by the distance η_D of the bead to the membrane surface obtained from the straight line which goes through the bead position and intersects the membrane surface perpendicularly. Therefore, we determine the tangential plane in this intersection point to calculate the distance of the polymer bead to this plane, see fig. 7.1. All points of the membrane surface are described by the position vector

$$\mathbf{l} \;=\; \begin{pmatrix} x_1 \\ x_2 \\ l(x_1, x_2) \end{pmatrix} . \tag{7.7}$$

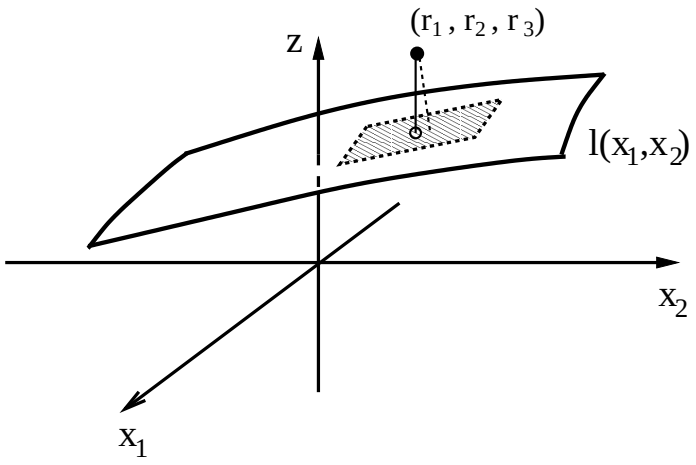

Figure 7.1: Schematic picture: The polymer bead is located at position (r_1, r_2, r_3) above the membrane surface, which is parameterized by $l(x_1, x_2)$.

The normal vector of the surface is given by

$$\mathbf{n} = \left(\frac{\partial \mathbf{l}}{\partial x_1} \times \frac{\partial \mathbf{l}}{\partial x_2}\right) \Big/ \left|\frac{\partial \mathbf{l}}{\partial x_1} \times \frac{\partial \mathbf{l}}{\partial x_2}\right| = \frac{1}{N} \begin{pmatrix} -\partial_{x_1} l \\ -\partial_{x_2} l \\ 1 \end{pmatrix} \tag{7.8}$$

with normalization

$$N = \sqrt{1 + \left(\frac{\partial l}{\partial x_1}\right)^2 + \left(\frac{\partial l}{\partial x_2}\right)^2} \, . \tag{7.9}$$

Assuming, that all gradients of $l(x_1, x_2)$ are small, which is true for our ansatz, we can in first order approximation describe the surface as a plane, containing the point $(r_1, r_2, l(r_1, r_2))$, which is the surface point below the polymer bead. Then the Hesse form of the surface is given by

$$\frac{1}{N} \left[\begin{pmatrix} x_1 \\ x_2 \\ l(x_1, x_2) \end{pmatrix} - \begin{pmatrix} r_1 \\ r_2 \\ l(r_1, r_2) \end{pmatrix} \right] \begin{pmatrix} -\partial l/\partial x_1 \\ -\partial l/\partial x_2 \\ 1 \end{pmatrix} = 0 \, . \tag{7.10}$$

The distance of the polymer bead at position (r_1, r_2, r_3) is found by inserting the position vector into the Hesse form, i.e.

$$r_D = \frac{1}{N} \left[\begin{pmatrix} r_1 \\ r_2 \\ r_3 \end{pmatrix} - \begin{pmatrix} r_1 \\ r_2 \\ l(r_1, r_2) \end{pmatrix} \right] \begin{pmatrix} -\partial l/\partial x_1 \\ -\partial l/\partial x_2 \\ 1 \end{pmatrix} \, . \tag{7.11}$$

Expanding in powers of $l(x_1, x_2)$ we conclude that

$$\begin{aligned} r_D &= [r_3 - l(r_1, r_2)] \left(1 - \left(\frac{\partial l}{\partial x_1}\right)^2 - \left(\frac{\partial l}{\partial x_2}\right)^2\right) \\ &= [r_3 - l(r_1, r_2)] + \mathcal{O}\left(\left(\frac{\partial l}{\partial x_1}\right)^2, \left(\frac{\partial l}{\partial x_2}\right)^2\right) \, . \end{aligned} \tag{7.12}$$

Since our perturbative calculation is performed to linear order, it turns out, that it is consistent to neglect the second order corrections of the distance. In consequence, the polymer partition function is given by

$$\begin{aligned}\mathcal{Z}_p\{l\} &= \int' \mathcal{D}\{\mathbf{r}\}\ \delta[r_1(0)]\,\delta[r_2(0)]\,\delta[r_3(0)-l(\underline{0})] \\ &\quad \exp\left(-\frac{3}{2R_p^2}\int_0^1 \mathrm{d}s\ [\mathrm{d}\mathbf{r}(s)/\mathrm{d}s]^2 - \int_0^1 \mathrm{d}s\ \frac{V[r_3(s)-l(r_1(s),r_2(s))]}{T}\right) \quad . \quad (7.13)\end{aligned}$$

The substitution $r_3 \to r_3 + l(r_1, r_2)$ leads to the analogue calculation, which we have performed in chapter 2, see eq. (2.14). The expansion in small deviations of l with respect to the flat geometry leads to an effective system, where the polymer is anchored on a flat surface. The monomer potential V, as shown in the above calculation, only depends on the z-direction.

We will therefore, in the following, investigate the adsorption properties of a polymer anchored on the flat substrate. In case of the Gaussian chain one can separate the three spatial coordinates in order to end up with a free polymer in the lateral directions and a half-space polymer in the z-direction, which is influenced by a z-dependent and (x_1, x_2)-independent potential.

7.2 Solution of the Schrödinger-type equation

Starting from (7.1) we will in the following measure the potential in units of T and solve the z-dependent Schrödinger-type equation

$$\left[\partial_s - \frac{R_p^2}{6}\partial_z{}^2 + V(z)\right]\mathcal{Z}(z_0, z|s) = 0 \quad , \ s > 0 \quad (7.14)$$

for the general potential

$$V(z) = \begin{cases} \infty & \text{for } z \le 0 \text{ on the membrane,} \\ V_I(z) & \text{for } 0 < z \le z_V, \\ = 0 & \text{for all } z > z_V. \end{cases} \quad (7.15)$$

with z_V denoting the range of attraction. For the moment it is not necessary to specify the form of the potential in the region $0 < z \le z_V$. The diffusion equation is solved by the method of Laplace transforms [89]. The calculation follows [83]. Using

$$G(z_0, z|t) = \int_0^\infty \mathrm{d}s\ \exp(-st)\mathcal{Z}(z_0, z|s) \quad (7.16)$$

one finds the ordinary differential equation for the propagator $G(z_0, z|t)$

$$\left[-\frac{R_p^2}{6}\partial_z^2 + t + V(z)\right]G(z_0, z|t) = \delta(z_0 - z) \quad . \quad (7.17)$$

This expression is only valid for $t > 0$. Thus, the sign convention we used here is for negative energies. In case of a square well potential with depth w e.g. the situation above could describe a polymer with energy $t < w$ leading to solutions with eigenfunctions $\sin$ and $\cos$ inside the range of

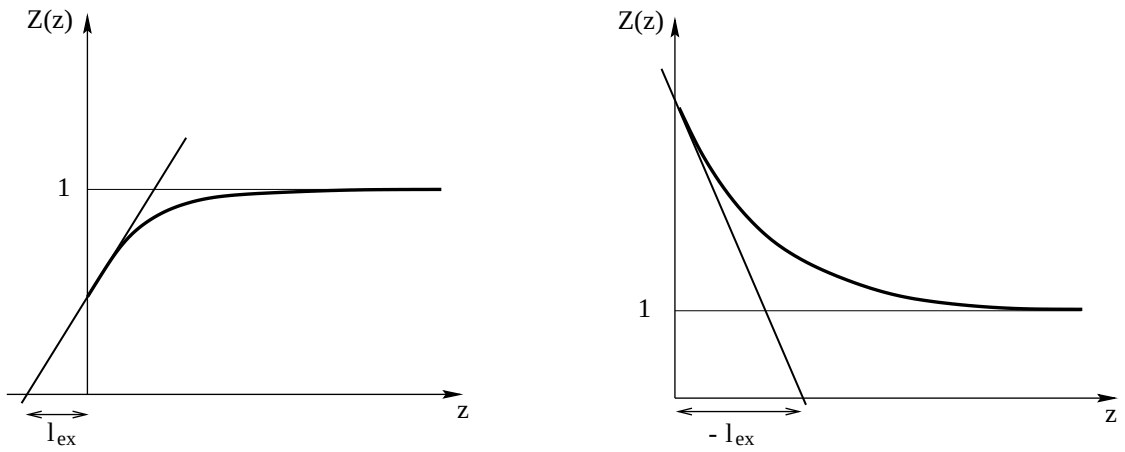

Figure 7.2: Extrapolation length: for desorption l_{ex} is positive (left) and for adsorption l_{ex} is negative (right).

attraction of the potential, and a damped exponential solution outside the attraction range. Eq. (7.17) is solved by the following ansatz [90]

$$G(z_0, z|t) \quad = \quad \psi_0(z_0, t)\ \psi_\infty(z, t) \tag{7.18}$$

where the ψ-parts obey the boundary conditions

$$\psi_0(0, t)\ =\ 0 \quad \text{and} \quad \lim_{z\to\infty} \psi_\infty(z, t)\ =\ 0\ . \tag{7.19}$$

Additionally we have to assume $z_0 \leq z$. Otherwise one has to interchange ψ_0 and ψ_∞.

The solution outside the potential range z_V, where $V(z) = 0$ is thus given by

$$G(z_0, z|t) = A_1 \left[\exp(\sqrt{6}\sqrt{t}\frac{z_0}{R_p}) + A_2 \exp(-\sqrt{6}\sqrt{t}\frac{z_0}{R_p})\right] \exp(-\sqrt{6}\sqrt{t}\frac{z}{R_p}) \quad . \tag{7.20}$$

The remaining constant A_1 is obtained by taking into account the Delta-function on the right site of eq. (7.17). This condition is equivalent to solving the equation

$$\psi_\infty(z)\partial_z\psi_0(z) - \psi_0(z)\partial_z\psi_\infty(z) = \frac{6}{{R_p}^2}\ . \tag{7.21}$$

which yields $A_1 = \sqrt{6}/2\sqrt{t}R_p$.

A_2 is fixed by the continuity and differentiability of G inside and outside the potential range at z_V, which we will investigate now.

Since so far we did not specify the potential for $z \leq z_V$ we consequently do not know the inner solution. Nevertheless we can define the logarithmic derivative at z_V, which corresponds to the boundary condition for both the unknown solution inside the potential range and for the outer solution. The logarithmic derivative in the limit of vanishing potential range $z_V \to 0$ defines a length scale which fully characterizes the potential. This length scale is the so called extrapolation length given by

$$\left.\frac{\partial_z G(z, z_e|t)}{G(z, z_e|t)}\right|_{z=z_V} \quad = \quad \left.\frac{\partial_z \mathcal{Z}(z, z_e|s)}{\mathcal{Z}(z, z_e|s)}\right|_{z=z_V} \quad = \quad \frac{1}{l_{ex}}\ . \tag{7.22}$$

In the following we call $1/l_{ex}$ the inverse extrapolation length, which defined the distance from the adsorption/desorption transition, see below. This transition is a real phase transition only in the limit of infinitely long chains, i.e. for $1/l_{ex} < 0$ the polymer is adsorbed and for $1/l_{ex} > 0$ the polymer is desorbed [91]. In case of finite chains adsorption is only possible if there is a reservoir given by the bulk concentration of polymers. Of course, the extrapolation length is a function of the potential V, which, depending on the special form of V, can be complicated. For a square well potential it is easy to realize that l_{ex} is a function of the depth w of the potential and the range z_V. We will later calculate the exact expression. In this chapter we will emphasize the situation of vanishing range z_V. In this limit, l_{ex} and $1/l_{ex}$, respectively, contain all the information on the potential.

In terms of $1/l_{ex}$ one can identify the following limiting cases

- total desorption for $1/l_{ex} \to \infty$ ($l_{ex} \searrow 0$),
- adsorption/desorption transition at $1/l_{ex} = 0$ ($l_{ex} \to \infty$),
- total adsorption for $1/l_{ex} \to -\infty$ ($l_{ex} \nearrow 0$).

We write down the general solution of a polymer in a half space under the influence of a potential, which we do not specify in detail. The only assumptions on the potential are: $V(z) \to \infty$ for $z = 0$, and $V(z) = 0$ for $z > z_V$. In addition, we demand the potential to scale in such a way that in the limit $z_V \to 0$ the inverse extrapolation length, which governs the adsorption/desorption behavior, stays constant.

The Greens function in the limit $z_V \to 0$ (more accurate $z_V\sqrt{t} \to 0$) is

$$G(z_0, z|t) = \sqrt{\frac{3}{2t}}\frac{1}{R_p}\left[\exp(-\sqrt{6t}\frac{z-z_0}{R_p}) + \frac{\sqrt{6t} - R_p/l_{ex}}{\sqrt{6t} + R_p/l_{ex}}\exp(-\sqrt{6t}\frac{z+z_0}{R_p})\right] . \quad (7.23)$$

The inverse Laplace transformation

$$\mathcal{Z}(z_0, z|s) = \frac{1}{2\pi i}\int_{\mathcal{I}} \mathrm{d}t\; G(z_0, z|t)\exp(st) \quad (7.24)$$

finally leads to the l_{ex}-dependent polymer partition function [51, 50]

$$\begin{aligned}\mathcal{Z}(z_0, z|s) = {} & \sqrt{\frac{3}{2\pi s}}\frac{1}{R_p}\left[\exp\left(-\frac{3}{2s}\frac{(z-z_0)^2}{R_p^2}\right) + \exp\left(-\frac{3}{2s}\frac{(z+z_0)^2}{R_p^2}\right)\right] \\ & -\frac{1}{l_{ex}}\exp\left(\frac{R_p^2}{6l_{ex}^2}s + \frac{z+z_0}{l_{ex}}\right)\operatorname{erfc}\left(\frac{R_p}{l_{ex}}\sqrt{\frac{s}{6}} + \sqrt{\frac{3}{2s}}\frac{z+z_0}{R_p}\right) \quad .(7.25)\end{aligned}$$

The details of the inverse Laplace transformation and the choice of the integration path are described in the appendix C.

Having the partition function of a polymer in a half-space for all strengths of the adsorption potential one can give a more vivid description of the extrapolation length l_{ex}. For a free polymer confined by a flat wall the integrated partition function

$$Z(z) = \int_0^\infty \mathrm{d}z_0\; \mathcal{Z}(z_0, z|1) \quad (7.26)$$

is proportional to the probability of finding the end of the polymer at position z. The corresponding profile is plotted in figure 7.2 in the desorption regime (left), where the probability decreases due

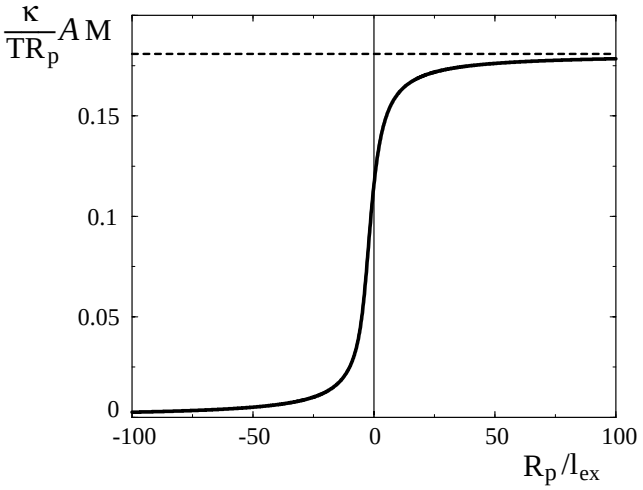

Figure 7.3: The integrated curvature plotted versus the inverse extrapolation length R_p/l_{ex} as obtained by the perturbative approach. The dashed line denotes the limiting curvature for strong desorption.

to depletion in the vicinity of the wall, and in the adsorption regime (right), where the probability increases close to the wall. Far from the wall $Z(z)$ always attains 1 corresponding to the bulk value. Due to the definition as given in eq. (7.22) l_{ex} is the length on the z-axis given by linear extrapolation of $Z(z)$ at $z = 0$, i.e. on the wall. As a consequence the extrapolation length is infinite at the adsorption/desorption transition where $Z(z) = 1$ for all values of z.

7.3 Membrane curvature induced by adsorbed polymers

So far we have considered the polymer and the solution of the Schrödinger-type equation in the half-space. We now come back to the compound polymer/membrane system. As we have already seen in eq. (7.13) the adsorption problem is described by the same partition function as used in chapter 2 with an additional interaction potential acting in the perpendicular direction. Consequently, the perturbative approach which we introduced in section 2.2 also holds in the adsorption regime. Since we can describe the polymer by the partition function (7.25) for all values of l_{ex}, it is possible to calculate the membrane curvature and shape by generalizing the previous investigations to the l_{ex}-dependent case.

The most important formula which we use in the following sections is eq. (2.61), which relates the integrated curvature of the membrane to the mean distance of the polymer end from a flat substrate:

$$\mathcal{A}\overline{M} = \frac{T}{4\kappa}\langle z(1)\rangle_{hs} \ . \tag{7.27}$$

This relation implies, that the membrane curvature does not change its sign for any value of the inverse extrapolation length, because of $\langle z(1)\rangle_{hs} \geq 0$. The remaining task is to determine $\langle z(1)\rangle_{hs}$ with the given l_{ex}-dependent partition functions of the polymer. One finds [92]

$$\mathcal{A}\overline{M} = \frac{T}{4\kappa}\ l_{ex}\left(\frac{\exp(-R_p^2/6l_{ex}^2)}{\mathrm{erfc}(R_p/\sqrt{6}l_{ex})} - 1\right) \tag{7.28}$$

which recovers the limits of total depletion and adsorption. The profile of the integrated curvature as a function of the inverse extrapolation length is plotted in fig. 7.3. In the region of total adsorption the integrated spontaneous curvature of the membrane vanishes, since the expectation value of the z-position of the polymer end point is zero. In consequence, the polymer is located on the membrane and cannot exert any non-vanishing pressure on the membrane. The resulting averaged shape is flat like in the unperturbed case without polymer. Note that this result only holds for a vanishing range of attraction z_V of the interaction potential between polymer and membrane.

It is important to point out, that the calculation we performed uses the partition function of a polymer anchored on a flat surface in order to calculate the spontaneous curvature and the shape profile of the membrane. In this case it is clear that the extrapolation length initially does not depend on the curvature.

This situation changes if one starts with the partition function of a polymer anchored on a curved surface, where it is not clear anymore whether or not the extrapolation length stays curvature independent [93]. This question is of particular interest in case of potentials, which do not explicitly depend on the curvature.

As can be shown for a square well potential of range z_V and depth w on a sphere the inverse extrapolation length yields for small z_V and close to the adsorption transition [87]

$$\frac{1}{l_{ex}} \sim \frac{\pi}{2}\frac{\sqrt{6}}{R_p}\left(\frac{\pi}{2\sqrt{6}}\frac{R_p}{z_V} - \sqrt{w}\right) - \frac{1}{R} \tag{7.29}$$

which corresponds to an extrapolation length

$$l_{ex} = l_0\left(1 + \frac{l_0}{R}\right) \quad \text{with} \quad l_0 = \left[\frac{\pi}{2}\frac{\sqrt{6}}{R_p}\left(\frac{\pi}{2\sqrt{6}}\frac{R_p}{z_V} - \sqrt{w}\right)\right]^{-1} . \tag{7.30}$$

Therefore the extrapolation length is curvature dependent. This is especially important, since the square well potential used here does not explicitly depend on the curvature.

If one considers anchored polymers on a sphere, one compares the free energy difference of the polymer on the curved surface to the flat situation and expands in powers of the curvature $M = 1/R$ of the spherical substrate. One finds

$$\Delta\mathcal{F}_{po}/T \quad = \quad -\ln(\mathcal{Z}/\mathcal{Z}_{hs}) = \Omega_\lambda(\frac{1}{\sqrt{6}l_{ex}}R_p)R_pM + \mathcal{O}((R_pM)^2) \tag{7.31}$$

with the scaling function Ω_λ [44] given by

$$\Omega_\lambda(y) \quad = \quad \frac{1}{\sqrt{6}y}\left[1 - 2\lambda y^2 - \frac{1 - 2\lambda y/\sqrt{\pi}}{\exp(y^2)\mathrm{erfc}(y)}\right] . \tag{7.32}$$

The parameter λ is defined as $\lambda = 1 - l_1/l_0$ with $l_{ex} = l_0(1 + l_1M)$, see eq. (7.29). One has $\lambda = 1$ in the case of the curvature independent extrapolation length and $\lambda = 0$ if the extrapolation length has the form given by the square well potential. The resulting integrated spontaneous curvature is given by

$$\mathcal{A}\overline{M} = -\frac{T}{4\kappa}R_p^2\Omega_\lambda(R_p/\sqrt{6}l_{ex}) \quad . \tag{7.33}$$

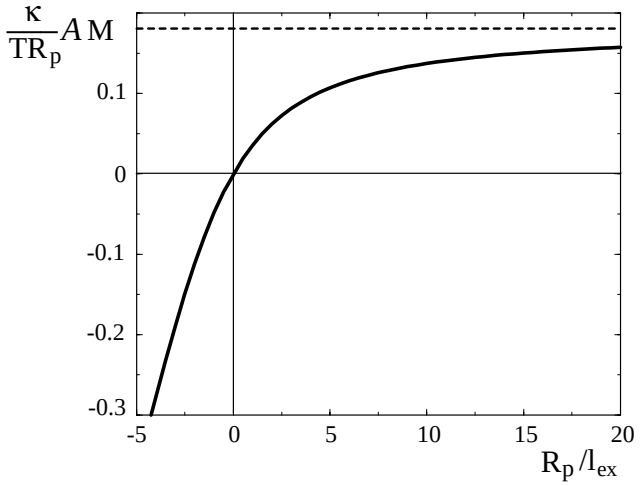

Figure 7.4: The integrated curvature plotted versus the inverse extrapolation length R_p/l_{ex} obtained by a curvature expansion with curvature independent extrapolation length.

For $\lambda = 0$, this result is identical with eq. (7.28). In case of the curvature independent extrapolation length we find, that the curvature of the membrane changes sign at $R_p/l_{ex} = 0$, i.e. at the adsorption-desorption transition and reaches the asymptotic limit of total depletion (large positive R_p/l_{ex}). In case of the strong adsorption limit, the curvature does not vanish, but diverges, as shown in fig. 7.4 . Although in our previous calculation we did not take into account any curvature dependency of the extrapolation length, since we expanded around the flat geometry, we ended up with a result corresponding to a curvature dependent extrapolation length. This might proof, that in the limit of vanishing potential range z_V the extrapolation length attains the universal curvature dependency of the square well potential. We will later extend our calculation to the case of non-vanishing potential range z_V and study the effects on the curvature behavior.

So far we considered the total (spontaneous) curvature of the membrane influenced by the adsorption behavior of the polymer. We will now have a closer look at both the configuration of the polymer and the membrane close to the adsorption/desorption transition and in the strong adsorption case. The restriction to the limiting cases is necessary since it is not possible to calculate analytically the average bead distance of the polymer in the z-direction, namely $\langle z(s)\rangle_{hs}$ as a function of the inverse extrapolation length R_p/l_{ex} for all values of R_p/l_{ex}. For large positive R_p/l_{ex}, we recover the limit of total desorption as can easily be verified.

7.3.1 Adsorption/desorption transition

In the region where $R_p/l_{ex} \simeq 0$ the polymer changes from the desorbed to the adsorbed state. The corresponding partition function is given by a series expansion for small R_p/l_{ex}

$$\mathcal{Z}(z_0, z|s) \approx \sqrt{\frac{3}{2\pi s}}\frac{1}{R_p}\left[\exp\left(-\frac{3}{2s}\frac{(z-z_0)^2}{R_p^2}\right) + \exp\left(-\frac{3}{2s}\frac{(z+z_0)^2}{R_p^2}\right)\right]$$

$$-\frac{1}{l_{ex}}\,\mathrm{erfc}\left(\sqrt{\frac{3}{2s}}\frac{z+z0}{R_p}\right)\,. \tag{7.34}$$

We can now calculate the average distance from the surface which leads to

$$\langle z(s)\rangle_{hs} \;=\; \sqrt{\frac{2}{3\pi}}R_p\sqrt{s}+\frac{R_p^2}{l_{ex}}\frac{2s}{3\pi}\left(\frac{\pi}{4}+\frac{1}{\sqrt{s}}-\sqrt{\frac{1-s}{s}}-\arctan\left(\sqrt{\frac{s}{1-s}}\right)\right)\,. \tag{7.35}$$

Using the average lateral distance

$$\sqrt{\langle x^2\rangle} \;=\; \sqrt{\langle x_1^2\rangle+\langle x_2^2\rangle}=\sqrt{\frac{2}{3}}\sqrt{s}R_p \tag{7.36}$$

the relation between lateral and perpendicular distance at $R_p/l_{ex}=0$ is linear at the adsorption/desorption transition:

$$\langle z(s)\rangle_{hs} \;=\; \frac{1}{\pi}\sqrt{\langle x^2\rangle}\,. \tag{7.37}$$

The pressure at $R_p/l_{ex}=0$ is consequently given by

$$P(\underline{x}) \;=\; \begin{cases} -\infty & x=0 \\ \frac{1}{3}\left(\frac{3}{2\pi}\right)^{3/2}\frac{1}{x^3}\left(\frac{x^3}{R_p^3}(3+\frac{R_p^2}{x^2})\exp(-\frac{3}{2}\frac{x^2}{R_p^2})+\sqrt{\frac{\pi}{6}}\mathrm{erfc}(\sqrt{\frac{3}{2}}\frac{x}{R_p})\right) & x>0 \end{cases}\,. \tag{7.38}$$

The form of the pressure is similar to the depletion case. It is positive for all distances larger than 0 and diverges for small x. In $x=0$ the sign is opposite, which corresponds to the pulling in the anchor point.

Using this pressure we finally obtain numerically the corresponding shape profile as depicted in figure 7.5. In addition, we plotted the corrections in R_p/l_{ex} in the vicinity of the adsorption/desorption transition. The analytic expression for the shape profile at $R_p/l_{ex}=0$ is given by

$$\begin{aligned}\langle l(x)\rangle-\langle l(0)\rangle \;=\; & -\frac{R_p}{4\pi}\frac{T}{\kappa}\left\{\frac{x}{R_p}\mathrm{erfc}\left(\sqrt{\frac{3}{2}}\frac{x}{R_p}\right)+\right. \\ & \left.+\frac{1}{\sqrt{6\pi}}\left[\gamma+2\left(1-\exp\left(-\frac{3}{2}\frac{x^2}{R_p^2}\right)\right)+\mathrm{E}\left(1,\frac{3}{2}\frac{x^2}{R_p^2}\right)+\ln\left(\frac{3}{2}\frac{x^2}{R_p^2}\right)\right]\right\}\end{aligned} \tag{7.39}$$

where γ is the Euler constant and $\mathrm{E}(1,z)$ is the elliptic integral of the second kind [55]. The asymptotic limits are given by the cone for small x, as in the case of the totally desorbed polymer

$$\langle l(x)\rangle-\langle l(0)\rangle \;\sim\; -\frac{1}{4\pi}\frac{T}{\kappa}x \tag{7.40}$$

and by the catenoid for large distances from the anchor point

$$\langle l(x)\rangle-\langle l(0)\rangle \;\sim\; -\frac{1}{4\pi}\frac{R_p}{\sqrt{6\pi}}\frac{T}{\kappa}\left(2+\gamma+\ln\left(\frac{3}{2}\frac{x^2}{R_p^2}\right)\right)\,. \tag{7.41}$$

The integrated curvature yields

$$\mathcal{A}\overline{M} \;=\; \frac{1}{2\kappa}\left(\frac{R_p}{\sqrt{6}}\frac{1}{\sqrt{\pi}}+\frac{R_p^2}{6l_{ex}}\left(\frac{2}{\pi}-\frac{1}{2}\right)\right) \tag{7.42}$$

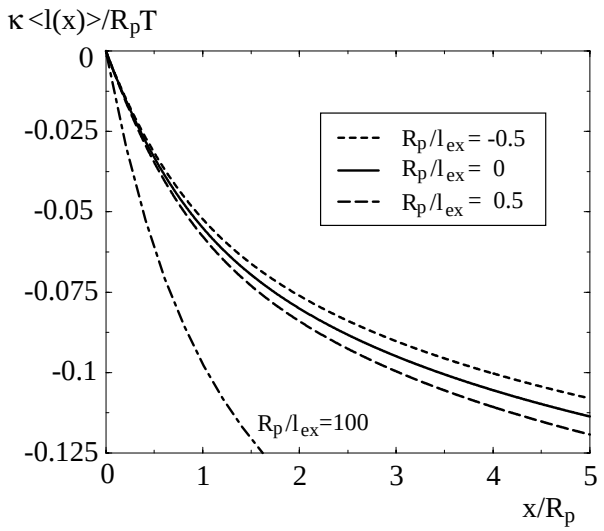

Figure 7.5: The membrane shape profile for the adsorption/desorption transition around $R_p/l_{ex} = 0$. In addition, we plot the profile in the strong desorption limit.

which we expanded to linear order in the inverse extrapolation length R_p/l_{ex}. At the adsorption/desorption transition the membrane shape is similar to the situation of total depletion. The only difference is due to the magnitude of the sharp bend at the anchor, which is smaller at $R_p/l_{ex} = 0$.

The integrated curvature is by factor of $2/\pi$ smaller than in the desorption case which indicates that the effect on the membrane exerted by the polymer is decreased if adsorption is included.

7.3.2 Total adsorption

Denoting $R_p/l_{ex} = -R_p/|l_{ex}|$ one finds the expression for the limiting solution

$$\begin{aligned} \mathcal{Z}(z_0, z|s) \quad \sim \quad & \sqrt{\frac{3}{2\pi s}} \frac{1}{R_p} \left[\exp\left(-\frac{3}{2s} \frac{(z-z_0)^2}{R_p^2} \right) - \exp\left(-\frac{3}{2s} \frac{(z+z_0)^2}{R_p^2} \right) \right] \\ & + \frac{2}{|l_{ex}|} \exp\left(\frac{s}{6} \frac{R_p^2}{|l_{ex}|^2} - \frac{z+z_0}{|l_{ex}|} \right) \ . \end{aligned} \tag{7.43}$$

The limit of total adsorption leads to a subtle behavior of all related quantities except for the integrated curvature as we will show in the following.

The expectation value $\langle z(s) \rangle_{hs}$ attains the limiting behavior

$$\langle z(s) \rangle_{hs} \quad \sim \quad \begin{cases} 0 & s = 0 \\ |l_{ex}|/2 & 0 < s < 1 \\ |l_{ex}| & s = 1 \end{cases} \ . \tag{7.44}$$

It is not possible to obtain a more controlled expansion for large $R_p/|l_{ex}|$. The mathematical reason for this is the combination of $R_p/|l_{ex}|s$ and $R_p/|l_{ex}|(1-s)$ in $\mathcal{Z}(z_0, z|s)$ and $\mathcal{Z}(z, z_e|1-s)$ respectively. The limit for large $1/|l_{ex}|$ is always in conflict with the limit of small s and the limit $s \approx 1$. Thus,

from the beginning we have to split off the cases $s = 0$ and $s = 1$ in order to perform the calculations separately.

Investigating eq. (7.44) we immediately see that the dominating length scale for strong adsorption is, as expected, the extrapolation length l_{ex}. The polymer is located in a distance from the adsorbing surface between 0, the z-position of the anchor point fixed on the surface, and $|l_x|$, the distance of the polymer end bead. For all other beads of the polymer, the average distance from the surface is half the extrapolation length. In the limit of total adsorption $R_p/|l_{ex}| \to \infty$ the polymer is located on the surface. However, the mathematical discontinuity for $s = 0$ and $s = 1$ stays valid and contributes to the polymer pressure. In fact, the only contribution to the pressure arises form the anchor point and the end point, since for all other beads $\mathrm{d}\langle z(s)\rangle_{hs}/\mathrm{d}s$ is zero and in consequence the corresponding pressure vanishes. Using

$$\frac{\mathrm{d}}{\mathrm{d}s}\langle z(s)\rangle_{hs} \quad = \quad \frac{|l_{ex}|}{2}\Big[\delta(s) + \delta(s-1)\Big] \tag{7.45}$$

leads for $R_p/|l_{ex}| \to \infty$ to the pressure

$$P(x) \quad \sim \quad \begin{cases} -\infty & x = 0 \\ \frac{9}{4\pi}\frac{1}{R_p^3}\frac{|l_{ex}|}{R_p}\left(\frac{3}{2}\frac{x^2}{R_p^2} - 1\right)\exp\left(-\frac{3}{2}\frac{x^2}{R_p^2}\right) & x > 0 \end{cases} . \tag{7.46}$$

The x-dependent part is nothing but the monomer pressure $P(s = 1, x)$ of the last polymer bead.

Finally one obtains the membrane shape profile

$$\langle l(x)\rangle - \langle l(0)\rangle \quad \sim \quad -\frac{T}{8\pi\kappa}|l_{ex}|\left[\frac{3}{2}\gamma + \frac{1}{2}\Gamma\left(0, \frac{3}{2}\frac{x^2}{R_p^2}\right) + \ln\left(\frac{3}{4}\frac{x^2}{R_p^2}\right)\right] . \tag{7.47}$$

The limiting behavior is given by logarithmic divergences for small and for large distances from the anchor point, respectively. The catenoidal shape close to the anchor point is a new feature which did not occur for the shape profiles in the other limits. It arises from the form of the pressure which exhibits a divergence for $x = 0$ which is not balanced by a divergence of opposite sign for small $x > 0$.

However it is important to realize that the membrane shape profile for all $0 < x < \infty$ scales with $|l_{ex}|$ and therefore vanishes in the limit of total adsorption. From a physical point of view it is clear that the depicted mathematical subtlety is not relevant, since we do not have infinitely extended membranes on the one hand, and we do not have membranes which are continuous on all length scales. On the scales of the lipids the membrane can not be described by the curvature Hamiltonian anymore. Thus, in the limit of small x the divergence in the anchor point, which becomes discontinuous in the limit of large $1/|l_{ex}|$, will never occur. Especially, in all discretized systems with finite membrane size, as given by a Monte Carlo simulation with periodic boundary conditions, the limiting membrane shape for total adsorption is $\langle l(x)\rangle - \langle l(0)\rangle = 0$. The integrated (spontaneous) curvature behaves nicer. Mathematically, it is given by eq. (7.27) and thus only depends on the average z-position of the end point. Inserting leads to

$$\mathcal{A}\overline{M} \approx \frac{T}{4\kappa}|l_{ex}| \tag{7.48}$$

which attains 0 for large $1/|l_{ex}|$. This is well-defined, since in the problematic regions for small and for large x the membrane shape attains a catenoid and consequently a minimal surface with vanishing curvature contribution. Everywhere else, the membrane is flat and does not contribute to the curvature either.

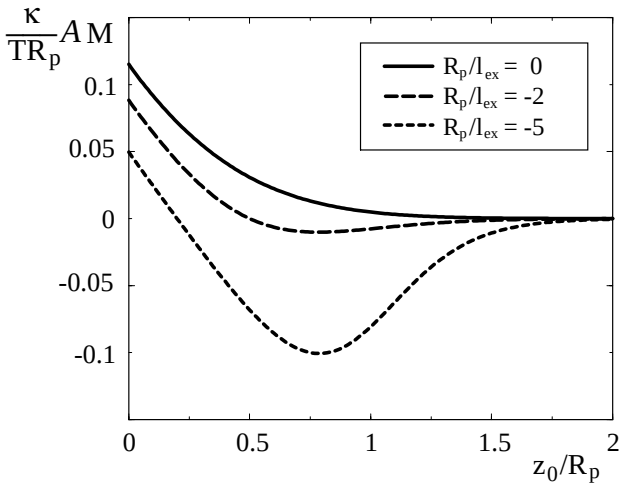

Figure 7.6: The integrated (spontaneous) membrane curvature as a function of the anchor distance z_0 for different values of the inverse extrapolation length R_p/l_{ex}. The curvature changes sign at $z_0 = -l_{ex}$ in the adsorption regime.

7.4 Polymers with non-vanishing anchor distance

In the previous section we studied geometries, in which the polymer was anchored directly on the membrane surface. From a physical point of view it is also interesting to study situations where the polymer is anchored in a distance z_0 from the surface. This is relevant because the anchor segment which is used to insert the polymer in the bilayer has non-vanishing size and normally extrudes from the membrane, see figure 1.4. Since the anchor is chemically different from the rest of the polymer it is justified to start the polymer chain in the anchor distance z_0. The membrane spontaneous curvature is now given by the modified relation

$$\mathcal{A}\overline{M} \;=\; \frac{T}{4\kappa}\left(\langle z(1)\rangle_{hs} - z_0\right) \tag{7.49}$$

where $\langle z(1)\rangle_{hs}$ also depends parametrically on z_0. Using the partition function (7.25) for the averaging one finds

$$\mathcal{A}\overline{M}_{z_0} \;=\; \frac{T}{4\kappa}\left(z_0 + l_{ex}\right)\left[\frac{1}{\operatorname{erf}\left(\sqrt{\frac{3}{2}}\frac{z_0}{R_p}\right) + \exp\left(\frac{R_p}{6l_{ex}}(\frac{R_p}{l_{ex}} + 6\frac{z_0}{R_p})\right)\operatorname{erfc}\left(\frac{R_p/l_{ex}+3z_0/R_p}{\sqrt{6}}\right)} - 1\right]. \tag{7.50}$$

The spontaneous curvature as a function of the anchor distance z_0 is shown in figure 7.6 for different values of R_p/l_{ex}. The important result is the change in the sign of the curvature if z_0 is increased. For large z_0 the curvature approaches zero, since the polymer is not able to influence the membrane anymore. It is easy to show that the curvature sign changes at $z_0 = -l_{ex}$. Thus, we only obtain a negative curvature where the membrane bends towards the polymer, if we are in the adsorption region with $R_p/l_{ex} < 0$. For $R_p/l_{ex} \geq 0$ the curvature stays positive for all values of z_0. In figure 7.6 the limiting plot for $R_p/l_{ex} = 0$ is given by the solid curve. For strong adsorption the curvature

becomes strongly negative for non-vanishing values of z_0. Note, that this does not correspond to a physically realistic limit, since the polymer configuration in this limit has an anchor bond of length z_0 and is therefore strongly over-stretched. The Gaussian model allows these configurations, but physical polymers always have restricted bond lengths.

Let us apply the result to vesicles covered with N_p polymers. The situation is analogue to section 4.2. We consider polymers anchored on the membrane in the adsorption regime. If the polymer is anchored in a distance $|l_{ex}| + l_{an}$ with $l_{an} > 0$ and both $|l_{ex}|$ and l_{an} are small compared to R_p we have guaranteed that the induced curvature is negative. We find for the adsorption-induced curvature the expression

$$M_{sp}^{(ad)} = -\frac{T}{4\kappa} l_{an} B \Gamma_p \tag{7.51}$$

where Γ_p is the polymer coverage-density and B denotes the absolute value of the square bracket in eq. (7.50). Furthermore we find a curvature contribution due to the repulsive polymer/polymer-interaction which is calculated as in eq. (4.11) and which yields

$$M_{sp}^{(pp)} = \frac{T}{4\kappa} b_2 (R_p + |l_{ex}| + l_{an}) \Gamma_p^2 \tag{7.52}$$

where b_2 is the second virial coefficient. Since the latter contribution leads to the opposite curvature compared to $M_{sp}^{(ad)}$ the membrane curvature changes its sign as a function of the coverage density. The density, at which the sign changes, is given by

$$\Gamma_p^* = \frac{B}{b_2} \frac{l_{an}}{R_p + |l_{ex}| + l_{an}} \, . \tag{7.53}$$

For smaller densities the curvature is negative and thus the membrane bends toward the anchored polymers whereas for higher coverage densities the membrane bends away from the polymers. Consequently the coverage density provides a curvature switch.

Chapter 8

Adsorbed Polymers: Square Well Potential

The contact potential, which we discussed in the previous chapter, is an idealized situation. In this chapter, we will extend the previous calculation to a non-vanishing range of attraction z_V of the interaction potential between polymer beads and the membrane. In this case, it is necessary to solve the Schrödinger-type equation inside and outside the potential range. The investigation for finite potential range z_V is necessary in order to compare our results for the Monte Carlo simulation with the theoretical prediction, since we expect deviations from the results for vanishing z_V in the case of our discretized system in the simulation.

8.1 General solution

We start writing down the Schrödinger-type equation as done in the previous chapter, where we already separate the perpendicular direction:

$$\left[\partial_s - \frac{R_p^2}{6}\Delta_z + V(z)\right] \mathcal{Z}(z_0, z|s) = 0 \tag{8.1}$$

with s denoting the internal length which ranges from 0 to 1. The potential is already rescaled with temperature. The equation is solved by Laplace transformation which yields the stationary Schrödinger-type equation

$$\left[t - \frac{R_p^2}{6}\partial_z^2 - w\Theta(z_V - z)\right] G(z_0, z|t) = \delta(z_0 - z)\ . \tag{8.2}$$

Here we already inserted the square well potential of depth w and range z_V.

In our ansatz for solving the equation, we will split the solutions into the three parts denoted in fig. 8.1, namely region I, where the polymer starts and ends in the potential well, region II, where the polymer starts in the well and ends outside the potential range, and region III, where the polymer's start and end point are outside the potential range. We write down the general ansatz:

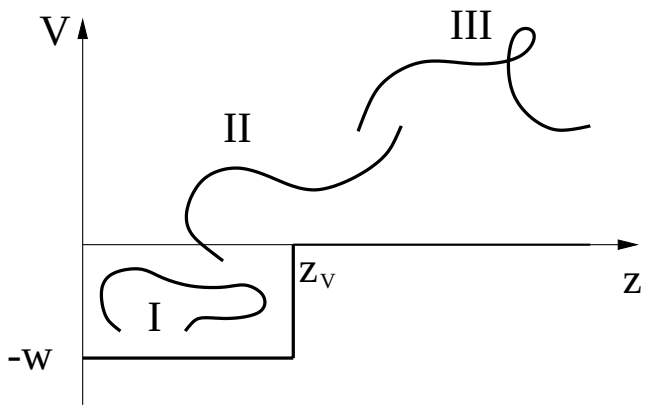

Figure 8.1: Schematic picture of the three regions of solutions for the Schrödinger-type equation.

$$
\begin{aligned}
G_I &= A_1 \sin(\sqrt{6}q\tfrac{z_0}{R_p}) \left[\cos(\sqrt{6}q\tfrac{z}{R_p}) + A_2 \sin(\sqrt{6}q\tfrac{z}{R_p})\right] && z_0 \le z \le z_V \ , \\
G_{II} &= B \sin(\sqrt{6}q\tfrac{z_0}{R_p}) \exp(-\sqrt{6}k\tfrac{z}{R_p}) && z_0 \le z_V \le z \ , \\
G_{III} &= C_1 \left[\exp(\sqrt{6}k\tfrac{z_0}{R_p}) + C_2 \exp(-\sqrt{6}k\tfrac{z_0}{R_p})\right] \exp(-\sqrt{6}k\tfrac{z}{R_p}) && z_V \le z_0 \le z \ ,
\end{aligned}
\tag{8.3}
$$

where q is the wavenumber inside the well, i.e. $q = \sqrt{w-t}$, and $k = \sqrt{t}$ is the wavenumber outside the well. Each of these solutions is the product of two parts, one of which, namely ψ_0, solves the boundary condition for $z \to 0$, and ψ_∞ solves the boundary condition for $z \to \infty$. So far, we have five unknown prefactors which have to be determined by boundary conditions at the matching point of both solutions z_V. A_1 and C_1 are calculated using the fact, that the solutions I and III must correctly reproduce the δ-function for z_0 and z and therefore have to obey the condition (7.21) for the two limiting parts of the solution. One finds

$$
A_1 \;=\; \frac{\sqrt{6}}{R_p}\frac{1}{\sqrt{w-t}} \quad , \quad C_1 \;=\; \frac{\sqrt{6}}{R_p}\frac{1}{2\sqrt{t}} \ . \tag{8.4}
$$

In addition, the continuity and differentiability conditions for G_I and G_{II} at $z = z_V$ with respect to the end point of the polymer and for G_{II} and G_{III} at $z = z_V$ with respect to the starting point of the polymer yield

$$
\begin{aligned}
A_2 &= \frac{q - k\cot(\sqrt{6}q\frac{z_V}{R_p})}{k + q\cot(\sqrt{6}q\frac{z_V}{R_p})} \ , \\
B &= \frac{\sqrt{6}}{R_p}\frac{\exp(\sqrt{6}k\frac{z_V}{R_p})}{q}\left(\cos\left(\sqrt{6}q\frac{z_V}{R_p}\right) + A_2\sin\left(\sqrt{6}q\frac{z_V}{R_p}\right)\right) \quad ,
\end{aligned}
\tag{8.5}
$$

and

$$
\begin{aligned}
C_2 &= \exp\left(2\sqrt{6}k\frac{z_V}{R_p}\right)\frac{1 - q/k\cot(\sqrt{6}q\frac{z_V}{R_p})}{1 + q/k\cot(\sqrt{6}q\frac{z_V}{R_p})} \ , \\
B &= \frac{\sqrt{6}}{R_p}\frac{\exp(\sqrt{6}k\frac{z_V}{R_p})}{k\sin(\sqrt{6}q\frac{z_V}{R_p}) + q\cos(\sqrt{6}q\frac{z_V}{R_p})} \ .
\end{aligned}
\tag{8.6}
$$

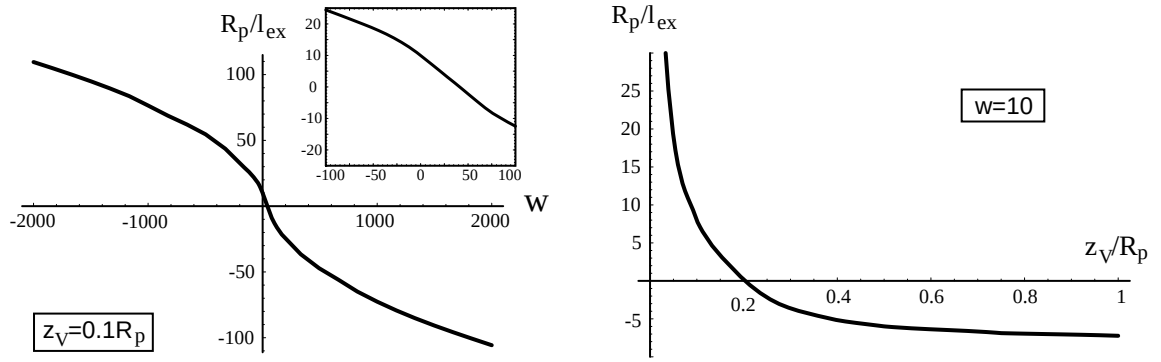

Figure 8.2: The inverse extrapolation length R_p/l_{ex} (a) plotted against the depth of the potential w at fixed value of the potential range $z_V = 0.1R_p$, in the inset: zoom close to the origin. (b) R_p/l_{ex} plotted against the potential range z_V for fixed depth $w = 10$.

It is easy to verify that both expressions for B are identical. Consequently, we do not obtain any further conditions for q and k, i.e. no condition for t.

However, note, that there is a scattering edge for t which separates a continuous spectrum from a discrete one obtained by a finite sum over the eigenstates. The condition for the discrete spectrum arises from G_{II}. Since the eigenfunction inside the potential well is $\sin(\sqrt{6}qz/R_p)$ and the eigenfunction outside $\exp(-\sqrt{6}kz/R_p)$ equating of the function and its derivative at $z = z_V$ yields the transcendental equation

$$k = -q \cot\left(\sqrt{6}q\frac{z_V}{R_p}\right) \ . \tag{8.7}$$

The value of the inverse extrapolation length is given by the logarithmic derivative of the solution inside the potential well evaluated at the first bound state which occurs, namely

$$\frac{1}{l_{ex}} = \frac{\sqrt{6}q_1}{R_p} \cot\left(\sqrt{6}q_1\frac{z_V}{R_p}\right) \ . \tag{8.8}$$

At the adsorption/desorption transition and in the desorption range, in which there are no bound states, the definition is extended to $q_1 = \sqrt{w}$. In figure 8.2 we plot the inverse extrapolation length as a function of the potential depth w for fixed potential range z_V (left) and for fixed w as a function of z_V (right). In the limit of large negative w, i.e. for repulsion out of the inner part, the inverse extrapolation length R_p/l_{ex} diverges to positive infinity, corresponding to the limit of total desorption. The adsorption/desorption transition takes place at the first zero of the cot-function occuring at $w = \pi^2 R_p^2/24z_V^2$. The R_p/l_{ex}-values in the adsorption range are obtained by solving the transcendental condition for q_1 numerically.

The bound states become dominant in the limit of total adsorption for large negative R_p/l_{ex}. In this limit it is justified to neglect the continuum solution.

Due to the transcendental condition for the bound states, it is not possible to calculate the solution in an analytically closed way. To take into account several bound states, the sum has to be evaluated numerically. However, for an infinitely long chain (which of course is not the case in our system) one

can neglect all but the lowest energy level E_1. In this so-called ground state-approximation one can analytically treat the problem. In the limit of small potential ranges $z_V \ll R_p$ we will use the ground state-approximation in order to calculate the membrane curvature.

Our calculation is again split into three parts: We start with the strong desorption regime, which is reached for general values of the potential depth w in the limit of small z_V/R_p, and for large repelling potential inside the well for arbitrary z_V/R_p. In a next step we consider the behavior at the adsorption/desorption transition and finally the limit of total adsorption. In the desorption case as well as at the adsorption/desorption transition we use the continuous solutions, whereas we use the discrete spectrum in case of total adsorption.

8.2 Limit of total desorption

As one can easily verify via eq. (8.8) the limit of total desorption for large positive R_p/l_{ex} can be obtained by two possible ways:

At any value of w kept constant the inverse extrapolation length $1/l_{ex} \sim 1/z_V$ for small z_V and thus approaches the desorption case of large positive R_p/l_{ex}. If one inserts the expansions for small z_V into the solutions G_I and G_{II} of the Schrödinger-type equation the expectation value $\langle z(1)\rangle_{hs}$ for the polymer end point, with which one calculates the spontaneous curvature induced on the membrane, is given by

$$\langle z(1)\rangle_{hs} \;=\; \lim_{z_0\to 0} \frac{\int_0^{z_V} \mathrm{d}z\; z\mathcal{Z}_I(z_0,z|s=1) + \int_{z_V}^{\infty} \mathrm{d}z\; z\mathcal{Z}_{II}(z_0,z|s=1)}{\int_0^{z_V} \mathrm{d}z\; \mathcal{Z}_I(z_0,z|s=1) + \int_{z_V}^{\infty} \mathrm{d}z\; \mathcal{Z}_{II}(z_0,z|s=1)} \; . \tag{8.9}$$

It is advantageous to calculate numerator and denominator separately, using the propagators G_I and G_{II}, expand both in powers of z_V and afterwards perform the inverse Laplace transform. This leads to the controlled expansion

$$\langle z(1)\rangle_{hs} \;=\; \sqrt{\frac{\pi}{6}}R_p + 2z_V\frac{z_V^2}{R_p^2}|w| + \mathcal{O}(z_V^4) \tag{8.10}$$

which via eq. (2.61) yields the spontaneous curvature

$$\mathcal{A}\overline{M} \;=\; \frac{T}{4\kappa}\langle z(1)\rangle_{hs} \;=\; \frac{1}{4}\frac{T}{\kappa}\sqrt{\frac{\pi}{6}}R_p + \frac{1}{2}\frac{T}{\kappa}z_V\frac{z_V^2}{R_p^2}|w| \; . \tag{8.11}$$

As we have expected in the limit of vanishing z_V we recover the result for total desorption, i.e. the result where only the steric repulsion of polymer beads and the membrane surface are taken into account. This holds irrespective of the strength w of the initial square well potential. If we now increase the range z_V without changing w we also increase the mean z-distance of the last bead, which immediately leads to an increase in the induced spontaneous curvature.

There is another possibility of reaching $1/l_{ex} \to \infty$, namely for fixed z_V and $w \to -\infty$. In consequence, the polymer beads are repelled from the potential well (which is a step now). Inside the potential range the solution G_I vanishes for $w \to -\infty$, i.e. there is no polymer bead inside the well except the anchor bead on the surface. The remaining contribution is due to G_{II}. Inserting $q = \sqrt{w-t} = i\sqrt{|w|+t}$ leads to the average z-distance of the polymer end point

$$\langle z(1)\rangle_{hs} \;=\; \left(\sqrt{\frac{\pi}{6}} - \frac{1}{\sqrt{6|w|}}\right) R_p \;+\; z_V \tag{8.12}$$

and to the spontaneous curvature

$$\mathcal{A}\overline{M} \;=\; \frac{1}{4}\frac{T}{\kappa}\left(\sqrt{\frac{\pi}{6}} - \frac{1}{\sqrt{6|w|}}\right) R_p \;+\; \frac{1}{4}\frac{T}{\kappa} z_V \quad . \tag{8.13}$$

First, we note that, as we expect, in the limit of vanishing z_V and large $|w|$, we recover the result for total desorption.

The second feature which is important to point out is, that eq. (8.13) does not contain any expansions for small z_V but only for large $|w|$. Eq. (8.13) is exact for all values of z_V in the limit $|w| \to \infty$. For larger z_V this implies that the Gaussian polymer which is fixed by the anchor bead on the membrane surface, is strongly over-stretched in the first bond between the anchor and the following bead. This leads to the intuitive picture in which the end point of the polymer is shifted by the value of z_V in the z-direction. However, for large z_V this result is not physical anymore, since it plays with an artifact of the Gaussian model. The spring between anchor and next bead can be extended to infinity, which is not true for real polymers. The Gaussian model breaks down in this limit and is consequently not applicable anymore. For small z_V however we expect the predictions of eq. (8.13) to be correct. We will use the relation in order to compare our Monte Carlo data in the region of large positive R_p/l_{ex} and fixed $z_V = 0.1R_p$.

8.3 Behavior at the adsorption/desorption transition

Here we focus on the adsorption/desorption transition at $1/l_{ex} = 0$. The adsorption/desorption transition, where the first bound state (with energy $t = 0$) occurs, is given by the first zero of the righthand-side of eq. (8.8). The solution is

$$\sqrt{6w}\frac{z_V}{R_p} = \frac{\pi}{2} \; . \tag{8.14}$$

The advantage of this restriction to $1/l_{ex} = 0$ is due to the fact, that it is possible to vary z_V without changing the value of $1/l_{ex}$.

Inserting (8.14) into q yields

$$q = \sqrt{\frac{\pi^2}{24}\frac{R_p^2}{z_V^2} - t} = \frac{\pi}{2\sqrt{6}}\frac{R_p}{z_V} - \frac{\sqrt{6}}{\pi} t \frac{z_V}{R_p} + \mathcal{O}(z_V^3) \; . \tag{8.15}$$

In order to calculate the effect on the curvature we again need $\langle z(1)\rangle_{hs}$, i.e. the expectation value for the z-position of the polymer end point. Here, we have to use the different solutions inside and outside z_V. Since the polymer is anchored at $z_0 = 0$ the solution for $z_V < z_0 < z$ (region III) plays no role anymore. Inserting the solutions and expanding in z_V leads to

$$\langle z(1)\rangle_{hs} \;=\; \sqrt{\frac{2}{3\pi}} R_p + \frac{(\pi+4)(\pi-2)}{2\pi^2} z_V + \mathcal{O}(z_V^2) \; . \tag{8.16}$$

As we expect, the first term of the expansion reproduces the result for vanishing z_V at $1/l_{ex} = 0$. Consequently, the membrane curvature

$$\mathcal{A}\overline{M} \;=\; \frac{T}{4\kappa}\left(\sqrt{\frac{2}{3\pi}} R_p + \frac{(\pi+4)(\pi-2)}{2\pi^2} z_V\right) \tag{8.17}$$

is increased further, if one increases z_V.

There is another limiting case which is of interest to study, namely the limiting behavior of the curvature and membrane shape profile for large z_V. It is clear by intuition that in this case we have to obtain the limit of total desorption again, since the polymer is not affected by a potential gradient, i.e. by a force, anymore.

The only Greens function which survives the limiting process (if we neglect the asymptotic corrections in z_V) is G_I. In fact, the insertion of the limiting $q = i\sqrt{t}$ leads to the half space propagator and, in consequence, to the same spontaneous curvature as for total desorption.

8.4 Limit of total adsorption

The limit of total adsorption with large negative R_p/l_{ex} is not characterized by the continuum but by the bound states. If the potential has N_b bound states the solution of the stationary Schrödinger-type equation is given by

$$G(z_0 \to 0, z|t) = \sum_{n=1}^{N_b} \frac{1}{t+E_n} \left(\tilde{G}_I^{(n)} \theta(z_V - z) + \tilde{G}_{II}^{(n)} \theta(z - z_V) \right) \tag{8.18}$$

with the modified Greens functions $\tilde{G}_I^{(n)}$, $\tilde{G}_{II}^{(n)}$ given by

$$\tilde{G}_I^{(n)} = \frac{6}{R_p} q_n \frac{z_0}{R_p} \left(1 + \cot^2(\sqrt{6} q_n \frac{z_V}{R_p}) \right) \sin(\sqrt{6} q_n \frac{z}{R_p}) \quad \text{for } z_0 \le z \le z_V \,, \tag{8.19}$$

$$\tilde{G}_{II}^{(n)} = \frac{6}{R_p} q_n \frac{z_0}{R_p} \csc\left(\sqrt{6} q_n \frac{z_V}{R_p} \right) \exp\left(\sqrt{6} q_n \frac{z - z_V}{R_p} \cot(\sqrt{6} \frac{z_V}{R_p}) \right) \quad \text{for } z_0 \le z_V \le z \,, \tag{8.20}$$

in which the divergences at $k_n = -q_n \cot(\sqrt{6} q_n z_V / R_p)$ are split off. Since the polymer is anchored on the membrane, the solution $\tilde{G}_{III}$ does not occur.

The inverse Laplace transformation yields

$$\mathcal{Z}(z_0, z|s \equiv 1) = \sum_{n=1}^{N_b} \exp(-E_n) \left(\tilde{G}_I^{(n)} \theta(z_V - z) + \tilde{G}_{II}^{(n)} \theta(z - z_V) \right) . \tag{8.21}$$

E_n is the energy level of state n, which is, of course, negative and given by $E_n = -t_n = -(w - q_n^2)$.

The expectation value of the polymer end-point which leads to the integrated membrane curvature is given by

$$\langle z(1) \rangle_{hs} = \lim_{z_0 \to 0} \frac{\sum_{n=1}^{N_b} \exp(-E_n) \left(\int_0^{z_V} \mathrm{d}z \; z \; \tilde{G}_I^{(n)}(z_0, z|1) + \int_{z_V}^{\infty} \mathrm{d}z \; z \; \tilde{G}_{II}^{(n)}(z_0, z|1) \right)}{\sum_{n=1}^{N_b} \exp(-E_n) \left(\int_0^{z_V} \mathrm{d}z \; \tilde{G}_I^{(n)}(z_0, z|1) + \int_{z_V}^{\infty} \mathrm{d}z \; \tilde{G}_{II}^{(n)}(z_0, z|1) \right)} \,. \tag{8.22}$$

For small potential range z_V one can calculate the strong adsorption limit analytically. If we approximate the polymer as an infinitely long chain, which is justified for $z_V \ll R_p$ it is correct to apply the

ground state-approximation, i.e. it is justified to take into account only the lowest bound state with energy E_1. One finds

$$\langle z(1)\rangle_{hs} \;=\; \lim_{z_0\to 0}\frac{\int_0^{z_V}\mathrm{d}z\; z\;\tilde{G}_I^{(1)}(z_0,z|1)+\int_{z_V}^{\infty}\mathrm{d}z\; z\;\tilde{G}_{II}^{(1)}(z_0,z|1)}{\int_0^{z_V}\mathrm{d}z\;\tilde{G}_I^{(1)}(z_0,z|1)+\int_{z_V}^{\infty}\mathrm{d}z\;\tilde{G}_{II}^{(1)}(z_0,z|1)}\;. \tag{8.23}$$

For large negative R_p/l_{ex} the transcendental condition (8.7) yields $q_1 = \pi R_p/\sqrt{6}z_V$. The limiting ground state (gs) solutions are

$$\tilde{G}_I^{(gs)} \;=\; \sqrt{6}\pi\frac{1}{z_V}\frac{z_0}{R_p}D^2\sin\left(\pi\frac{z}{z_V}\right)\;, \tag{8.24}$$

$$\tilde{G}_{II}^{(gs)} \;=\; \sqrt{6}\pi\frac{1}{z_V}\frac{z_0}{R_p}D\exp\left(\pi D\,(1-\frac{z}{z_V})\right)\;, \tag{8.25}$$

where we introduced the factor $D=\lim_{q\to q_1}\csc(\sqrt{6}qz_V/R_p)$ which diverges in the limiting process. Inserting and performing the integration finally yields for total adsorption the important results

$$\langle z(1)\rangle_{hs} \;=\; \frac{z_V}{2} \qquad\text{and}\qquad \mathcal{A}\overline{M} \;=\; \frac{1}{8}\frac{T}{\kappa}z_V\;. \tag{8.26}$$

Note that these results are correct also from an intuitive point of view. The limit of strong adsorption in a square well potential of range z_V in the z-direction is equivalent to the situation of confining a polymer between two parallel plates in a distance z_V. We expect the average position in the z-direction to be $z_V/2$.

However, if z_V is increased we have to take into account higher energy levels, at least the ground state and the neighboring level. The reason for this is the assumption of the infinite polymer length in ground state approximation. Irrespective of the size of z_V the expectation value always stays at $\langle z(1)\rangle_{hs} = z_V/2$. An additional length scale which includes the finite end-to-end distance R_p does not occur. Only if we take into account the second energy level, the additional length scale occurs and respects the finite R_p. This always leads to a lowering of $\langle z(1)\rangle_{hs}$ as we expect. In particular, for large z_V we expect that the bound state contribution leads to an expectation value $\langle z(1)\rangle_{hs}$ which is identical with the result for total desorption and thus governed only by R_p and not by z_V anymore. We will proof this in the following section.

8.4.1 Bound states for large potential range z_V

As we have already seen bound states are given by the condition $q_n = n\pi R_p/\sqrt{6}z_V$ with integer n. The solution which remains in the limit of large z_V is G_I. Inserting q_n one ends up with

$$G_I^{(n)} \;=\; n\pi\frac{\sqrt{6}}{z_V}\frac{z_0}{R_p}\sin\left(n\pi\frac{z}{z_V}\right) \;=:\; n\pi\frac{C}{z_V}\sin\left(n\pi\frac{z}{z_V}\right)\;. \tag{8.27}$$

The prefactor C cancels when calculating averages.

The energies in eq. (8.22) are given by

$$E_n \;=\; -(w-q_n^2)\;. \tag{8.28}$$

Dividing numerator and denominator of eq. (8.22) by $\exp(-E_1)$ yields the numerator

$$\int_0^{z_V}\mathrm{d}z\; z\; G_I^{(1)}+\sum_{n=2}^{N_b}\exp(E_1-E_n)\int_0^{z_V}\mathrm{d}z\; z\; G_I^{(n)}\;. \tag{8.29}$$

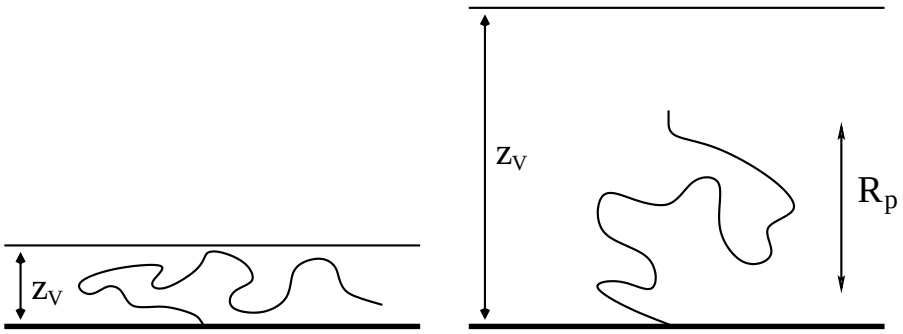

Figure 8.3: Adsorption behavior in the limit of total adsorption for $z_V/R_p \ll 1$ (left) and for $z_V/R_p \gg 1$ (right). The polymer on in the small slot is strongly deformed, whereas the polymer in the large slot is unperturbed.

The denominator follows in analogy. The energy difference is

$$E_1 - E_n \quad = \quad -(n^2-1)\frac{\pi^2}{6}\frac{R_p^2}{z_V^2} =: -(n^2-1)\; x \; . \tag{8.30}$$

The solutions of the integrations are

$$\int_0^{z_V} \mathrm{d}z \; z \; G_I^{(n)} = -\; (-1)^n \; C \; z_V \quad \text{and} \quad \int_0^{z_V} \mathrm{d}z \; G_I^{(n)} = \Big(1-(-1)^n\Big) \; C \tag{8.31}$$

which lead to the average distance

$$\langle z(1) \rangle_{hs} \quad = \quad - \; \frac{\sum_{n=1}^{\infty} (-1)^n \exp(-n^2 x)}{\sum_{n=1}^{\infty} \exp(-n^2 x) - \sum_{n=1}^{\infty} (-1)^n \exp(-n^2 x)} \; z_V \; . \tag{8.32}$$

It is possible to evaluate the sums analytically,

$$S_1 \quad := \quad \sum_{n=1}^{\infty} (-1)^n \exp(-n^2 x) = \frac{1}{2}\Big(\vartheta_4(0|\exp(-x)) - 1\Big) \quad \text{and} \tag{8.33}$$

$$S_2 \quad := \quad \sum_{n=1}^{\infty} \exp(-n^2 x) = \frac{1}{2}\Big(\vartheta_3(0|\exp(-x)) - 1\Big) \; , \tag{8.34}$$

where ϑ are Elliptic theta functions. The limit of large potential ranges z_V is equivalent to the limit of small x, see the definition above. For small x one obtains the asymptotics

$$S_1 \sim -0.5 \;\; \text{and} \;\; S_2 \sim 0.886 \frac{1}{\sqrt{x}} \; . \tag{8.35}$$

The prefactors are evaluated numerically [56].

Inserting into eq. (8.32) finally yields

$$\langle z(1) \rangle_{hs} \quad \approx \quad 0.7238 \; R_p \; \approx \; \sqrt{\frac{\pi}{6}} R_p. \tag{8.36}$$

The result recovers the limit of total desorption. This is expected, since the polymer is not affected by the potential gradient anymore, if the potential step located at z_V is at a much larger distance from the surface than the polymer beads. In consequence, we obtain the same polymer and membrane configuration as in the case of no adsorbing potential, see figure 8.3 .

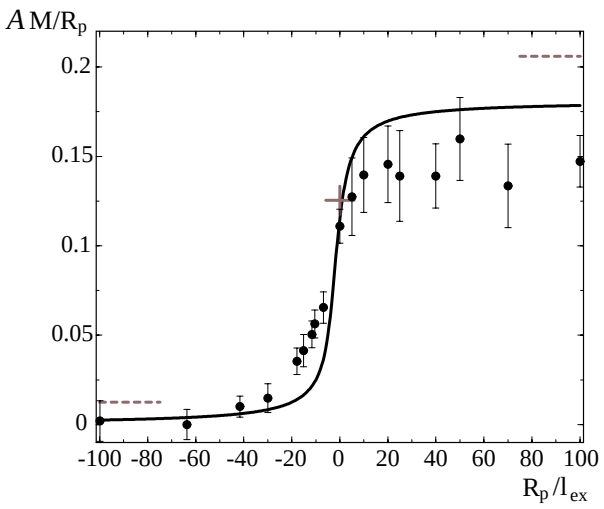

Figure 8.4: The integrated curvature plotted versus the inverse extrapolation length R_p/l_{ex} as obtained by the small gradient expansion for a contact potential and by Monte Carlo simulations. The dashed lines in the limits of strong desorption and adsorption and the cross at the adsorption/desorption transition are the corrections for the square well of range $z_V = 0.1R_p$, which is the potential used in the simulation. The Monte Carlo data is obtained for $\kappa/T = 1$. The membrane discretization is $a_m/R_p = 0.5$ and the polymer discretization $a_p/R_p = 0.0625$.

8.5 Comparison with Monte Carlo simulations

We will now compare the analytic results with Monte Carlo-simulations. As in chapter 3 both membrane and polymer are discretized. The membrane can move continuously in the perpendicular direction above a two dimensional lattice with lattice parameter a_m.

The anchored polymer is described by the bead-spring model, in which the neighboring pointlike beads are coupled by harmonic springs. This model corresponds to an ideal chain. The Kuhn length a_p provides the average bond length. One Monte Carlo step of the compound system corresponds to a single move of each membrane segment and each polymer bead.

We use periodic boundary conditions in the lateral directions. The lateral membrane size is chosen about eight times larger than the polymer end-to-end distance R_p, which corresponds to the dilute coverage (mushroom) regime, i.e. the polymers do not penetrate each other.

The square well potential, which acts on each bond is included by measuring the distance in z-direction of a polymer bead, which represents a bond, and the membrane segment which is located beneath the bead. In order to avoid large discretization effects it is necessary to choose the discretization of the polymer, i.e. the bond length, smaller than the potential range z_V. The interesting quantity which we are going to measure is the induced spontaneous curvature of the membrane. It is not possible to integrate the membrane curvature of all membrane segments, since due to the periodic boundary condition this integral will vanish. Therefore we choose an area of integration corresponding to a circle of radius R_p, which is basically the area in which the polymer interacts with the membrane. The area takes into account the 13 inner segments in the vicinity of the anchor. Results vary slightly if one increases the integration area, but do not change the diagram qualitatively. The major contribu-

tion to the curvature arises from the cone-like bend in the anchor segment. It is therefore justified to choose the area small in order to avoid boundary effects. The integrated curvature as a function of the inverse extrapolation length is shown in figure 8.4. The solid curve displays the analytic solution for the curvature in case of a contact potential. Since in the simulation we do not use a contact potential but a square well of range $z_V = 0.1R_p$ the results of the contact potential will be shifted according to our analytic calculations. The shifts are displayed in the diagram for the limiting cases of strong adsorption and desorption, respectively and for the adsorption/desorption transition.

For strong adsorption the curvature does not vanish, since the polymer moves in a volume of height z_V above the membrane. Thus, it still exerts a pressure, leading to a small but positive membrane curvature, analytically given by $z_V T/8\kappa$ in the limit $1/l_{ex} \to -\infty$. For the values of $z_V = 0.1R_p$ this leads to a shift of $\mathcal{A}\overline{\Delta M} = 0.0125R_pT/\kappa$, which we denoted by the dashed line in the left part of the diagram. At the adsorption/desorption transition we have calculated the shift to higher curvatures if $z_V > 0$, which is given by $\mathcal{A}\overline{\Delta M} \approx 0.04R_pT/\kappa$, denoted by the cross in the diagram at $R_p/l_{ex} = 0$. For strong desorption the shift is given by $\mathcal{A}\overline{\Delta M} = 0.025R_pT/\kappa$ and denoted by the dashed line on the right side of the diagram.

There is a general trend that the simulation data is below the analytic predictions. In addition to the already mentioned effect due to the choice of the integration area there are two important reasons for the difference:

(i) Discretization effects: Since both, the membrane and the polymer are discretized, one expects differences to the analytic predictions. The Kuhn length of the polymer is always chosen smaller than the range of the potential $z_V = 0.1R_p$. We choose a Kuhn length $a_p = 0.0625R_p$, corresponding to 257 beads. We did not increase the system size further due to restriction of calculation time. However, if the Kuhn length of the polymer is chosen larger than the range of the potential, one expects systematic errors, since the potential in the simulation does not act on the bonds but on the polymer beads. Consequently each bead represents one polymer bond. The error is small, if a_p is reduced to lengths which are small compared to z_V. The membrane discretization is determined by the lattice parameter $a_m = 0.5R_p$, corresponding to 289 membrane segments. If one compares results obtained with $a_m = R_p$ with the finer discretization the effect on the integrated curvature is small. Nevertheless, the discretization of the membrane leads to an increase of the curvature (a trend in the correct direction) as one would expect from our results in the total desorption MC simulation. The slope of the cone increases for better discretizations.

(ii) Boundary effects: Since we use periodic boundary conditions the membrane shape profile differs from the free boundary case, which we use in the analytic calculation. This is especially important, since we did not confine the membrane by a harmonic potential, which leads to a finite parallel correlation length. If the parallel correlation length is small compared to the lateral membrane size one expects boundary effects to be small. In case of vanishing confining potential the membrane is a critical object with diverging parallel correlation length and thus always influenced by the system boundaries.

In fig. 8.5 we plot the membrane shape profile for different values of R_p/l_{ex} as obtained by the MC simulation. Additionally we insert the analytic prediction for strong desorption and for the adsorption/desorption transition in case of free membrane boundaries (thick solid curves) and in case of periodic boundaries with a finite amount of Fourier modes (thick dashed lines). At the periodic boundaries the thick dashed profiles become flat, as expected. The slope difference in the anchor point is due to the finite amount of Fourier modes which were taken into account. Apart from the

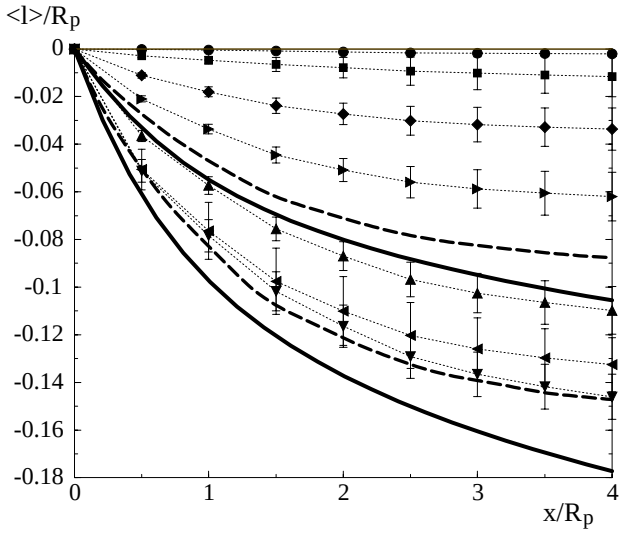

Figure 8.5: Membrane shape profile obtained by MC simulations, using the same parameters as in figure 8.4: For (i) $R_p/l_{ex} = 100$ (triangle down) to compare with the analytic curve for a membrane with free boundaries in the desorption limit (lower thick solid curve) and to compare with the analytic desorption limit for a membrane with periodic boundary conditions (lower thick dashed curve). In the latter case we performed a numerical discrete Fourier transform [56] taking into account 30 Fourier modes. (ii) $R_p/l_{ex} = 25$ (triangle left). (iii) $R_p/l_{ex} = 0$ (triangle up). To compare with the corresponding analytical solution for the membrane with free boundaries (upper thick solid curve) and the analytic profile in periodic boundaries (upper thick dashed curve). (iv) $R_p/l_{ex} = -6.8$ (triangle right). (v) $R_p/l_{ex} = -17.8$ (diamond). (vi) $R_p/l_{ex} = -41.6$ (square). (vii) $R_p/l_{ex} = -100$ (circle).

above mentioned discretization and boundary effects the agreement between analytic calculation and simulation is good.

There is another interesting quantity in our simulation, namely the average squared distance of the first polymer bead, which is anchored on the membrane, and the last bead in the perpendicular direction. It is intuitively clear that this quantity decreases for increasing adsorption, since the polymer is located close to the surface in the strong adsorption limit. In fig. 8.6 we plot the square-root of the average squared end-to-end distance in the z-direction. We compare this quantity with the theoretical prediction for the related half-space distance $\langle z(1)\rangle_{hs}$. of a polymer anchored to a flat surface. However note, that both quantities are mathematically different and refer to different geometries (fluctuating versus flat surface). If we compare with the theoretical prediction for the contact potential and the corrections due to the square well, the agreement is surprisingly good, especially with respect to the square well shift. This confirms the postulated relation (2.61) of our perturbative calculation between the integrated membrane curvature and the average distance of the polymer-end to the flat surface, if one generalizes the latter observable to the situation of a fluctuating boundary as given by the membrane in the simulation.

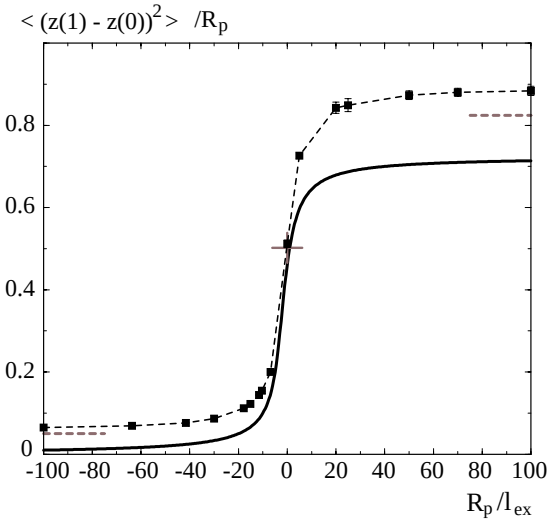

Figure 8.6: The polymer end-to-end distance in the z-direction as obtained by the MC-simulation plotted against the inverse extrapolations length. We compare this quantity with the related theoretical half-space values $\langle z(1)\rangle_{hs}$ for the contact potential (solid) and the square well (dashed corrections).

Chapter 9

Membranes Exposed to Polymer Solutions

In the remainder of this thesis we detach the polymers from the membrane and focus on free polymers in solution. This is a completely different physical situation, since the bending properties of the membrane are now determined by the depletion zone in the vicinity of the surface, whereas in case of the anchored polymer the behavior is governed by the individual pressure distribution induced by each polymer. In terms of entropy, the bending in case of the polymer solution is determined by their translational and configurational entropy, whereas the bending due to anchoring is determined only by configurational entropy.

There are contradictory results concerning the spontaneous curvature of fluctuating surfaces influenced by the polymers. In a paper of Podgornik the spontaneous curvature is predicted to bend the membrane towards the polymer-rich phase in case of adsorption and to bend away for desorption [88, 94], whereas calculations done by Eisenriegler et al. show the opposite behavior [83] and point out mistakes due to the integration boundaries of the polymers in a half-space in [88]. Furthermore, the density profile of the polymers near a spherical particle is studied [95]. In a mean-field approach of Clement and Joanny [96] the spontaneous curvature is determined by the excluded-volume term of the polymer solution, which in second order approximation vanishes for ideal polymers. Recently, the vesicular budding induced by polymers was studied. It is predicted that polymers adsorbed on vesicles initiate budding of the vesicle and thus increase the curvature of the membrane [97]. Furthermore the effect on the membrane rigidity is studied, where some authors predict stiffening due to adsorbed polymers [98, 99], other authors calculate a decrease in the membrane rigidity [100, 101, 102].

As in the previous chapters we discuss the interaction of polymers with the membrane both, entropically and energetically. The polymers do not penetrate the membrane, but can interact with it via a short-range potential. The polymers itself are considered in the θ-regime, where the individual excluded volume interaction along the chain is neglected. In addition we neglect the pairwise interaction of different polymers, which arise from three-point interactions described by the third virial coefficient.

In figure 7.2 we have already shown the concentration profile of polymers in solution close to a wall, depending on the strength of the interaction between wall and polymers. In case of a pure steric repulsion, i.e. in the desorption regime, where there is no additional energetic interaction, the polymers are repelled from the surface in such a way, that the segment density in the vicinity

of the surface decreases to zero. In the other limit of strong adsorption the polymers want to be close to the surface. Consequently, the segment density in the vicinity of the wall increases and diverges for infinite potential strength. The adsorption and the desorption regime are separated by the transition line, where the entropic and the energetic effect cancel such that the concentration profile is constant. i.e. the bulk value of the concentration is maintained at the surface. The control parameter which describes the adsorption behavior is the inverse extrapolation length $1/l_{ex}$. At the adsorption/desorption transition the inverse extrapolation length vanishes.

Since the polymer solution will lead to a homogeneous bending on the membrane, we will in the following calculate the membrane curvature in a small curvature expansion, starting from the initial partition function of the polymers on a curved geometry.

In order to introduce the formalism we will first investigate the simpler system of colloidal particles which interact with a large sphere, but do not interact among themselves. In the limit of pure entropy the partition function of each particle is given by the volume which is accessible, i.e. the volume of the system subtracted by the volume of the depletion zone in the vicinity of a boundary. For a large sphere of radius R surrounded by small colloidal particles of radius R_c this depletion volume is easily calculated,

$$\mathcal{V}_{\rm depl} \;=\; \frac{4}{3}\pi(R+R_c)^3 - \frac{4}{3}\pi R^3 \;=\; \mathcal{A}\left(R_c + \frac{R_c^2}{R} + \frac{1}{3}\frac{R_c^3}{R^2}\right) \tag{9.1}$$

where $\mathcal{A}$ is the lateral area. The first term in the brackets represents the depletion volume of the half-space, whereas the second term contains the correction due to bending. If the sphere bends away from the particles, the depletion volume is increased. Thus, compared to the flat geometry it is favorable for the particles to have a sphere which bends towards them.

In the following we will generalize this argument to the case of polymers, which are in solution under the presence of a curved boundary. The polymers do not interact among each other, but interact with the wall. Consequently the partition function of the particles separate, according to $\mathcal{Z}_{N_p} = [\mathcal{Z}_1]^{N_p}/N_p!$, where $\mathcal{Z}_1$ is the single polymer partition function.

The correct calculation is done in the grand canonical ensemble, since the number of particles in the bulk solution should in average stay constant for all strengths of the adsorbing potential. This can only be regulated by a chemical potential. The grand canonical partition function reads

$$\mathcal{Z}_g \;=\; \sum_{N_p} \exp(\mu N_p/T)\,[\mathcal{Z}_1]^{N_p}\,\frac{1}{N_p!} \;=\; \exp(\lambda \mathcal{Z}_1)\;, \tag{9.2}$$

where we introduced the fugacity $\lambda = \exp(\mu/T)$. The average number of polymers is given by

$$\langle N_p\rangle \;=\; \lambda\frac{\partial \ln \mathcal{Z}_g}{\partial\lambda} \;=\; \lambda\mathcal{Z}_1\;. \tag{9.3}$$

We identify the average number of polymers with the bulk value N_b and conclude that the fugacity is given by

$$\lambda \;=\; \frac{N_b}{\mathcal{Z}_1}\;. \tag{9.4}$$

Thus, if we calculate the free energy of N_b polymers in solution we write down the canonical free energy which is derived from the grand canonical potential ψ by the Legendre transformation $\mathcal{F}_{N_b} =$

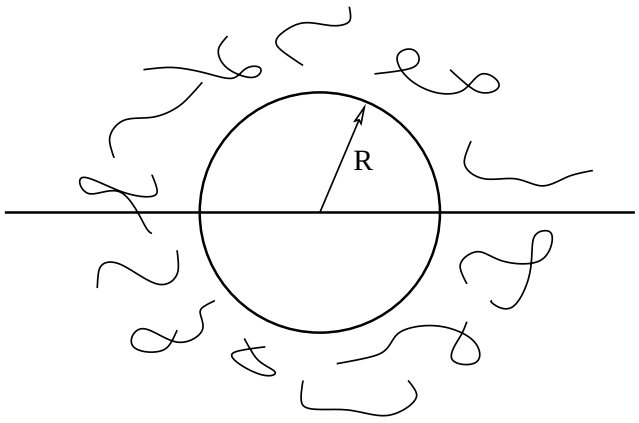

Figure 9.1: Sphere of radius R in a polymer solution: The system of reference is put in the origin of the sphere, which divides the solution into two half-spaces.

$\psi + \mu N_b$ and find

$$\begin{aligned} \mathcal{F}_{N_b} &= -T\lambda\mathcal{Z}_1 + TN_b \ln\lambda \\ &= -T\left(N_b - N_b \ln N_b + N_b \ln \mathcal{Z}_1\right) . \end{aligned} \tag{9.5}$$

The remaining task is to calculate the single polymer partition function $\mathcal{Z}_1$.

In fig. 9.1 we display a large sphere of radius R located in a polymer solution. Using this situation we will introduce our system of reference in which we describe the polymer solution above a curved surface in the limit of large curvature radii R. The surface l_{sp} of the large sphere leads us to the corresponding integration boundaries in the partition function. Shifting the system of reference into the origin of the sphere leads to

$$l_{sp}(\underline{r}) = \begin{cases} R\sqrt{1-\frac{r^2}{R^2}} & , r \le R \\ 0 & , r > R \end{cases} \tag{9.6}$$

where r is the lateral distance from the origin. The volume of the solution outside the sphere is thus given by

$$\mathcal{V} = \int_{-\infty}^{\infty} \mathrm{d}^2 r \left[\int_{-\infty}^{-l_{sp}(\underline{r})} \mathrm{d}r_3 + \int_{l_{sp}(\underline{r})}^{\infty} \mathrm{d}r_3 \right] . \tag{9.7}$$

Expanding l_{sp} for large R the integration boundary attains $l_{sp}(\underline{r}) = R - r^2/2R + \mathcal{O}(R^{-3})$.

Due to the symmetry with respect to the two half-spaces above and below the sphere both integrals in the sum of (9.7) are identical. In order to calculate the half-space solution above the curved surface we are going to omit the integral of the lower half-space. This leads to a missing factor 2 if one compares the results we will obtain with results for the large sphere in the entire solution, see reference 32 in [87].

Shifting the origin of our system of reference in the r_3 direction to $r_3 \mapsto r_3 + R$ leads us to the partition function of a single polymer bounded by a curved surface of large curvature radius R and

influenced by a contact potential V which is measured in units of T and characterized by the inverse extrapolation length:

$$\mathcal{Z}_1 = \int_{-\infty}^{\infty} \mathcal{D}\{\underline{r}\} \int_{-\varepsilon\frac{r^2}{2}}^{\infty} \mathcal{D}\{r_3\} \exp\left(-\frac{3}{2R_p^2}\int_0^1 \mathrm{ds}\, \left[\frac{\mathrm{d}}{\mathrm{ds}}\mathbf{r}(\mathrm{s})\right]^2 - \int_0^1 \mathrm{ds}\, \mathrm{V}(\mathbf{r}(\mathrm{s}))\right) \quad . \tag{9.8}$$

where we introduced $\varepsilon = 1/R$. The expansion of the integral for small ε yields

$$\mathcal{Z}_1 = \sum_{n=1}^{\infty} \frac{1}{n!}\mathcal{Z}_1^{(n)}\varepsilon^n \quad \text{with} \quad \mathcal{Z}_1^{(n)} = \left.\frac{\mathrm{d}^n\mathcal{Z}_1}{\mathrm{d}\varepsilon^n}\right|_{\varepsilon=0} . \tag{9.9}$$

The first term of the expansion is the half-space solution

$$\begin{aligned}\mathcal{Z}_1\{0\} &= \mathcal{V}_{hs} - \left(\sqrt{\frac{2}{3\pi}} + \frac{l_{ex}}{R_p}\left[\exp\left(\frac{R_p^2}{6l_{ex}^2}\right)\mathrm{erfc}\left(\frac{R_p}{\sqrt{6}l_{ex}}\right) - 1\right]\right) R_p\mathcal{A} \\ &=: \mathcal{V}_{hs} - \Upsilon_{\mathrm{depl}}^{(0)}\, R_p\mathcal{A}\,, \end{aligned} \tag{9.10}$$

where $\mathcal{Z}(\underline{x}_0, \underline{x}|1)$ is the lateral polymer partition function in the free space as given by eq. (2.22) and $\mathcal{Z}_{hs}(z_0, z_e|1)$ is the half-space partition function as given by eq. (2.24).

Using the expression in the brackets one can define an effective radius R_e and thus treat the polymer as a colloidal sphere of this radius [87], similar to the situation, in which nanoparticles interact with membranes [103]. In the limit of total desorption this radius is given by $R_e = \sqrt{2/3\pi}R_p$. Adsorption leads to a decrease of this radius until it vanishes at the adsorption/desorption transition. Due to this analogy one expects that the curvature contribution to the depletion volume, which is proportional to the size of the small particles, vanishes at the adsorption/desorption transition $R_p/l_{ex} = 0$. In the adsorption regime $R_p/l_{ex} < 0$ the analogy to the particle radius breaks down, since the effective radius becomes negative. However, the hard sphere-model does not take into account the configurational entropy of the polymers which allows the polymer to deform in the vicinity of the curved surface. Another important argument refers to the extrapolation length l_{ex}. As we already pointed out the extrapolation length depends on the curvature. If one neglects the curvature dependence of l_{ex} the next term in the curvature expansion (9.10) $\mathcal{Z}_1^{(1)}$ is given by

$$\begin{aligned}\mathcal{Z}_1^{(1)} = \int_0^1 \mathrm{d}s \int_{-\infty}^{\infty} \mathrm{d}^2x_0 \int_{-\infty}^{\infty} \mathrm{d}^2x\, \frac{x^2}{2}\mathcal{Z}(\underline{x}_0, \underline{x}|s) \quad \times \\ \times \int_0^{\infty} \mathrm{d}z_0 \int_0^{\infty} \mathrm{d}z_e\, \mathcal{Z}_{hs}(z_0, 0|s)\mathcal{Z}_{hs}(0, z_e|1-s)\,, \end{aligned} \tag{9.11}$$

where we used the Leibniz formula to differentiate the integral in eq. (9.8) [55].

Analogous to the half-space part $\mathcal{Z}_1\{0\}$ we split off the volume term of the polymer configuration in the z-direction, which, after integration of the lateral part in eq. (9.11), leads to the curvature correction

$$\begin{aligned}\mathcal{Z}_1^{(1)} &= R_p^2\mathcal{A}\int_0^1 \mathrm{d}s\, \frac{s}{3}\left[1 - \underbrace{\left(1 - \exp\left(\frac{R_p^2}{6l_{ex}^2}\right)\mathrm{erfc}\left(\frac{R_p}{\sqrt{6}l_{ex}}\sqrt{1-s}\right)\mathrm{erfc}\left(\frac{R_p}{\sqrt{6}l_{ex}}\sqrt{s}\right)\right)}_{\text{depletion zone}}\right] \\ &=: \left(\frac{1}{6} - \Upsilon_{\mathrm{depl}}^{(1)}\right) R_p^2\mathcal{A}\,. \end{aligned} \tag{9.12}$$

The first term in the bracket is the change in volume for the polymer due to the bending of the membrane. The second term gives the depletion volume above the curved surface.

Since the half-space partition functions $\mathcal{Z}_{hs}$ of the polymer in the perpendicular direction explicitly depend on the extrapolation length l_{ex} there occurs an additional term if one takes into account the curvature dependence of l_{ex}. In case of a square well potential (and the contact potential we consider arises from the square well in the limit of vanishing range z_V) this curvature dependence is given by $l_{ex}(\varepsilon) = l_{ex}(1 + l_{ex}\varepsilon)$. Therefore the inverse extrapolation length reads $1/l_{ex}(\varepsilon) = 1/l_{ex} - \varepsilon$ and the second term in the curvature contribution is

$$\mathcal{Z}_1^{(1,\mathrm{l_{ex}})} \;=\; \mathcal{A}\int_0^\infty \mathrm{d}z_0 \int_0^\infty \mathrm{d}z_e \left(\frac{\mathrm{d}}{\mathrm{d}\varepsilon}\mathcal{Z}_{hs}(z_0, z_e|1)\right)\Big|_{\varepsilon=0} . \tag{9.13}$$

In this equation the volume term is directly subtracted, since it does not depend on ε and cancels in the differentiation. Thus, one immediately finds

$$\begin{aligned}\mathcal{Z}_1^{(1,\mathrm{l_{ex}})} \;&=\; -R_p^2\mathcal{A}\,\frac{l_{ex}^2}{R_p^2}\left(\sqrt{\frac{2}{3\pi}}\frac{R_p}{l_{ex}} + \left(1 - \frac{1}{3}\frac{R_p^2}{l_{ex}^2}\right)\exp\left(\frac{R_p^2}{6l_{ex}^2}\right)\mathrm{erfc}\left(\frac{R_p}{\sqrt{6}l_{ex}}\right) - 1\right) \\ &=:\; -\Upsilon_{\mathrm{depl}}^{(1,\mathrm{l_{ex}})}\,R_p^2\mathcal{A}\,. \end{aligned} \tag{9.14}$$

Merging all contributions one obtains the complete single polymer partition function up to linear order in the curvatures

$$\mathcal{Z}_1 \;=\; \Big(\underbrace{\mathcal{V}_{hs} \;+\; \frac{1}{6}\frac{R_p^2\mathcal{A}}{R}}_{\mathcal{V}_{\mathrm{bulk}}} \;-\; \underbrace{\Upsilon_{\mathrm{depl}}^{(0)}R_p\mathcal{A}}_{\mathcal{V}_{\mathrm{depl}}^{(0)}}\Big) - \underbrace{\left(\Upsilon_{\mathrm{depl}}^{(1)} + \Upsilon_{\mathrm{depl}}^{(1,\mathrm{l_{ex}})}\right)\frac{R_p^2\mathcal{A}}{R}}_{\mathcal{V}_{\mathrm{depl}}^{(1)}} . \tag{9.15}$$

In the limit of total desorption $R_p/l_{ex} \to \infty$ the contribution $\mathcal{Z}_1^{(1,\mathrm{l_{ex}})}$ vanishes and the single polymer partition function of one polymer on a curved surface is given by

$$\mathcal{Z}_1 \;=\; \mathcal{V}_{\mathrm{bulk}} - \mathcal{V}_{\mathrm{depl}} \;=\; \mathcal{V}_{\mathrm{bulk}} - \mathcal{A}\left(\sqrt{\frac{2}{3\pi}}R_p + \frac{1}{6}\frac{R_p^2}{R}\right) \tag{9.16}$$

which is identical to the result in [87].

If we now calculate the corresponding membrane curvature the physically important contribution of the polymer solution arises from the change in the depletion volume $\mathcal{V}_{\mathrm{depl}}^{(1)}$ due to bending. Denoting $V_0 = \mathcal{V}_{\mathrm{bulk}} - \mathcal{V}_{\mathrm{depl}}^{(0)}$ eq. (9.15) leads to

$$\frac{\mathcal{Z}_1}{\mathcal{V}_0} \;=\; 1 - \frac{\mathcal{V}_{\mathrm{depl}}^{(1)}}{\mathcal{V}_0} \;\approx\; 1 - \frac{\mathcal{V}_{\mathrm{depl}}^{(1)}}{\mathcal{V}_{hs}} + \mathcal{O}(R^{-2}) , \tag{9.17}$$

where we used the smallness of the half-space depletion volume $\mathcal{V}_{\mathrm{depl}}^{(0)}$ compared to the half-space volume V_{hs}.

Using eq. (9.5) the free energy difference of the curved geometry compared to the half-space leads to $\Delta\mathcal{F}_{N_b} = TN_b\mathcal{V}_{\mathrm{depl}}^{(1)}/\mathcal{V}_{hs}$ and to the free energy per area of the compound polymer/membrane system

$$\frac{\mathcal{F}}{\mathcal{A}} \;=\; 2\kappa M^2 + \frac{\Delta\mathcal{F}_{N_b}}{\mathcal{A}} . \tag{9.18}$$

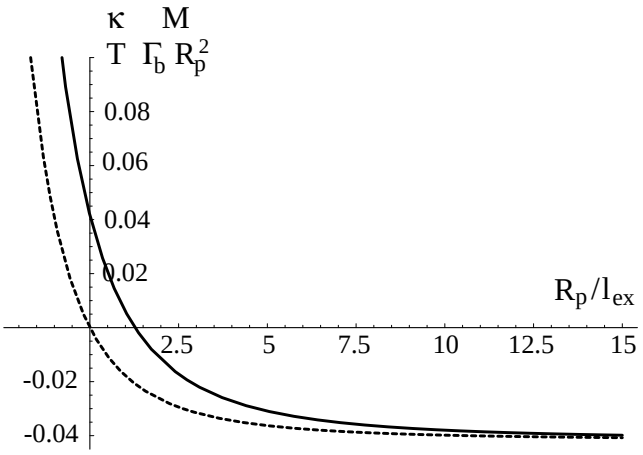

Figure 9.2: Polymer solution: The integrated membrane curvature versus the inverse extrapolation length for curvature independent l_{ex} (dashed), and for the correct curvature dependence of l_{ex} (solid).

Minimization with respect to the curvature M and insertion of the depletion volume $\mathcal{V}_{\rm depl}$ as given by eq. (9.15) finally leads to the curvature

$$M = -\frac{T}{4\kappa}\Gamma_b \left(\Upsilon^{(1)}_{\rm depl} + \Upsilon^{(1,l_{\rm ex})}_{\rm depl}\right) R_p^2 \,, \tag{9.19}$$

where $\Gamma_b = N_b/\mathcal{V}_{hs}$ is the bulk concentration of polymers in the half-space.

In fig. 9.2 we plot both the membrane curvature for curvature independent extrapolation length, which corresponds to the neglect of $\Upsilon^{(1,l_{\rm ex})}_{\rm depl}$ and for curvature dependent extrapolation length. In both cases the limit of total desorption is identical. The membrane bends towards the polymer solution. The curvature in this limit is

$$M_{\rm des} = -\frac{1}{24}\frac{T}{\kappa}\Gamma_b R_p^2 \,. \tag{9.20}$$

As one concludes the polymer solution behaves opposite to the case of anchored polymers, where the membrane bends away from the polymers in the desorption limit. The physical reason is that the anchor situation is governed by the change in polymer configurational entropy due to bending, whereas the solution is additionally governed by the difference in the translational entropy of each polymer due to the bending. If the membrane bends towards the solution the volume of the depletion zone is decreased.

In the limit of strong adsorption the membrane bends away from the polymer solution in order to increase the adsorption volume above the membrane surface. This bending, in principle, does not saturate and therefore diverges.

The basic difference between the two cases of curvature dependent and independent l_{ex} occurs in the vicinity of the adsorption/desorption transition. In the curvature independent case, the membrane bending changes its sign at the adsorption/desorption transition. However, in the curvature dependent case the sign of the membrane curvature changes already at a value of the inverse extrapolation length, which is larger than zero, $R_p/l_{ex} \approx 1.27$.

Chapter 10

Conclusions and Outlook

Membranes, which are decorated by polymers, are perturbed by the presence of the chains. Both anchored [43, 46] and non-anchored [87] polymers influence the shape, curvature and rigidity of the membrane. In chapters 2 to 8, we study the influence of anchored polymers on the shape and curvature of the membrane.

The initial partition function of the compound system contains the fluctuating membrane surface and the fluctuating polymer. In the perturbative calculation presented in chapter 2, the partition function is expanded in powers of deviations of the local membrane height from the flat reference state. Since the polymer partition function solves the corresponding Schrödinger-type equation, the degrees of freedom of the polymer can be integrated out.

In the resulting partition function the polymer part leads to a location-dependent pressure of the polymer. The polymer pushes the membrane away from it, but pulls at the membrane in the anchor point. For large distances from the anchor the pressure vanishes exponentially, whereas close to the anchor it diverges. Since there are no external forces applied on the compound system the polymer can not provoke a center-of-mass motion, and the integrated pressure vanishes.

The pressure allows us to calculate the explicit shape of the membrane under the influence of the polymer. Far away from the anchor, the membrane is not affected by the polymer and approaches a profile of vanishing curvature. Since the polymer interacts with the membrane on a range given by its end-to-end distance, the membrane is strongly perturbed in the vicinity of the anchor point. The resulting shape is a cone and consequently leads to a sharp bend with diverging curvature in the anchor point. However, the integrated (spontaneous) curvature of the membrane is finite. The shape for large distances is a catenoid, which does not contribute to the integral anymore [54]. The integrated curvature of the membrane is directly proportional to the average perpendicular distance of the polymer-end-point in the half-space.

In order to check whether the perturbative approach is justified, we perform extensive Monte Carlo simulations which are compared with the analytic predictions in chapter 3, especially the membrane shape profile. In order to avoid the influence due to the periodic boundary conditions, the lateral size of the membrane is chosen large compared to the polymer end-to-end distance. Furthermore, the membrane is confined by a harmonic potential. The simulation results depend on both the polymer and the membrane discretization. The continuum limit is approached for finer discretizations.

Since our perturbative approach extends to linear order, the effect of several anchored polymers is given by superposition of the single polymer effects. Therefore, the curvature due to polymer/membrane interaction is proportional to the surface coverage density of polymers. In chapter

4, we also consider the effect of polymer/polymer interactions. The membrane-induced pairwise interaction between polymers is attractive. However, the attraction takes place in a range where polymers intersect. Therefore, steric repulsion of the polymers is dominant and the attraction can be neglected [54]. The repulsive polymer/polymer interaction leads to a curvature contribution which is quadratic in the coverage density. The predictions on the membrane curvature are compared with experiments, in which vesicles are covered by anchored polymers [74]. For small coverage densities, one expects a regime dominated by the polymer/membrane interaction, whereas for larger densities the polymer/polymer interaction becomes dominant.

The above method is generalized to polymers, which are anchored with both ends, and to polymers which translocate the membrane. In the first situation, the polymer acts effectively as a single anchored polymer, if the anchors are close together. For large distances, the polymer acts as a spring, pulling the membrane upwards. A polymer with freely diffusing anchors does not induce curvature on the membrane.

The translocation of a polymer is interesting from a biological point of view since it deals with the problem of DNA passing through the cell membrane. We consider the effect on the shape during the translocation, given by superposition of oppositely anchored polymers of different length. Consequently, if half of the polymer has passed the membrane, the average profile is flat.

Application of lateral forces on the membrane leads to an additional tension contribution in the membrane Hamiltonian. The tension term changes the behavior of the membrane from the limiting case of the catenoid for large anchor distances to the case of an exponentially decaying, finally flat profile. Perpendicular forces which are applied to the polymer end point, lead to a change in the polymer configuration and to corrections of the membrane profile.

The adsorption of anchored polymers due to short-range interactions is studied in chapters 7 and 8. First, a pure contact potential is considered. The adsorption leads to a decrease in the entropically induced initial membrane curvature. The integrated curvature as a function of the inverse extrapolation length is monotonic and vanishes in the limit of strong adsorption, where the average membrane shape is flat. The polymer which is located directly on the membrane surface can not exert any pressure in this limit. Only in the case of non-vanishing anchor distances, the polymer induces a membrane bending towards it in the limit of strong adsorption. The result shows that it is necessary to take into account the curvature dependence of the extrapolation length. Furthermore, a square-well potential is considered, which leads to corrections to the contact potential. In general, the finite potential range increases the membrane curvature, especially for strong adsorption, where the polymer can still move in the well above the membrane surface. In the limit of large potential ranges, one always recovers the limit of total desorption, since the polymer of finite size is not affected by the potential gradient anymore. The results are in good agreement with corresponding Monte Carlo simulations [92].

In the final chapter 9 we consider free polymers in solution above the membrane. The curvature of the membrane is now governed by both the translational and configurational entropy of the polymers and not, as in the anchored case, only by the configurational entropy compared to the flat geometry. In case of desorbed polymers in solution, the membrane curves towards the polymers [87], since the depletion volume, in which the polymers cannot enter, is decreased. In the limit of strong adsorption, the membrane bends away from the polymers in order to increase the volume in which the polymers can adsorb on the surface.

Future work will consider more realistic potentials, especially the effect of long-range interaction, in which the interaction energy is integrated over the whole membrane surface. In addition, the effect

of excluded volume in the polymer can be considered perturbatively, which might lead to an increase of the induced membrane curvature, since the polymer size is increased and the integrated curvature is proportional to the end-to-end distance of the polymer. It is furthermore of major importance to compare the theoretical predictions with experiments, in which polymers are anchored to vesicles.

Appendix A

Schrödinger-type Equation

Here, we derive the Schrödinger-type equation for the polymer chain, which actually corresponds to a diffusion problem, starting from the polymer Hamiltonian with an external potential V acting on each monomer. For simplicity, but sufficient for our needs, we restrict the derivation to the z-direction. The Hamiltonian reads

$$\mathcal{H} = \int_0^1 \mathrm{d}s\, T \left[\frac{3}{2R_p^2}\left(\frac{\mathrm{d}z}{\mathrm{d}s}\right)^2 + \frac{V(z)}{T}\right] . \tag{A.1}$$

The internal length of the polymer corresponds to the time in this diffusion process. We now discretize the Hamiltonian and end up with

$$\mathcal{H}_d = \sum_i \Delta s\, T \left[\frac{3}{2R_p^2}\left(\frac{z(s_i)-z(s_{i+1})}{\Delta s}\right)^2 + \frac{V(z(s_{i+1}))}{T}\right] \tag{A.2}$$

which we can rewrite into

$$\mathcal{H}_d = T\sum_i \Delta s\, H(z(s_i), z(s_{i+1})) . \tag{A.3}$$

The probability of the segment $(i+1)$ being located at position z given the condition that segment i is located at position z' is now

$$\begin{aligned}\mathcal{Z}(z|s_{i+1}) &= \int \mathrm{d}z'\, \frac{\sqrt{3}}{\sqrt{2}R_p} \exp\left(-\Delta s H(z',z)\right)\ \mathcal{Z}(z'|s_i) \\ &= \exp\left(-\Delta s \frac{V(z)}{T}\right)\int \mathrm{d}z'\, \frac{\sqrt{3}}{\sqrt{2}R_p} \exp\left(-\frac{3}{2R_p^2\Delta s}(z'-z)^2\right)\mathcal{Z}(z'|s_i) . \end{aligned} \tag{A.4}$$

The exponential in this integral is called transfer matrix. Expanding $\mathcal{Z}(z|s_i)$ around z yields

$$\mathcal{Z}(z'|s_i) = \exp\left[(z'-z)\frac{\partial}{\partial z}\right]\mathcal{Z}(z|s_i) . \tag{A.5}$$

Substituting $\bar{z} = (z'-z)$ we find

$$\mathcal{Z}(z|s_{i+1}) = \exp\left(-\Delta s \frac{V(z)}{T}\right)\int \mathrm{d}\bar{z}\, \frac{\sqrt{3}}{\sqrt{2}R_p} \exp\left(-\frac{3}{2\Delta s}\frac{\bar{z}^2}{R_p^2} + \bar{z}\frac{\partial}{\partial z}\right)\ \mathcal{Z}(z|s_i) . \tag{A.6}$$

If one solves the integral one ends up with

$$\mathcal{Z}(z|s_{i+1}) \;=\; \exp\left(-\Delta s\frac{V(z)}{T}\right)\,\left(\frac{\pi\Delta s}{2}\right)^{1/2}\exp\left(\Delta s\frac{R_p^2}{6}\frac{\partial^2}{\partial z^2}\right)\,\mathcal{Z}(z|s_i)\;. \tag{A.7}$$

The next step is to expand the exponentials in powers of Δs up to first order. We neglect the term $(\pi\Delta s/2)^{1/2}$ which leads to a shift in the origin and scale of the free energy and does not change the final result. The expansion yields

$$\mathcal{Z}(z|s_{i+1}) \;=\; \left(1-\Delta s\frac{V(z)}{T}+\Delta s\frac{R_p^2}{6}\frac{\partial^2}{\partial z^2}\right)\mathcal{Z}(z|s_i)\;. \tag{A.8}$$

In the limit of $\Delta s\to 0$ we find the Schrödinger-type equation

$$\frac{\partial\mathcal{Z}(z|s)}{\partial s} \;=\; -\frac{\hat{H}}{T}\mathcal{Z}(z|s) \tag{A.9}$$

with the Hamilton operator

$$\hat{H} \;=\; V(z)-T\frac{R_p^2}{6}\frac{\partial^2}{\partial z^2}\;. \tag{A.10}$$

Appendix B

Limiting Behavior of Bessel Functions

In this chapter, we summarize the behavior of some Bessel functions and Bessel related functions which we use in the main part[55, 57, 104].

For small arguments, the series expansions of the Bessel function of the first kind $J_\nu(z)$ and the modified Bessel function $I_\nu(z)$ are given by

$$\begin{aligned} J_\nu(z) &= \left(\frac{z}{2}\right)^2 \sum_{k=0}^{\infty} \frac{(-z^2/4)^k}{k!\,\Gamma(\nu+k+1)} \qquad \text{and} \\ I_\nu(z) &= \left(\frac{z}{2}\right)^2 \sum_{k=0}^{\infty} \frac{(z^2/4)^k}{k!\,\Gamma(\nu+k+1)} \,. \end{aligned} \tag{B.1}$$

In particular one has

$$\begin{aligned} J_0(z) &= 1 - \frac{1}{4}z^2 + \mathcal{O}(z^4)\,, \\ I_0(z) &= 1 + \frac{1}{4}z^2 + \mathcal{O}(z^4) \qquad \text{and} \\ I_1(z) &= \frac{z}{2} + \frac{1}{16}z^3 + \mathcal{O}(z^5)\,. \end{aligned} \tag{B.2}$$

The asymptotic expansions for large arguments yield

$$J_\nu(z) \sim \sqrt{\frac{2}{\pi z}} \left(\cos(z - \frac{1}{2}\nu\pi - \frac{1}{4}\pi)\right) \tag{B.3}$$

and

$$I_\nu(z) \sim \frac{\exp(z)}{\sqrt{2\pi z}} \left(1 - \frac{4\nu^2 - 1}{8z} + \mathcal{O}(z^{-2})\right) \,. \tag{B.4}$$

The Thomson functions ker and kei are related to the modified Bessel function K_0 via

$$\mathrm{ker}(z) + i\mathrm{kei}(z) = K_0(z\sqrt{i})\,. \tag{B.5}$$

For small arguments the series expansion of kei leads to

$$\mathrm{kei}(z) = \frac{z^2}{4}\left(1 - \gamma + \ln\left(\frac{2}{z}\right)\right) + \mathcal{O}(z^4) \tag{B.6}$$

where γ is Euler's constant.

The asymptotics of kei for large argument are given by

$$\mathrm{kei}(z) \quad \sim \quad \sqrt{\frac{\pi}{2z}} \exp\left(-\frac{z}{\sqrt{2}}\right) \sin\left(-\frac{z}{\sqrt{2}} - \frac{\pi}{8}\right) \ . \tag{B.7}$$

Appendix C

Inverse Laplace Transformation

The inverse Laplace transform is given by the complex integral

$$\mathcal{Z}(z_0, z|s) \quad = \quad \frac{1}{2\pi i}\int_{\eta-i\infty}^{\eta+i\infty} \mathrm{d}t \ \exp(st) G(z_0, z|t) \ . \tag{C.1}$$

Note that it is important to introduce a positive η in order to ensure that the initial Laplace transformation, defined in 7.16, is a convergent integration. In fact, one obtains the final result in the limit $\eta \searrow 0$.

The method, which we use for the solutions of the adsorption in a contact potential and in the square well potential, is easily demonstrated for the Greens function of the polymer in free space, as given by $G(z_0, z|t) = \sqrt{6}/2\sqrt{t}R_p \cdot \exp(-\sqrt{6t}(z - z_0)/R_p)$. The corresponding partition function is

$$\mathcal{Z}(z_0, z|s) \quad = \quad \lim_{T\to\infty} \frac{1}{2\pi i}\int_{-iT}^{+iT} \mathrm{d}t \ \exp(st) \frac{\sqrt{6}}{2\sqrt{t}R_p} \exp\left(-\sqrt{t}(z - z_0)\frac{\sqrt{6}}{R_p}\right) \ . \tag{C.2}$$

Substituting $t' = \sqrt{t}$ leads to

$$\mathcal{Z}_T(z_0, z|s) \quad = \quad \frac{1}{2\pi i}\int_{T(1-i)}^{T(1+i)} \mathrm{d}t' \exp(st'^2) \frac{\sqrt{6}}{R_p} \exp\left(-t'(z - z_0)\frac{\sqrt{6}}{R_p}\right) \tag{C.3}$$

where we used the correct definition of the square root in the complex plane. The resulting shift in the integration path is depicted in figure C.1. Substitution of $\tau = it$ and neglecting the imaginary shift in the exponent (Goursats lemma [105]) yields

$$\begin{aligned}\mathcal{Z}_T(z_0, z|s) \quad = \quad & \frac{1}{2\pi} \exp\left(-\frac{3}{2s}\frac{(z - z_0)^2}{R_p^2}\right) \left[(1 - i)\int_0^T \mathrm{d}\tau \ \exp(2is\tau^2)\right. \\ & \left. + (1 + i)\int_0^T \mathrm{d}\tau \ \exp(-2is\tau^2)\right] \ .\end{aligned} \tag{C.4}$$

Using the relations

$$(1 \pm i)\int_0^\infty \mathrm{d}x \ \exp(\mp ix^2) = \sqrt{\frac{\pi}{2}} \tag{C.5}$$

we in the limit $T \to \infty$ end up with

$$\mathcal{Z}(z_0, z|s) \quad = \quad \sqrt{\frac{3}{2\pi s}}\frac{1}{R_p} \exp\left(-\frac{3}{2s}\frac{(z - z_0)^2}{R_p^2}\right) \ . \tag{C.6}$$

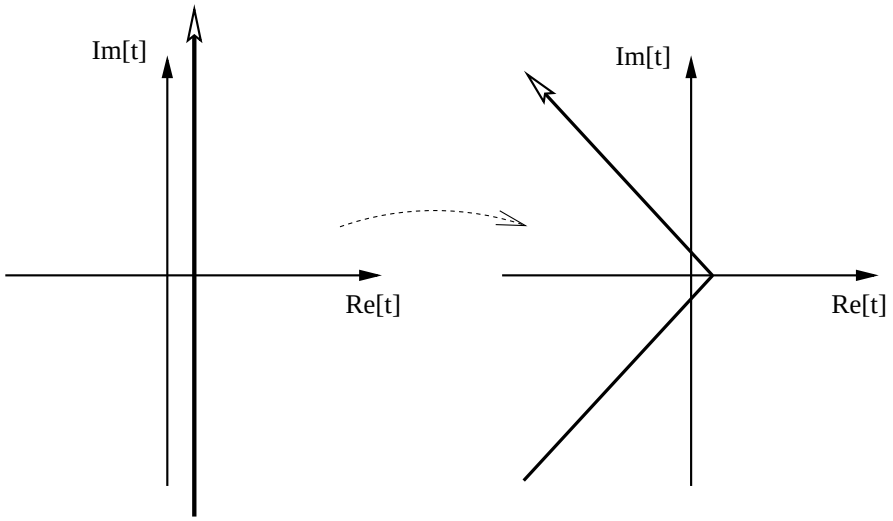

Figure C.1: The shift of the integration path in the complex plane as used in the inverse Laplace transformation.

In the same formalism it is easy to show that the inverse Laplace transform of $G_{hs}(z_0, z|t) = \sqrt{6}/R_p\sqrt{t} \cdot \sin(\sqrt{6t}\, z_0/R_p) \sin(\sqrt{6t}\, z/R_p)$ leads to the half-space partition function

$$\mathcal{Z}_{hs}(z_0, z|s) = \sqrt{\frac{3}{2\pi s}} \frac{1}{R_p} \left(\exp\left(\frac{3}{2s} \frac{(z - z_0)^2}{R_p^2} \right) - \exp\left(\frac{3}{2s} \frac{(z + z_0)^2}{R_p^2} \right) \right) . \qquad \text{(C.7)}$$

Appendix D

List of important symbols

a_m	membrane discretization
a_p	Kuhn length
$\mathcal{A}$	area
A_{an}	area per anchor molecule
$\mathcal{A}\overline{M}$	integrated membrane curvature
b_2	second virial coefficient
C	correlation function
E_n	discrete energy levels
F	external force
$\mathcal{F}$	free energy
$G(z_0, z\|t)$	polymer Greens function with energy $-t$
G	Gaussian curvature
$\gamma(\underline{x})$	generating field
Γ_b	bulk concentration of polymers
Γ_p	polymer coverage density on the membrane
$\mathcal{H}_{me}$	membrane Hamiltonian
$\mathcal{H}_p$	polymer Hamiltonian
k	wavenumber of the Greens function outside the potential range
K	membrane kernel
κ	bending rigidity
κ_G	Gaussian bending rigidity
l	membrane height
L	lateral membrane size
l_{ex}	extrapolation length
l_{me}	membrane thickness
λ	fugacity
M	mean curvature
μ	chemical potential
N	monomer number of the polymer
N_p	number of polymers
P	polymer pressure

q	wavenumber of the Greens function inside the potential range
$\mathbf{r}(s)$	spacial position of monomer s
R	curvature radius
R_p	polymer end-to-end distance
R_{ve}	vesicle radius
s	internal (contour) length of the polymer
S_p	entropy of the polymer
Σ	membrane surface tension
t	negative energy $-E$ (notational convenience)
T	absolute temperature (generally in energy units)
v_2	harmonic potential parameter
V	interaction potential between polymer and membrane
$\mathcal{V}$	volume
w	depth of the square well potential
$\mathrm{w}(\underline{x}, z)$	polymer segment density
$\underline{x}$	lateral directions x_1, x_2
$\xi_{\parallel}$	parallel membrane correlation length
$\xi_{\perp}$	perpendicular membrane correlation length (roughness)
z	perpendicular direction
z_V	range of the square well potential
$\mathcal{Z}_p$	polymer partition function
$\mathcal{Z}$	free polymer partition function
$\mathcal{Z}_{hs}$	half-space polymer partition function
$\mathcal{Z}_{\parallel}$	polymer partition function in the lateral directions
$\mathcal{Z}_{\perp}$	polymer partition function in the perpendicular direction
$\mathcal{Z}_{me}$	membrane partition function
$\mathcal{Z}_g$	grand canonical partition function

Bibliography

[1] B. Alberts, D. Bray, J. Lewis, M. Raff, K. Roberts, and J.-D. Watson. *Molecular biology of the cell*. Garland Publishing, New York, 1994.

[2] B. Alberts, D. Bray, A. Johnson, J. Lewis, M. Raff, K. Roberts, and P. Walter. *Essential cell biology*. Garland Publishing, Inc., New York, London, 1998.

[3] W. Hoppe, W. Lohmann, H. Markl, and H. Ziegler. *Biophysics*. Springer, Berlin, 1983.

[4] J. Darnell, H. Lodish, and D. Baltimore. *Molecular cell biology*. Scientific American Books, New York, 1990.

[5] C. Tanford. *The hydrophobic effect: formation of micelles and biological membranes*. Krieger Pulb. Comp., Malabar, 1991.

[6] E. Egberts and H.J.C. Berendsen. Molecular-dynamics simulation of a smectic liquid-crystal with atomic detail. *J. Chem. Phys*, 89:3718, 1988.

[7] H.E. Alper, D. Bassolino, and T.R. Stouch. Computer-simulation of a phospholipid monolayer-water system - the influence of long-range forces on water-structure and dynamics. *J. Chem. Phys*, 98:9798, 1993.

[8] R. Goetz and R. Lipowsky. Computer simulations of bilayer membranes: Self-assembly and interfacial tension. *J. Chem. Phys.*, 108:7397, 1998.

[9] R. Goetz, G. Gompper, and R. Lipowsky. Mobility and elasticity of self-assembled membranes. *Phys. Rev. Lett.*, 82:221, 1999.

[10] D. Chiras. *Human biology*. Jones and Bartlett Pub., 1999.

[11] G. Decher, E. Kuchinka, H. Ringsdorf, J. Venzmer, D. Bitter-Suermann, and C. Weisgerber. Interaction of amphiphilic polymers with model membranes. *Angew. Makromol. Chem.*, 166/167:71, 1989.

[12] J. Simon, M. Kühner, H. Ringsdorf, and E. Sackmann. Polymer-induced shape changes and capping in giant liposomes. *Chem. Phys. Lipids*, 76:241, 1995.

[13] V. Frette, I. Tsafrir, M.-A. Guedeau-Boudeville, L. Jullien, D. Kandel, and J. Stavans. Coiling of cylindrical membrane stacks with anchored polymers. *Phys. Rev. Lett.*, 83:2465, 1999.

[14] B. Jakobs, T. Sottmann, R. Strey, J. Allgaier, L. Willner, and D. Richter. Amphiphilic block copolymers as efficiency boosters for microemulsions. *Langmuir*, 15:6707, 1999.

[15] R. Lipowsky. Flexible membranes with anchored polymers. *Colloids Surfaces A: Physicochem. Eng. Aspects*, 128:255, 1997.

[16] R. Lipowsky. Vesicles and biomembranes. *Encycl. Appl. Phys.*, 23:199, 1998.

[17] D.D. Lasic. *Applications of liposomes.* In: R. Lipowsky and E. Sackmann, *Structure and dynamics of membranes - from cells to vesicles*, volume 1A of *Handbook of biological physics*, pp. 491-520. Elsevier, Amsterdam, 1994.

[18] M.C. Woodle and D.D. Lasic. Sterically stabilized liposomes. *Biochim. Biophys. Acta*, 1113:171, 1992.

[19] T.M. Allen. Liposomal drug delivery. *Curr. Opin. Coll. Int. Sci.*, 1:645, 1996.

[20] G. Blume and G. Cevc. Liposomes for the sustained drug release in vivo. *Biophys. Acta*, 1029:91, 1990.

[21] A.K. Kenworthy, S.A. Simon, and T.J. McIntosh. Structure and phase behavior of lipid suspensions containing phospholidids with covalently attached poly(ethylene glycol). *Biophys. J.*, 68:1903, 1995.

[22] D.D. Lasic and D. Papahadjopoulos. Liposomes revisited. *Science*, 267:1275, 1995.

[23] R. Dimova. private communication.

[24] R. Lipowsky. The conformation of membranes. *Nature (London)*, 349:475, 1991.

[25] R. Lipowsky and E. Sackmann. *Structure and dynamics of membranes*. Elsevier, Amsterdam, 1995.

[26] M. Shinitzky. *Biomembranes*. VCH Verlagsgesellschaft, Weinheim, 1993.

[27] M. P. do Carmo. *Differential geometry of curves and surfaces*. Prentice-Hall, New Jersey, 1976.

[28] P.M. Chaikin and T.C. Lubensky. *Principles of condensed matter physics*. Cambridge University Press, Cambridge, 1995.

[29] W. Helfrich. Elastic properties of lipid bilayers: Theory and possible experiments. *Z. Naturforsch. C*, 28:693, 1973.

[30] M. Spivak. *A comprehensive introduction to differential geometry I-IV*. Publish or Perish, Houston, 1979.

[31] H.-G. Döbereiner. *Fluctuating vesicle shapes.* In: P.L. Luigi and P. Walde: *Giant vesicles*. John Wiley and Sons Ltd., 2000.

[32] U. Seifert, K. Berndl, and R. Lipowsky. Shape transformations of vesicles: Phase diagrams for spontaneous-curvature and bilayer-coupling models. *Phys. Rev. A*, 44:1182, 1991.

[33] K. Berndl, J. Käs, R. Lipowsky, E. Sackmann, and U. Seifert. Shape transformations of giant vesicles: Extreme sensitivity to bilayer asymmetry. *Europhys. Lett.*, 13:659, 1990.

[34] H.-G. Döbereiner, E. Evans, M. Kraus, U. Seifert, and M. Wortis. Mapping vesicle shapes into the phase diagram: A comparison of experiment and theory. *Phys. Rev. E*, 55:4458, 1997.

[35] L. Miao, U. Seifert, M. Wortis, and H.-G. Döbereiner. Budding transitions of fluid-bilayer vesicles: the effect of area-difference elasticity. *Phys. Rev. E*, 49:5389, 1994.

[36] W. Wintz, H.-G. Döbereiner, and U. Seifert. Starfish vesicles. *Europhys. Lett.*, 33:403, 1996.

[37] M. Doi. *Introduction to polymer physics*. Clarendon Press, Oxford, 1996.

[38] M. Doi and S.F. Edwards. *The theory of polymer dynamics*. Oxford Science Publication, Oxford, 86.

[39] G.R. Strobl. *The physics of polymers*. Springer, Berlin, 1997.

[40] P.J. Flory. *Principles of polymer chemistry*. Cornell University Press, Ithaka, 1971.

[41] J. des Cloizeaux. *Polymers in solution: their modelling and structure*. Clarendon Press, Oxford, 1990.

[42] K. Binder. *Critical behaviour at surfaces* in: *Phase transitions and critical phenomena*, vol. 8. Academic Press, New York, 1983.

[43] R. Lipowsky. Bending of membranes by anchored polymers. *Europhys. Lett.*, 30:197, 1995.

[44] C. Hiergeist, V. Indrani, and R. Lipowsky. Membranes with anchored polymers at the adsorption transition. *Europhys. Lett.*, 36:491, 1996.

[45] C. M. Marques and J. B. Fournier. Deviatoric spontaneous curvature of lipid membranes induced by siamese macromolecular cosurfactants. *Europhys. Lett.*, 35:361, 1996.

[46] C. Hiergeist and R. Lipowsky. Elastic properties of polymer-decorated membranes. *J. Phys. II France*, 6:1465, 1996.

[47] P.G. de Gennes and C. Taupin. Microemulsions and the flexibility of oil-water interfaces. *J. Phys. Chem. US*, 86:2294, 1982.

[48] W. Helfrich. Effect of thermal undulations on the rigidity of fluid membranes and interfaces. *J. Phys. Paris*, 46:1263, 1985.

[49] L. Peliti and S. Leibler. Effects of thermal fluctuations on systems with small surface tension. *Phys. Rev. Lett.*, 54:1690, 1985.

[50] H. Carslaw and J. Jaeger. *Conduction of heat in solids*. Oxford at the Clarendon Press, Oxford, 1959.

[51] Y. Lepiné and A. Caillé. The configuration of a polymer chain interacting with a plane interface. *Can. J. Phys.*, 56:403, 1978.

[52] A. Silberberg. The adsorption of flexible macromolecules. part i. the isolated macromolecule at a plane interface. *J. Phys. Chem.*, 66:1872, 1962.

[53] E.A. diMarzio. Proper accounting of conformations of a polymer near a surface. *J. Chem. Phys.*, 42:2101, 1965.

[54] M. Breidenich, R. R. Netz, and R. Lipowsky. The shape of polymer-decorated membranes. *Europhys. Lett.*, 49:431, 2000.

[55] M. Abramowitz and I. A. Stegun. *Handbook of mathematical functions*. Dover Publications, Inc., New York, 1972.

[56] Mathematica, Wolfram Research Inc., 100 Trade Center Drive Champaign, IL 61820-7237, USA.

[57] I. S. Gradshteyn and I. M. Ryzhik. *Table of integrals, series and products*. Academic Press, London, 1994.

[58] D. Needham, K. Hristova, T. McIntosh, and D. Lasic. Repulsive interactions and mechanical stability of polymer-grafted lipid membranes. *Biochim. Biophys. Acta*, 1108:40, 1992.

[59] K. Hristova and D. Needham. The influence of polymer-grafted lipids on the physical properties of lipid bilayers: A theoretical study. *J. Coll. Interf. Sci.*, 168:302, 1994.

[60] S.T. Milner. Polymer brushes. *Science*, 251:905, 1991.

[61] S.T. Milner, T.A. Witten, and M.E. Cates. Theory of the grafted polymer brush. *Macromolecules*, 21:2610, 1988.

[62] J.M.H.C. Scheutjens and G.J. Fleer. Statistical theory of the adsorption of interacting chain molecules. 1. partition-function, segment density distribution, and adsorption-isotherms. *J. Phys. Chem.*, 83:1619, 1979.

[63] R.R. Netz and M. Schick. Polymer brushes: From self-consistent field theory to classical theory. *Macromolecules*, 31:5105, 1998.

[64] W. Helfrich. Hats and saddles in lipid membranes. *Liquid Crystals*, 5:1647, 1989.

[65] W. Helfrich. Flexibility and roughness of mixed and partially polymerized bilayers in terms of the hat model and local bending frustration. *J. Phys. II France*, 4:1427, 1994.

[66] R. Golestrian, M. Goulian, and M. Kardar. Fluctuation-induced interactions between rods on membranes and interfaces. *Europhys. Lett.*, 33:241, 1996.

[67] R. Holzlöhner and M. Schoen. Attractive forces between anisotropic inclusions in the membrane of a vesicle. *Eur. Phys. J. B*, 12:413, 1999.

[68] N. Dan, P. Pincus, and S.A. Safran. Membrane-induced interactions between inclusions. *Langmuir*, 9:2768, 1993.

[69] R. Bruinsma, M. Goulian, and P. Pincus. Self-assembly of membrane junctions. *Biophys. J.*, 67:746, 1994.

[70] J.B. Fournier. Nontopological saddle-splay and curvature instabilities from anisotropic membrane inclusions. *Phys. Rev. Lett.*, 76:4436, 1996.

[71] R.R. Netz and P. Pincus. Inhomogeneous fluid membranes: Segregation, ordering, and effective rigidity. *Phys. Rev. E*, 52:4114, 1995.

[72] R. R. Netz. Inclusions in fluctuating membranes: exact results. *J. Phys. I France*, 7:833, 1997.

[73] K. Hristova and D. Needham. Influence of bilayer fluctuations on the steric interactions between polymer-grafted bilayers. *Liquid Crystals*, 18:423, 1995.

[74] H.-G. Döbereiner, A. Lehmann, W. Goedel, O. Selchow, and R. Lipowsky. Membrane curvature induced by sugar and polymer solutions. *Mat. Res. Soc. Symp. Proc.*, 489:101, 1998.

[75] C. Hiergeist. *Elastische Eigenschaften Polymer-dekorierter Membranen*. Dissertation, Universität Potsdam, 1997.

[76] R. Lipowsky, H.-G. Döbereiner, C. Hiergeist, and V. Indrani. Membrane curvature induced by polymers and colloids. *Physica A*, 249:536, 1998.

[77] P.G. de Gennes. Problems of DNA entry into a cell. *Physica A*, 1-2:1, 1999.

[78] P.G. de Gennes. Passive entry of a DNA molecule into a small pore. *Proc. Natl. Acad. Sci. USA*, 13:7262, 1999.

[79] P.J. Park and W. Sung. Polymer release out of a spherical vesicle through a pore. *Phys. Rev. E*, 57:730, 1998.

[80] M. Muthukumar. Polymer translocation through a hole. *J. Chem. Phys.*, 111:10371, 1999.

[81] J.J. Kasianowicz, E. Brandin and. D. Branton, and D.W. Deamer. Characterization of individual polynucleotide molecules using a membrane channel. *Proc. Natl. Acad. Sci. USA*, 93:13770, 1996.

[82] Maple, Waterloo Mapple Inc., 57 Erb Street W., Waterloo, Ontario, N2L6C2, Canada.

[83] E. Eisenriegler. *Polymers near surfaces*. World Scientific, Singapore, 1993.

[84] E. Eisenriegler, K. Kremer, and K. Binder. Adsorption of polymer chains at surfaces: scaling and Monte Carlo analyses. *J. Chem. Phys.*, 77:6296, 1982.

[85] P. G. de Gennes. *Scaling concepts in polymer physics*. Cornell University Press, Ithaca, 1979.

[86] A.N. Semenov, J.-F. Joanny, and A. Johner. *Polymer adsorption: mean field theory and ground state dominance approximation.* In: A. Grosberg: *Theoretical and mathematical models in polymer research*. Academic Press, Boston, 1998.

[87] E. Eisenriegler, A. Hanke, and S. Dietrich. Polymers interacting with spherical and rodlike particles. *Phys. Rev. E*, 54:1134, 1996.

[88] R. Podgornik. Polymer-boundary surface interactions and bilayer curvature elasticity. *Europhys. Lett.*, 21:245, 1993.

[89] D. Duffy. *Solving partial differential equations*. CRC Press, Boca Raton, 1994.

[90] V. I. Smirnov. *Höhere Mathematik (IV)*. Deutsch, Harri, Verlag GmbH, Thun und Frankfurt/M., 1988.

[91] P.G. de Gennes. *Rep. Prog. Phys.*, 32:187, 1969.

[92] M. Breidenich, R. R. Netz, and R. Lipowsky. Adsorption of polymer anchored on membranes. *in preparation*.

[93] R. C. Ball, M. Blunt, and W. Barford. Can surface bound states be induced by interfacial roughness? *J. Phys. A: Math. Gen.*, 22:2587, 1989.

[94] R. Podgornik. Surface polymer network model and effective membrane curvature elasticity. *Phys. Rev. E*, 51:3368, 1995.

[95] E. Eisenriegler. Polymers interacting with mesoscopic particles. *J. Phys.: Condens. Matter*, 12:A227, 2000.

[96] F. Clement and J.-F. Joanny. Curvature elasticity of an adsorbed polymer layer. *J. Phys. II France*, 7:973, 1997.

[97] Y.M. Kim and W. Sung. Vesicular budding induced by a long and flexible polymer. *Europhys. Lett.*, 47:292, 1999.

[98] P.G. de Gennes. Interactions between polymers and surfactants. *J. Phys. Chem.*, 94:8407, 1990.

[99] T. Garel, M. Kardar, and H. Orland. Adsorption of polymers on a fluctuating surface. *Europhys. Lett.*, 29:303, 1995.

[100] J. T. Brooks, C. M. Marques, and M. E. Cates. Role of adsorbed polymer in bilayer elasticity. *Europhys. Lett.*, 14:713, 1991.

[101] J. T. Brooks, C. M. Marques, and M. E. Cates. The effect of adsorbed polymer on the elastic moduli of surfactant bilayers. *J. Phys. II*, 1:673, 1991.

[102] M. Laradji. Polymer adsorption on fluctuating surfaces. *Europhys. Lett.*, 47:694, 1999.

[103] R. Lipowsky and H.-G. Döbereiner. Vesicles in contact with nanoparticles and colloids. *Europhys. Lett.*, 43:219, 1998.

[104] G.N. Watson. *A treatise on the theory of Bessel functions*. Cambridge University Press, Cambridge, 1995.

[105] R. Remmert. *Funktionentheorie*. Springer, Berlin, 1992.

Danksagung

Herrn Prof. Lipowsky danke ich für die interessante und vielschichtige Problemstellung, deren interdisziplinärer Charakter anregend war, zugleich Anlass bot für zahl- und lehrreiche Diskussionen.

Herrn Netz danke ich für stets offene Ohren und Gespräche zum Thema, die mich weitergebracht haben.

Meinen Gutachtern Prof. Lipowsky, Prof. Eisenriegler und Prof. Vilgis danke ich für ihre Arbeit und ihr Urteil.

Dank an die Mitarbeiter des Instituts, aktive wie ehemalige, die auf verschiedene Weise zu dieser Arbeit beigetragen haben: Félix Csaika, Rumiana Dimova, Hans-Günter Döbereiner, Willi Fenzl, Prof. Gerhard Gompper, Karl-Kuno Kunze, André Moreira, Paul van der Schoot, Christian Seidel, Udo Seifert, Julian Shillcock und Thomas Weikl.